Foredune restoration and dune system development, Mason Bay, Rakiura/Stewart Island, New Zealand

Megan K. Hankey

A thesis submitted in partial fulfilment of the degree of

Master of Science

At the University of Otago, Dunedin, New Zealand

July 2021

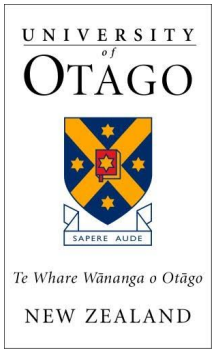

Abstract

Transgressive dune systems are naturally dynamic environments that have been actively stabilised through the 20th century. Awareness of the biodiversity of these systems has increased in recent years, globally, and in New Zealand. This has led to the Rakiura (Stewart Island) Dune Restoration Programme, one of the largest dune restoration projects in the world. Restoration of the largest dune system on Rakiura commenced at Mason Bay in 2000. Since 2010, work has focussed on removing *Ammophila arenaria* (marram grass) and destabilizing a Type I, *A. arenaria* foredune. The impacts of deliberately devegetating a foredune of this magnitude have not been previously examined, including the consequence of releasing large volumes of sand for downwind plant communities. This research aims to understand the impacts of foredune devegetation on (i) dune system morphology; (ii) rates and processes of aeolian sediment transport and landscape evolution; and (iii) deflation surface plants and plant communities at Mason Bay, downwind of this eroding foredune.

The study area includes three adjacent long-walled parabolic dunes (P4-P6). The foredune upwind of P6 was treated with herbicide to eradicate *A. arenaria* in 2010; whereas the foredune upwind of P4 and P5 was treated in 2015. This situation, coupled with a long-term vegetation monitoring programme, has provided a unique opportunity to address the objectives. Changes in the morphology of the foredune-parabolic dune complex were quantified by comparing digital surface models derived from UAV photogrammetry obtained in 2015 and 2020, topographical profiles and soil pits. Estimates of aeolian sand flux within the parabolic dunes were gained using sonic anemometers and sand traps during strong (typical) onshore wind events. Vegetation in six plots located in the deflation surfaces of each parabolic dune were monitored between 2015 and 2020. Changes in plant community composition were analysed to determine the influence of burial on deflation surface plant communities.

The morphology of the foredune (P6 section) changed slowly between 2010 and 2017. After 2017, the rate of change accelerated and the devegetated foredune became lower and wider and the crest shifted landward. About half of the sediment eroded from the foredune since 2017 has been deposited locally, in the lee of the foredune and across the

seaward half of the P6 deflation surface. Most of the remaining sediment has primarily been deposited in the depositional lobe of the parabolic dune, in conjunction with *Ficinia spiralis*, which has also extended inland. Less than 2% of the sediment eroded from the foredune and depositional lobe has been transported beyond the parabolic dunes, into the wider dune system.

Estimates of sand flux were made in P5 and P6 to compare sand input to the parabolic dunes from the eroding and largely intact sections of foredune. Sand flux rates recorded during a strong (15-20 ms^{-1}) onshore wind event downwind of the devegetated foredune in the P6 deflation surface were 575 times greater than downwind of the vegetated foredune in the P5 deflation surface. A second experiment examined shore-normal trends in sand transport between the beach and the depositional lobe. Sand transport increased with distance inland through the devegetated parabolic dune. Sediment transport recorded in the deflation surface and depositional lobes (0.90-1.65 $kg/m^2/min$) was almost three times greater than sediment transport recorded on the foredune crest (0.48-0.51 $kg/m^2/min$). A two-stage model of sedimentation is proposed. During low to moderate wind events (8-12 ms^{-1}) sediment is eroded from the stoss face of the foredune and deposited in the lee of the foredune. During stronger wind events (>15 ms^{-1}), this sediment is transported further inland, across the deflation surface and into the depositional lobe.

Foredune erosion and downwind sedimentation has implications for downwind plant communities. The species richness and abundance of plants in the seaward plot in the P6 deflation surface decreased between 2015 and 2020 (17 species in 2015 and 5 species in 2020). Most species were not able to keep up with the rate of sediment deposition (24-93 cm of accretion in the quadrats in the seaward P6 plot between 2015 and 2020). Prostrate, herbaceous species experienced the greatest decline. In contrast, the plant communities in the P4 and P5 deflation surfaces, where there has been less sand accumulation, showed little change between 2015 and 2020. *A. arenaria* seedlings were not recorded in the plots in the deflation surfaces, despite the existence of a large foredune seedbank. This indicates that as the foredune has eroded and seeds released, *A. arenaria* seeds are either not viable, are being transported further inland, beyond the parabolic dunes or the deflation surface environment is not conducive to germination or recruitment.

Foredune devegetation has restored dynamic geomorphic processes at Mason Bay. It is anticipated the rate of foredune erosion will slow and the former deflation surfaces associated with the parabolic dunes will be transformed into an undulating, hummocky, landscape, composed of *F. spiralis* nabkha and associated sand dune-specific species. It is expected the increase in dunal species within the foredune and deflation surface environment will enhance the deposition of sediment, as has occurred in the P6 deflation surface. Therefore, minimal sediment will be transported further inland, beyond the parabolic dunes. Subsequently, it is expected the area downwind of the restored foredune will become representative of the pre-*A. arenaria* landscape, resulting in enhanced biodiversity within the dune system.

Acknowledgements

To my supervisor, Associate Professor Mike Hilton, thank you for the support you have provided throughout this research. Your experience and knowledge on dune system dynamics has been invaluable. Thank you for introducing me to Mason Bay. It is a very unique part of the world, and I will forever be grateful for having the opportunity to complete my research here.

Doctor Teresa Konlechner, thank you for the support and knowledge you provided, particularly on the ecological aspects of this research. The long-term data set monitoring the deflation surface plant communities was invaluable for this research.

To the field assistants who helped with the collection of data for this research, Jarrod, Dave, Maddie, Pearl, Paulina, Sean and Carol. Special thanks to Campbell for the support and positive attitude you provided on the August trips where we worked through some tough conditions. Our naps in the dunes and breaks under the flax bushes while we waited for the rain to pass will be missed.

The staff in the School of Geography for your support during this research. Particularly Chris Garden, for your assistance with the GIS used in this thesis, and Nigel and Douglas, for your support in preparing equipment before field trips.

The Department of Conservation for the tireless effort you have put towards the eradication of *A. arenaria* at Mason Bay. This research would not have been possible without your support.

To my friends in the Geography Department, the coastal lab group, the map library crew, and my fifth-floor officemates. Thank you for the many fun times, lunchtime chats and support you have provided over the past two years.

Lastly, to my family and friends. Especially Mum, Dad and Leah, for the endless love, support and motivation you provided throughout the completion of this thesis. Thank you for always being a positive and encouraging influence in my life. I would not be the person I am today without you.

Table of Contents

List of Figures

Chapter 1

Chapter 2

Chapter 3

Chapter 4

Chapter 5

List of Tables

Chapter 3

Chapter 4

Chapter 5

Chapter 1

Introduction

1.1 Coastal sand dunes

Coastal sand dunes establish where there is a large supply of sand, adequate wind energy to transport sediment, vegetation present to trap sand and available accommodation space (Goldsmith, 1989; Elko *et al*., 2016). Transgressive dunefields contain episodically active and mobile sand deposits, sand dunes, that can be partially or fully vegetated and migrate across or alongshore, depending on the local wind regime (Hesp and Walker, 2013; Hesp *et al*., 2011). Transgressive dunefields encompass both erosional and accretional dune types (Hesp, 2013). Coastal dunes also have ecological value, including providing habitat for flora and fauna, feeding grounds and nesting sites for birds, as well as a refuge and corridor for migration (Elko *et al*., 2016).

Coastal sand dunes have been degraded in the past due to anthropogenic activities (Doody, 2001; Hilton, 2006). Past management of coastal dunes has primarily been concerned with suppressing active processes and controlling erosion by converting mobile dune systems into a state of stabilisation (Nordstrom *et al.*, 2000). Sand dunes have been stabilised either by the introduction of efficient sand binding species in managed dunes, or the invasion of exotic species in unmanaged dunes (Wiedemann and Pickart, 1996). *Ammophila arenaria* (marram grass) is a particularly effective sand binding species that has invaded dune systems well beyond its natural range, including in New Zealand (Wiedemann and Pickart, 1996; Hilton, 2006). The foredune is the transfer system between the beach and the hinterland, and therefore, this is often the most effective place for stabilisation to occur (Arens *et al.*, 2013a). The invasion of exotic sand binding species on the foredune alters the dune morphology and restricts active

geomorphic processes, which has further implications for the wider dune system (Arens *et al.*, 2013a; Walker *et al.*, 2013; Hilton *et al.*, 2005).

In New Zealand, there has been a 50-80% decrease in area of active sand dunes and there are six ecosystems associated with active dune systems that are classified as 'endangered' or 'critically endangered' (Holdaway *et al.*, 2012). Restoration on the west coast of Rakiura/Stewart Island is one of the largest dynamic dune restoration projects in the world (Hilton and Konlechner, 2010). The extensive scale of this project makes it difficult to compare to restoration at other sites. The dune system at Mason Bay covers a very large, complex area (776 ha, extending 3 km inland), that provides habitat to a number of rare native flora and fauna (Hart *et al*., 2012). The dune restoration project commenced at Mason Bay in 2000 and the dunes have subsequently been monitored regularly (Hilton and Konlechner, 2010). This provides a unique, long-term data set, recording the dune system response to the removal of *A. arenaria*. The different treatment histories of the foredune upwind of the parabolic dunes also provides a rare comparison to understand the processes that occur following foredune devegetation.

1.2 Dynamic dune restoration

In the last 30 years, awareness of the natural dynamic function of active dune systems has increased (Walker *et al.*, 2013). Dynamic landscapes stimulate geomorphic processes and provide habitats and ecosystems that are more resilient to environmental change (Walker *et al*., 2013). Therefore, mobile sand dunes often have a greater natural value than stable dunes (Heslenfeld *et al*., 2004). As specialist species diversity within coastal dune systems reduces globally, the importance of restoring these systems is becoming increasingly acknowledged (Arens *et al.*, 2013b; Konlechner *et al.*, 2014).

'Dynamic dune restoration' aims to restore active processes of sedimentation to sand dune systems (Nordstrom, 2008). Dynamic restoration not only focuses on restoring biodiversity, but also geomorphic diversity to enhance the active and open spaces for specialist species, adapted to young and dynamic environments (Arens *et al*., 2013a; Buckley *et al*., 2016). Dynamic dune restoration increases the complexity of the landscape through enhancing aeolian processes, dune development, topographic and environmental diversity, and consequently, habitat for specialist dune species (Creer *et al.,* 2020). These species should be protected and restored over common and/or generalist

species that often dominate modified environments and produce homogenous and stable dune systems (Doody, 2001).

The most effective way to achieve remobilisation of sand dunes is chemical or mechanical removal of vegetation (Arens *et al.*, 2013b; Hilton and Konlechner, 2010). Chemical removal is achieved through the application of herbicide. Methods of application include aerial or ground spraying and vary depending on the scale of the project, as well as presence of other species that may be affected by the herbicide (Hilton and Konlechner, 2010). Mechanical removal involves removing large sections of soil and vegetation from the dunes, typically initiated with excavators and bulldozers (Arens *et al.*, 2013b). Following mechanical removal, the time to achieve the desired foredune morphology is almost instantaneous, whereas repeated applications of herbicide are required over a number of years to achieve full restoration following chemical removal (Konlechner *et al.*, 2014).

In locations where restoration has occurred, it had been predicted that without intervention, the dune systems would have soon transformed into a state of complete stabilization (Heathfield and Walker, 2011; Hilton and Konlechner, 2010). This has a negative effect on the ability of the dune system to respond to changes in the environment. This includes the impacts of changes in storm event frequency and intensity and whether the dunes will be able to keep up with the predicted eustatic sea level rise (Seabloom *et al.*, 2013; Arens *et al.*, 2013b; de Winter and Ruessink, 2017). Therefore, there is a clear imperative to conserve biological diversity and geomorphic activity to help protect the resilience of these ecosystems and habitats in the future.

A. arenaria has invaded dune systems throughout New Zealand (Hilton, 2006). A. *arenaria* was first introduced to New Zealand in the late 1800s to stabilise coastal dunes and has since spread to coastal dunes throughout New Zealand via the marine dispersal of rhizome (Konlechner and Hilton, 2009). This has resulted in the displacement of native dune species, including the native sand binding species, *Ficinia spiralis* (locally 'pīkao'), a taonga to Māori, which forms low-lying, hummocky dunes in New Zealand (Hart *et al.*, 2012). *A. arenaria* has invaded all of the dunes in southern New Zealand, resulting in the development of high, stable foredunes, where none previously existed (Hilton *et al*., 2019). This prevents the transfer of sediment from the beach into the hinterland and

alters the natural character of the dunes. This arises the question of what occurs following dynamic dune restoration involving foredune devegetation, including, how downwind sedimentation changes and what the implications are for the plant communities that developed in these habitats.

1.3 Study site: Mason Bay, Rakiura/Stewart Island

Rakiura/Stewart Island contains some of the least modified active dune systems in New Zealand. The dune system at Mason Bay is the largest on Rakiura/Stewart Island (776 ha), and one of the largest in the South Island. Mason Bay contains 55% of the area of remaining high conservation value dune systems in the South Island. The dune system has a high biodiversity and 31 of the native plant species that inhabit the dune system at Mason Bay are listed as 'nationally threatened' or 'at risk' (de Lange *et al.*, 2018).

Mason Bay is located on the west coast of Rakiura/Stewart Island, New Zealand (Lat. S46°55', Long. E167°47', Fig. 1.1). The predominant wind direction is onshore, westerly winds. The central transgressive dunefield at Mason Bay extends 3 km inland between Duck Creek and Martins Creek and is 1.2 km wide (Fig. 1.1). This dune system is recognised as nationally significant (Johnson, 1992; Partridge, 1992). The dune system is characterized by a foredune, a series of parabolic dunes ranging from 600-800 m in length, consisting of a deflation surface, trailing arms and depositional lobe, and beyond these, a gently sloping deflation surface, known as the stonefield (Fig. 1.2).

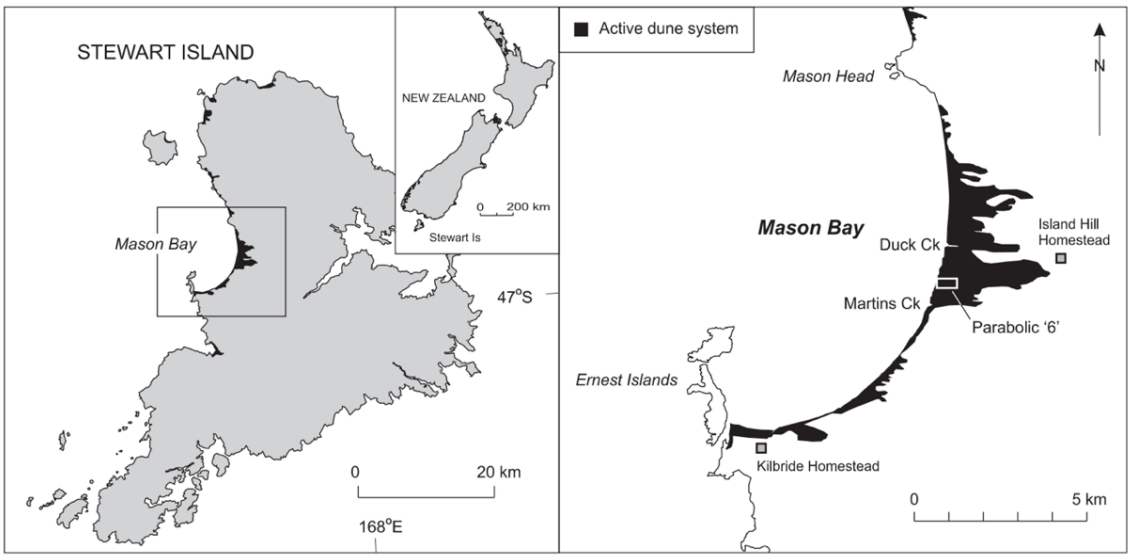

Figure 1.1: Location of the study site in Mason Bay, situated on the west coast of Rakiura/Stewart Island, New Zealand. The transgressive dune system that will be studied is located in the central dune system, between Duck Creek and Martins Creek (from Hart *et al*., 2012).

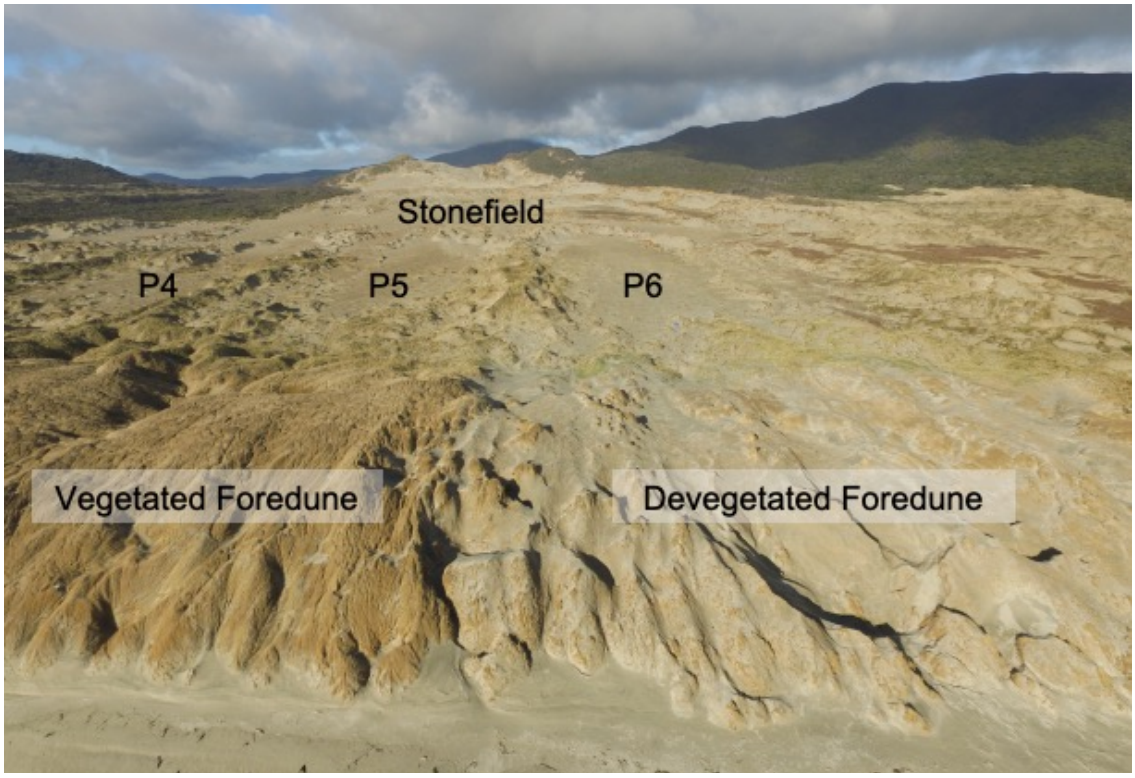

Figure 1.2: Oblique image of the study site, the central dunes in Mason Bay, Rakiura/Stewart Island, oriented onshore in September 2017. The devegetated foredune adjoins parabolic 6 (P6) and the vegetated foredune adjoins parabolic 4 and parabolic 5 (P4 and P5). The stonefield is located inland of the parabolic dunes (source: Dave Borrie).

Prior to the invasion of *A. arenaria*, the Mason Bay dunes consisted of an irregular foredune, mainly composed of low-lying (2-3 m high) nabkha associated with *F. spiralis* (Cokayne, 1990). This formed an undulating, geomorphically diverse landscape as sediment was transferred between the beach and the hinterland. *A. arenaria* was planted at Kilbride, a farm located in the southern dunes of Mason Bay, in the 1930's, and more recently near the Island Hill Homestead in the 1960's, to stabilise the dunes and protect agricultural land (Hilton *et al*., 2005). The marine dispersal of *A. arenaria* rhizome led to the subsequent invasion of *A. arenaria* in the central and northern dunes at Mason Bay. Following the introduction of *A. arenaria*, the foredune formed a steep, densely vegetated, uniform, Type I foredune (after Hesp, 1988), up to 11 m high and 120 m wide (Fig.1.3) (Hart *et al*., 2012; Konlechner *et al*., 2016). By 1998, *A. arenaria* had established across 68% of the active dune system in Mason Bay (Hesp and Hilton, 2013). The increase in vegetation cover led to a loss of mobility and stabilization of the dune system, threatening the habitats of a number of native species (Hart *et al*., 2012).

A series of parabolic dunes established following the introduction of *A. arenaria* at Mason Bay, probably as a result of the formation of *A. arenaria* shadow dunes in the first stages of invasion (Hart *et al.*, 2012). The southern-most parabolic dune, henceforth referred to as 'Parabolic 6' (or 'P6'), originated from a blowout following the introduction of *A. arenaria* to the dune system (Hart *et al*., 2012). The migration of the parabolic dunes has resulted in the enlargement of deflation surfaces. The area of deflation surface habitat in the central dune system at Mason Bay increased from 20% in 1978 to 31% in 2013 (Konlechner *et al*., 2016). These provide habitat for distinct plant communities, primarily composed of low-lying plant species such as *Raoulia hookeri var. hookeri* and *Colobanthus muelleri*.

Figure 1.3: Oblique image of the untreated foredune at Mason Bay in 2017. *A. arenaria* invaded the Mason Bay dune system, forming a steep and densely vegetated foredune, up to 11 m high and 120 m wide (source: Dave Borrie).

The Department of Conservation recognised the significance of the Mason Bay dune system. In 2000, they commenced one of the largest dynamic dune restoration projects in the world at Mason Bay. The aim of this project is to remove *A. arenaria* to stimulate geomorphic processes to promote the return of the dune system to a dynamic state. A grass-specific herbicide (Hurricane^{TM}) has been applied to the dunes using spray application methods including helicopters, argo and knapsacks (Hilton and Konlechner, 2010). Initial restoration efforts at Mason Bay were focussed on back-dune patches of *A. arenaria* (Hilton and Konlechner, 2010). Between 2000 and 2021, the area of *A. arenaria* control at Mason Bay has expanded from 35 ha to 341 ha.

Sections of the foredune have been treated since 2010. The foredune upwind of P6 was first sprayed in December 2010 (Fig. 1.4). Applications of herbicide over a seven year period were required to eradicate *A. arenaria* from the foredune. However, the foredune was not sprayed annually, some years were skipped, or only the stoss face of the foredune was sprayed (Fig. 1.4). The foredune upwind of parabolic 4 and parabolic 5 (P4 and P5) was first sprayed in 2015 (Fig. 1.4). Consequently, by 2019, the foredune upwind of P6

was devegetated, whereas *A. arenaria* remained on the foredune upwind of P4 and P5, primarily as regrowth and decaying roots. Thus, the sedimentation histories of P4 and P5 varies with P6. This provides an exceptional opportunity to understand the processes following foredune devegetation by comparing the changes in morphology and ecology of the parabolics and wider dune system at Mason Bay. Walker *et al.* (2013) stated an adjacent control site, with similar geomorphology, where treatment was not applied, is useful in understanding the response to devegetation.

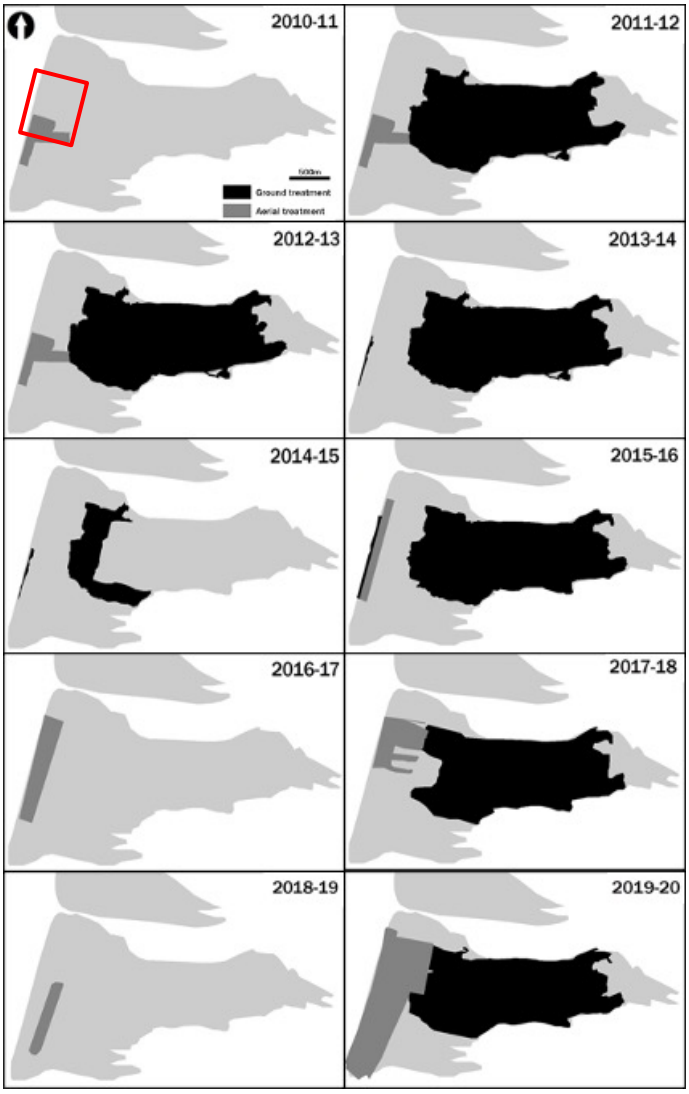

Figure 1.4: Sections of the central dunes at Mason Bay that were sprayed between 2010 and 2020. The section of the foredune sprayed in 2010 included the foredune upwind of P6. The foredune upwind of P4 and P5 was first sprayed in 2015. The black represents areas sprayed by ground operations and the grey represents helicopter spray operations. The study site, consisting of the foredune-parabolic dune complex, is outlined in red.

1.4 Research justification and aims

Foredune destabilization is still a relatively new management strategy. The geomorphic and ecological implications for the downwind environment are not completely understood, particularly as the response of devegetation at different sites is not always the same (Arens *et al.*, 2013b; Bird *et al.*, 2020). Previous dune restoration projects have shown the importance of returning dynamism to unique transgressive dune systems (Arens *et al*., 2013b; Walker *et al*., 2013). However, longer-term, follow-up monitoring on the response and effectiveness of restoration are lacking (Darke *et al.*, 2016). It is important to understand the rates and processes following devegetation to further predict how the landscape and plant communities will evolve in the future.

Further knowledge is required on the transfer of sediment between the beach, foredune and hinterland following devegetation (Arens *et al.*, 2013a). This includes understanding of the rate of foredune erosion and where sand is redistributed to within the dune system. This will be of particular importance for the plant communities that have established in the deflation surfaces downwind of the foredune at Mason Bay. The deflation surfaces formed as result of the sediment supply deficit, as the *A. arenaria* foredune prevented the transfer of sediment from the beach to the hinterland (Petersen *et al.*, 2011). The plant communities in the deflation surfaces are primarily composed of low-lying, herbaceous plants, that do not have a high tolerance to burial. Therefore, there is a risk these species will be displaced from the deflation surfaces of the parabolic dunes. Thus, it is important to understand how sedimentation processes downwind of the foredune change following devegetation and how the plant communities in the deflation surfaces respond to these changes.

Knowledge gained from dynamic dune restoration projects can aid managers in making informed decisions, with the natural function of the dune system at the forefront. This includes understanding the progressive release and movement of sand from the foredune, as well as the evolution of plant ecosystems. The long-term monitoring of the foredune and parabolic dunes following devegetation at Mason Bay provides an exceptional opportunity to understand the response to foredune destabilization. It is expected foredune devegetation will result in the release and downwind transport of large

quantities of sediment, however, it is unknown how rapidly this will occur, where this sediment will be deposited and what the implications will be for the plant communities that have established in the deflation surfaces. Findings from this research will aid in the future management of this site, particularly by understanding the implications for the threatened species located in the deflation surfaces of the parabolic dunes. These results can also provide an insight to what may occur following dynamic restoration at other sites.

The aim of this research is to understand processes of dune habitat evolution downwind of a partially restored (and completely devegetated) *A. arenaria* foredune in Mason Bay, Rakiura/Stewart Island. This research addresses key knowledge gaps through investigating the landscape and plant community response to foredune devegetation. Three research aims will be addressed to understand the rates and processes of foredune erosion, aeolian sediment transport and deposition downwind following foredune devegetation and the response of deflation surface plant communities to changed patterns of sedimentation downwind of the foredune.

Specifically, this research aims to determine:

1. The spatio-temporal patterns of sand erosion and deposition following foredune devegetation.

2. The rates, patterns and sources of aeolian sediment transport at Mason Bay.

3. How deflation surface plants and plant communities have responded to changes in sedimentation patterns.

1.5 Thesis structure

Chapter 1 has provided a brief overview to the context of this study. Awareness of the importance of dynamic dune systems has increased in recent years. This has led to the implementation of dynamic dune restoration projects, including at Mason Bay, where the Department of Conservation are eradicating *A. arenaria* from the dune system. However, there is still limited knowledge of the implications of remobilisation on dune system

development, including for the geomorphology and ecology of the dunes. The scale of restoration at Mason Bay is incomparable to other projects around the world and the partial treatment of different sections of the foredune provides an excellent opportunity to study dune system response to foredune destabilisation.

Chapter 2 provides a detailed review of relevant literature related to sand dune mobility, sediment transport, coastal dune ecology and dynamic dune restoration. The review identifies gaps in the current knowledge to justify the aims of the present study.

Chapter 3 examines how the morphology of the Mason Bay dune system has changed following foredune devegetation. The long-term data set, including ground photos, topographical profiles, and UAV surveys, is used to understand changes in dune system morphology at Mason Bay. This chapter will describe and explain the incremental breakdown of the foredune and where released sand has been deposited.

Chapter 4 investigates the rates and processes of sedimentation in the Mason Bay dune system. An empirical approach is taken, with two experiments completed. The first compares sediment transport downwind of a devegetated and vegetated foredune. The second experiment investigates sediment transport within a devegetated parabolic dune to identify the source of transported sediment.

Chapter 5 explores how downwind plant communities have responded to changes in sedimentation patterns identified in Chapter 3. Permanent plots established in the deflation surfaces of the parabolics were surveyed between 2015 and 2020 and this data is analysed to show how these plant communities have changed following foredune devegetation.

Chapter 6 presents the key findings of this thesis. Each research aim is addressed and discussed. This chapter closes with final conclusions for this thesis and identification of the potential for future research.

Chapter 2

Literature review

2.1 Introduction

This chapter reviews literature related to coastal sand dune dynamism, aeolian sediment transport, dune system ecology, and dynamic dune restoration. This review will aid in forming the research objectives for this study by considering the knowledge gaps based on current understanding in the literature.

Section 2.2 examines the factors that influence dune mobility. The trend of management of dune systems towards stabilization and how this alters dune system function is then outlined in Section 2.3. Sand dune system processes are discussed in Sections 2.4 and 2.5. These cover aeolian sediment transport and coastal dune ecology. Section 2.6 provides a review of dynamic dune restoration projects, including the current knowledge and understanding of the processes following devegetation from case studies around the world. The chapter concludes with a summary in Section 2.7.

2.2 Sand dune mobility

2.2.1 States of mobility

Sand dunes can exist in mobile or stable states. Mobile sand dunes often represent a young and dynamic phase in dune development. Coastal sand dunes, including transgressive dunes, migrate to a stable state where they are fixed in place (Arens *et al*., 2013a). Naturally, all stable dune systems once existed in an active state and became stabilized due to changes in climate, in particular, temperature and rainfall, as these factors influence vegetation growth (Tsoar, 2005). Sand dunes can exist in multiple states

of mobility (Tsoar, 2005). This includes blowouts which may develop in stable surfaces, or parabolic dunes, considered as active landforms, however, contain deflation surfaces which are a relatively stable surface (Jungerius and van der Meulen 1988). Sand dunes can also transition between stages of mobility and stability depending on long term cycles of change, such as perturbations in the climate (Darke *et al*., 2013; Hugenholtz and Wolfe, 2005). These cycles can range in length from decades to hundreds of years (Howe *et al*., 2012).

2.2.2 Mobile sand dunes

Hesp and Thom (1990) defined transgressive dune systems as comprising a broad, free-moving sand surface, that migrates landward or alongshore. Transgressive dune systems are highly dynamic and are primarily affected by sediment supply, climatic variables and vegetation (Hesp, 2013). They can be partially or highly vegetated dune systems that predominantly migrate in the direction of the prevailing wind (Hesp and Thom, 1990; Hesp *et al*., 2011). Forms of transgressive dunes include blowouts, parabolic dunes, barchans, transverse dunes, barchanoid chains and depositional lobes (Yizhaq *et al*., 2013).

Mobile sand dunes are geomorphically diverse. Morphodynamic indicators of mobile dune systems include enhanced aeolian activity, accretion and erosion (Darke *et al*., 2016; Walker *et al*., 2013). Transgressive dune systems often result in the development of geomorphic features such as blowouts and deflation surfaces which leads to geomorphic resilience (Hesp and Thom, 1990; Arens and Geelen, 2006).

The geomorphic diversity of dynamic dune systems also influences the ecology of the dunes, through the range of habitats they provide. These habitats can vary in space and time, including the upper beach, foredune and deflation surfaces (Martínez and Psuty, 2004). Subsequently, mobile dune systems exhibit high ecological diversity, which often leads to the presence of specialist plant species, only found in these unique environments (Nordstrom, 2008). Numerous plant species are able to survive in the coastal environment, however, very few require a dynamic landscape to thrive (Konlechner *et al*., 2014; Barchyn and Hugenholtz, 2013). The dynamic environment at Mason Bay provides habitat for a number of plant species. The native sand-binding species, *F. spiralis*, is the primary native dunal species, whereas the deflation surfaces provide

habitat for species that require a moist and stable surface to survive, resulting in a higher diversity of plant species (Konlechner *et al*., 2016).

Not only are active dune systems important for plant ecology, but they are also critical for shorebirds. Many shorebirds rely on coastal dunes for nesting and breeding. Shorebirds are very sensitive to changes in these environments and disturbances can affect their behaviour and survival, including parental care, foraging and nesting ability (Hubbard and Dugan, 2003). The geomorphic diversity of mobile dunes provides a range of habitats for shorebirds to survive and breed such as deflation surfaces and nabkha. The stonefield, located inland of the parabolic dunes at Mason Bay, provides habitat for the critically threatened southern New Zealand dotterel (Konlechner *et al*., 2016).

2.2.3 Sand dune stabilization

Sand dune stabilization is 'a reduction in active or open dune sand surface by colonizing vegetation' (Heathfield and Walker, 2011, p. 1196). Sand dunes that are in a stable state indicate ageing of the dune system (Provoost *et al*., 2011). As dunes migrate inland, they grow and upwind sections are initially stabilized, before eventually the whole dune system becomes fixed in place (Martinho *et al*., 2010). Processes that contribute to this include variation in the relative sea level, changes in climate, existing topography and beach morphodynamcis (Martinho *et al*., 2010). Sand dunes that are fully vegetated are considered to be stabilized, influencing aeolian activity and the geomorphic diversity of the dune system (Hugenholtz and Wolfe, 2005; Tsoar, 2005). Fixed dunes will remain stable unless an unnatural action destabilizes them (Tsoar, 2005). Simulations completed by Tsoar (2005) suggest wind power needs to be larger than 6000 DP to destabilize a dune system. This is unlikely to occur as wind power of this magnitude has only ever been recorded in Antarctica.

2.2.4 Foredunes

Hesp (2002, p. 245) defined foredunes as 'shore-parallel dune ridges formed on the top of the backshore by aeolian sand deposition within vegetation'. The development of foredunes are largely dependent on wind energy, sediment transport and the cover, density and distribution of plants. Foredunes can exist in a range of forms, discussed by Hesp (1984). There are two main types of foredunes, incipient and established. Incipient foredunes are developing, generally dominated by pioneer plant species. Incipient

foredunes develop into established foredunes as plants, such as woody species, colonise or incipient dune species form a dense population in the foredune environment. This results in the building of a higher and complex foredune (Hesp, 2002).

Foredunes are present in both mobile and stable dune systems. The stability of the foredune is largely dependent on the plant species present and the percentage of vegetation coverage. Foredunes can range in size from less than a metre in height to 30-35 m high (Hesp, 2002). Human interference is the primary reason for foredunes reaching these heights, through activities such as nourishment or planting vegetation, which has occurred globally (Arens *et al*., 2013a; Hilton, 2006; Gao *et al.*, 2020). The restrictive state of stable dunes has implications for the geomorphology of the dune system, for example in the Netherlands, it resulted in a prograded foredune and a steepened coastal profile (Arens *et al*., 2013a). Hesp (1984; 1988) classified high foredunes as Type I foredunes. These are typically homogenous and have a dense cover of vegetation. As the foredune builds higher, it acts as a barrier, often cutting off the sand supply to downwind environments, which has further implications for the hinterland and the plant communities that establish here (Arens *et al*., 2013a).

2.2.5 Parabolic dunes

Parabolic dunes are U- or V-shaped dunes, comprised of a central deflation basin, elongated lateral ridges and a depositional lobe (Hesp, 1991). The depositional lobe advances into vegetation, forming two trailing arms that are stabilized by vegetation (Hesp and Walker, 2013). The depositional lobe advances downwind and a deflation surface is formed upwind of the lobe. The deflation surface is eroded down to the water table and plants establish here, as sand is transported downwind, primarily deposited within the depositional lobe (Hesp and Walker, 2013; Widemann and Pickart, 1996). Parabolic dunes often form where vegetation is sparse or from blowouts (Goldsmith, 1989; Arens *et al*., 2007). It is thought that parabolic dunes are features of a transitional landscape between dune mobility and stability (Arens *et al*., 2004).

2.2.6 Factors influencing sand dune mobility

Hesp and Thom (1990) stated the driving forces that control sand dune mobility are sand availability, wind energy and the growing capacity of vegetation (Fig. 2.1). As the erosion versus deposition rate increases, the growth rate of vegetation decreases, in turn increasing the mobility of the dunes (Durán and Moore, 2013). Mobile dune systems are generally found where there are high wind speeds, high sand supply rates and factors that limit vegetation growth (Pye and Blott, 2017).

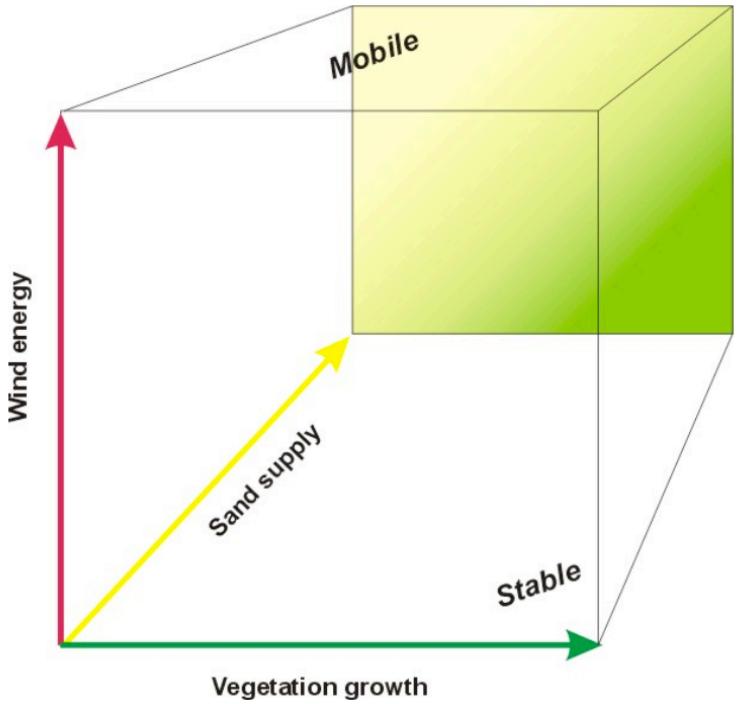

Figure 2.1: Factors that influence sand dune development and function; wind energy, sand supply and vegetation growth (from Hesp and Thom, 1990).

Sand availability

Sediment supply is important for determining the mobility of sand dunes. Sand is supplied either from the beach or from erosion of previously deposited sand (Arens *et al*., 2007). Sand supply is largely determined by coastal processes and sediment from rivers (Arens *et al*., 2013a). A high supply of sediment allows for large transgressive dune systems to develop. This also contributes to an increase in aeolian activity, leading to geomorphic diversity. Without a supply of fresh sand, aeolian activity reduces and dunes stabilise. Sand availability can also be influenced by human activities in a number of ways including mining, planting of vegetation and the construction of infrastructure such as canals or jetties (Arens *et al*., 2013a). Sand supply is extremely important in

allowing dune systems to migrate, which will be particularly significant with the predicted rises in eustatic sea level and whether dunes will be able to respond (Walker and Barrie, 2006).

Wind energy

As wind energy increases, so does the mobility of most dune systems (Tsoar, 2005). Aeolian sediment transport is the predominant form of sediment transport on coastal dunes (Maun, 2009). Wind energy has a direct influence on the aeolian activity of the dune system, thus, as the wind energy increases, the amount of sediment transported will also increase. Due to the lack of cohesiveness of dune soil, which is a porous substrate, composed of very fine particles, with a low infiltration capacity, erosion from wind is acknowledged as one of the primary factors that determines plant growth (Tsoar and Blumberg, 2002).

Mobility indices have been developed based on dune mobility in different parts of the world (Lancaster, 1988; Tsoar, 2005). A factor that is considered in a number of these is the degree of windiness. This can be expressed as the annual average wind speed or as a percentage of the number of days where the threshold velocity for sediment transport occurs. Mobile dune systems are found on coasts which are dominated by high wind energy, and thus, high rates of aeolian sediment transport, whereas naturally stable dunes are generally found on coasts with lower wind energy (Tsoar, 2005).

The growing capacity of vegetation

There is a strong relationship between wind power and vegetation growth. This can vary depending on dune system characteristics, however, high wind power often leads to erosion, creating less favourable conditions for vegetation to establish and grow. Tsoar (2005) developed a hysteresis curve to display the relationship between wind power and vegetation cover (Fig. 2.2). The lines represent a stable state, thus, factors that change the vegetation cover or wind power will cause a change in the stability of the dune system. For example, vegetation removal from dunes in the Netherlands lowered the stability point of the dune system (Arens *et al*., 2013b). Levin *et al*. (2008) studied the relationship between presence of perennial plants and aeolian activity on a dune system on the Mediterranean coast of Israel. They found there was a negative correlation

associated with vegetation cover and sand movement, although aeolian activity varied depending on the plant species present. Thus, vegetation cover is often used as an indicator for sand dune mobility. Mobile dune systems have sparsely distributed vegetation cover and higher rates of aeolian activity, whereas stable dunes are fixed due to the high percentage of vegetation cover, leading to higher rates of sediment deposition (Barchyn and Hugenholtz, 2013). Stable sand dunes are often present in environments with high and frequent rainfall and a high availability of nutrients, as these are conditions which favour vegetation growth (Pye and Blott, 2017).

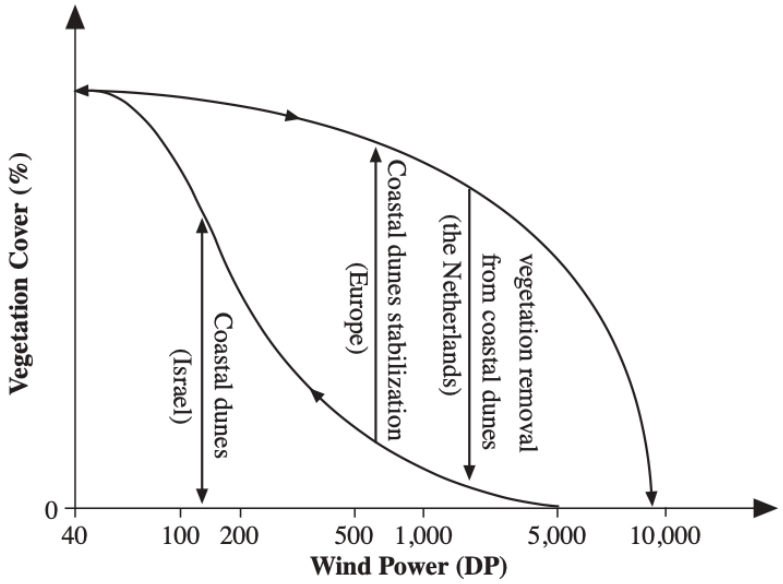

Figure 2.2: Hysteresis curve displaying the relationship between wind power (drift potential – DP) and vegetation cover (%) (from Tsoar, 2005).

2.3 Management towards stabilization

Sand dunes can progress to a stable state naturally through the influence of climatic factors, such as a rise in temperature and/or rainfall and reduction in wind energy. A study by Jackson *et al*. (2019) found there has been a global 'greening' of remote coastal dunes that have not been impacted by human activities, showing increases in vegetation cover from 1984-2017. This effect was attributed to changes in climate leading to increases in temperature, precipitation and nutrients, all favouring enhanced plant growth.

Human activities have also had a significant influence on the stabilization of dune systems. Stabilization aims to supress dynamic processes such as wind erosion, sand drift and dune migration (Walker *et al*., 2013). Gao *et al*. (2020) reviewed dune mobility over the past century and found the most common factor that has contributed to the stabilization of dune systems was human activity (Fig. 2.3). This includes through land use change, stabilization projects and sediment decline. Stabilization is often adopted to reduce erosion and protect surrounding agricultural areas, infrastructure and settlements. Management practices stabilizing sand dunes restrict free blowing sand and interfere with natural processes in the dune system as the landscape and vegetation are unable to rejuvenate (van der Meulen *et al*., 2004). As a result of the extensive effects of anthropogenic activities on the natural function of dune systems, there are very few remaining naturally functioning sand dune systems (Buffa *et al*., 2012).

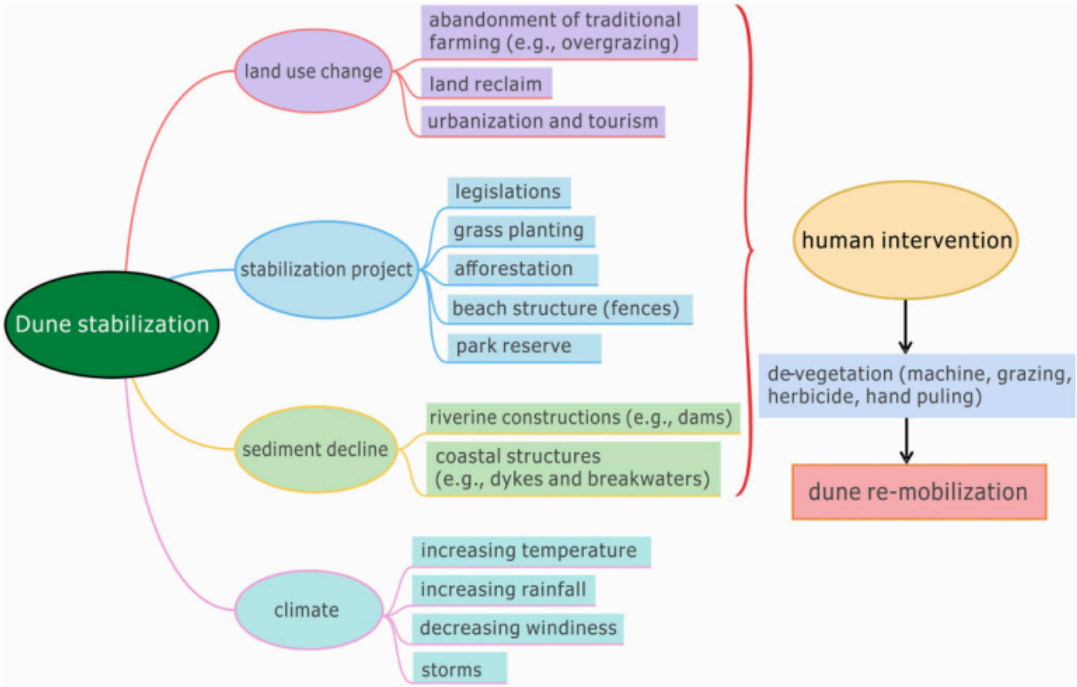

Figure 2.3: Factors contributing to sand dune stabilization. Changes in climate is a natural contributor, while land use change, stabilization project and sediment decline are a result of human intervention. Remobilization can be achieved through devegetation (from Gao *et al.*, 2020).

The majority of coastal dune systems in western Europe are in a state of stabilization (Provoost *et al*., 2011). Dunes in the Netherlands have been managed in the past to

control erosion through stabilization to reduce their mobility and loss of sand from the foredune (Arens *et al*., 2013b). This has resulted in the formation of foredunes which are steeper, higher and more densely vegetated. This is because vegetation interferes with the sediment exchange between the beach and the dunes, as it traps sand that would typically be transported further inland. Heathfield and Walker (2011) found that over a 34 year observation period of two transgressive dune systems in Canada, the active surface area of the dunes decreased by 27.8% and 29.9% respectively. This was a result of encroachment by introduced beach grasses on the foredune and woody plants on the transgressive dune surface.

A review of coastal restoration projects by Lithgow *et al*. (2013) found that 54% of restored dunes are stable dunes, whereas mobile dunes accounted for 27% of the restored dune types. The most common restoration method used was revegetation, accounting for 42%, whereas destabilization or vegetation removal made up less than 5% of the total restoration projects.

2.3.1 Vegetation planting and invasion of exotic species

Planting vegetation on the foredune is a common method used globally to stabilise coastal dune systems (Gao *et al*., 2020). This is because vegetation traps sand and is effective in supressing aeolian sediment transport into the hinterland. Not only does this alter the geomorphology of the dunes through creating a homogenous dune system, but also the ecology. In unmanaged dunes, the primary cause of stabilization is the invasion of exotic species. If invasive species are not controlled, they will often outcompete native species, altering the natural function of the dune system. Subsequently, the introduction of invasive species into the coastal environment has caused the loss of native and pioneer plant species and it has been recognised as one of the greatest threats to biodiversity (Biel *et al*., 2017). In New Zealand an association with increases in stability and a decline in biodiversity has been observed (Hilton, 2006).

2.3.2 *Ammophila arenaria* (marram grass)

Ammophila arenaria (marram grass) is often planted to stabilise dune systems, particularly on the foredune (Hilton, 2006; Wiedemann and Pickart, 1996). *A. arenaria* is highly efficient at trapping sand and can withstand high rates of burial, up to 1 m per year (Ranwell, 1958). Thus, *A. arenaria* accelerates the process of dune stabilization and

foredune building (Darke *et al*., 2016). This can result in the formation of high, homogenous, Type I foredunes (Hesp, 1989; Zarnetske *et al*., 2015). Foredunes on New Zealand beaches that are dominated by *A. arenaria* are generally stable and high compared to dunes formed by the native sand binding species, *F. spiralis* and *Spinifex sericeus* (Hilton, 2006).

A. arenaria has a number of adaptations that makes it a very successful invasive species. These include its ability to withstand low soil moisture, a range of soil pH, extreme tolerance to burial and the extensive seed bank it develops (Ranwell, 1958; Wiedemann and Pickart, 1996; Hilton *et al*., 2019). Konlechner and Hilton (2009) found *A. arenaria* rhizome is able to survive long-distance marine dispersal, particularly in cold water and during the winter months. Rhizome was able to grow after 70 days in seawater. This means *A. arenaria* has the ability to colonize remote environments, including where it was not introduced by humans. *A. arenaria* has thus invaded dune systems well beyond its natural range, including in New Zealand (Hilton *et al*., 2005).

The invasion of *A. arenaria* has further implications for the function of the dune system due to its influence on rates of burial and erosion. Willis *et al*. (1959) found on an *A. arenaria* dominated foredune, there was a substantial decline in wind speed close to the surface, resulting in high rates of deposition on both the windward and lee side of the dune. This alters the sediment budget of the dune system as very little sediment is transported further inland.

A. arenaria also directly influences the presence of other species. Examples from the Netherlands showed on *A. arenaria* dominated dunes, pioneer stages became rarer, the number of weeds increased and the biodiversity of the dunes decreased (Arens *et al*., 2007). Contrarily, in Doughboy Bay on Rakiura/Stewart Island, Konlechner *et al*. (2014) found that *A. arenaria* resulted in an increase in plant biodiversity, as it created an environment where other weeds could establish. However, this did not reflect the natural state of the dune system. This is because the stabilisation of the landscape caused by the presence of *A. arenaria* resulted in the ability for opportunistic species to colonise that may not have otherwise been able to establish in the natural, dynamic environment. Furthermore, increased vegetation growth alters soil nutrients and structure. The root system that results from the high rates of vegetation coverage further stabilises the

system, reducing the chance of erosion and trapping additional sediment, contributing to further growth of the foredune (Sigren *et al*., 2014).

A. arenaria has had an extensive impact on the dune system at Mason Bay, described by Hart *et al*. (2012). After initially being introduced to stabilise the dunes for farming at Kilbride, *A. arenaria* rapidly migrated north, establishing a dense population in the Mason Bay dune system. Between 1958 and 1998, the area of *A. arenaria* increased by 5204%, covering 74.9 ha of the central dunes at Mason Bay. By 2002, over 80% of the foredune was covered in *A. arenaria,* resulting in a different morphology to the pre-*A. arenaria* landscape, including significant accretion and progradation of the foredune. These changes had further implications on aeolian processes. Due to the density of *A. arenaria,* flow velocities were reduced, leading to a reduction in aeolian sediment transport, and thus, stabilization of the dune system (Petersen *et al*., 2011).

2.3.3 Dune restoration

Dune restoration aims to reverse the impacts of invasive species on coastal dunes. The goal of these projects includes to provide ecosystem services, conservation and to restore biodiversity (Lithgow *et al.*, 2013). Dune restoration can occur in two forms, destabilization or re-vegetation (Martinez *et al*., 2013). This thesis is focussed on the impacts following foredune devegetation. Due to the relatively new nature of these projects, there is still very little known about their implications, particularly for the downwind environment. This includes the rate sediment is released from the foredune and where it is deposited, as well as the impacts for hinterland plant communities.

To understand the processes following foredune destabilization, it is important to understand the interaction between aeolian sediment transport and vegetation and the influence these factors have on sand dune mobility. Processes that occur on the beach interact with the hinterland, resulting in a highly connected landscape (Hesp and Thom, 1990). It is expected that as vegetation is removed from the foredune, there will be an increase in aeolian activity, and therefore, dune mobility. This will have further implications for the ecology of the dune system.

2.4 Aeolian sediment transport

2.4.1 Forms of aeolian sediment transport

Aeolian sediment transport is the primary form of sediment transport in the coastal environment. Wave action provides sediment to the coast and from here it is deposited or transported inland (Goldsmith and Golik, 1980). Nickling and Davidson-Arnott (1991) described the primary forms of aeolian sediment transport (Fig. 2.4). Small particles (<60-70 um) are mainly transported through suspension, where particles are transported through eddies while held in the air. Saltation is the primary form of sediment transport, accounting for 75% of total aeolian sediment flux (Rotnicka, 2013). Saltation occurs where particles (60-100 um) are suspended in the air and transported by wind, bouncing along, hitting the surface and being resuspended in the air until they are deposited. Larger particles (>500 um) are transported through surface creep, where they are pushed along the surface largely as a result of the surrounding saltating grains. The wind velocity must be over the threshold for sediment transport to occur. The threshold value is at least 7-8 ms^{-1} for dry, fine-grained sand (Sherman and Lee, 2009; Davidson-Arnott and Bauer, 2009).

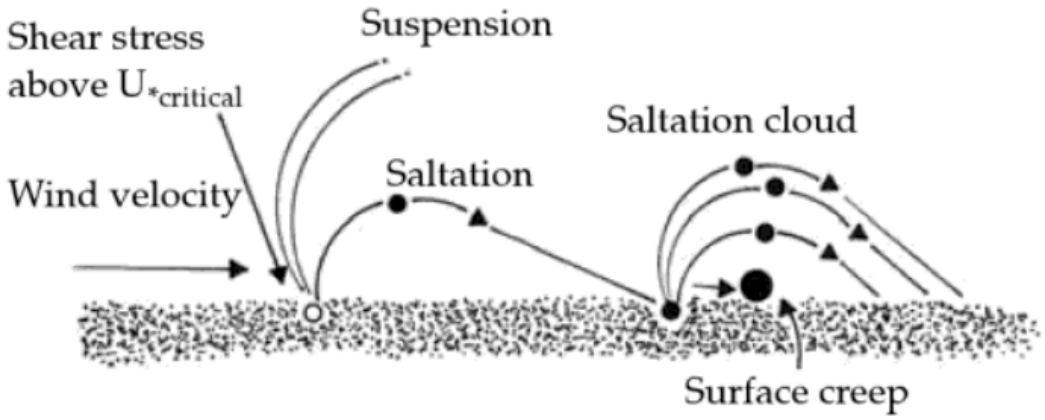

Figure 2.4: Modes of aeolian sediment transport; suspension, saltation and surface creep, initiated by wind velocity of at least 7-8 m/s (from Maun, 2009).

2.4.2 Factors influencing aeolian sediment transport

There are a number of factors that influence sediment transport in the coastal environment. Aeolian sediment transport rates are greatest when there are strong onshore winds, a high supply of fine-grained sand particles and a wide, flat beach (Pye, 1983;

Hesp, 1988). The predominant wind direction at Mason Bay is westerly, directly onshore and these winds can be very strong. Mason Bay has a DP of 260, and is therefore, classified as a high energy environment (Hart *et al*., 2012; Bullard, 1997). The sediment supply for coastal dunes originates from the zone between the low tide level and the backshore where vegetation is unable to survive as a result of wave energy and variations in the high tide mark (Nickling and Davidson-Arnott, 1990). On eroding or devegetated foredunes, sediment supply can also originate from the stoss face. The width of the beach controls the amount of sediment transported, including through determining the total volume of sediment available to be transported, the beach slope and form (Davidson-Arnottt and Lawt, 1996).

Coastline orientation has an important role in determining the level of wave and wind energy the coast is exposed to (Miot Da Silva and Hesp, 2010). The higher the exposure of the coastline to onshore winds, the higher the wind energy towards the coast will be, thus, more sediment will be transported. A large proportion of sediment is transported towards dunes by oblique or alongshore winds (Davidson-Arnott *et al*., 2018). Offshore winds can also have a significant role in sediment transport. However, fewer studies have been conducted on the role of offshore winds on sediment transport compared to onshore winds as it is often assumed they have a lesser importance on dune system development (Lynch *et al*., 2009). In Mason Bay, although the prevailing wind is onshore from the SW, the offshore, NE component is also strong and plays an important role in transporting sediment back towards the beach.

Topography has a strong influence on airflow which effects rates of sediment transport. As air flows up the stoss face of the foredune, a pressure gradient forms due to the compression of streamlines, causing flow acceleration (Walker and Hesp, 2013). Anderson and Walker (2006) recorded flow acceleration over a foredune 1.6 times greater than the incident wind speed. Consequently, sediment transport on the stoss face of the foredune is enhanced. As air flows over the foredune, deceleration occurs due to separation of flow as a result of the topography (Walker and Hesp, 2013). Subsequently, wind speeds decrease with distance inland, resulting in increased sediment deposition.

The interaction between sediment transport and vegetation is significant in controlling dune system function. This is because vegetation traps sediment that is transported

towards the dunes. The rate this occurs determines the morphology of the dune system. Van Dijk *et al.* (1999) stated that in unvegetated dune environments, the evolution of the morphology of the dune system largely depends on the interaction between topography, air flow and sediment transport. Whereas, in vegetated dune environments, dune development is dependent on the height and cover of vegetation as well as topography and the influence these factors have on aeolian activity.

Rates of sedimentation are controlled by wind velocity and vegetation density (Keijsers *et al.*, 2015). Typically, sediment transport will reduce as vegetation cover increases (Anderson and Walker, 2006). Petersen *et al*. (2011) studied the transport of sediment over the *A. arenaria* foredune at Mason Bay. They found sediment could reach up to 5 m high through suspension over the foredune, however, only about 2% of the sediment transported in this way surpassed the foredune environment, entering the hinterland. This resulted in no additional sediment being transported into the hinterland which had further implications for the deflation surface. The deflation surface increased in area and accounted for 31% of the dune system (Konlechner *et al.*, 2016). This led to a decline in the abundance of *F. spiralis* and increased deflation surface habitat.

Knowledge of the rates of sediment transport through parabolic dunes is limited, particularly based on empirical data (Delgado-Fernandez *et al.*, 2018). Understanding the transport of sediment from the beach, through the deflation surface and into the depositional lobes of the parabolic dunes is important to understand how the dune system will develop in the future. This is particularly necessary for dunes that have been destabilized, such as Mason Bay, to determine the implications of changes in sedimentation patterns for the downwind environment.

2.5 Coastal sand dune ecology

Evidently, vegetation plays an integral role in the formation of coastal dunes as a result of plants trapping sand (Durán and Moore, 2013). Vegetation acts as a stabilizer for sand dunes by decreasing the shear stress of wind as it flows over the dune, causing sand to be trapped and deposited where plants grow (Luna *et al.*, 2011). As this process continues, more sand is deposited and the foredune grows in height and width. The

amount of sediment deposited is largely controlled by wind velocity, dune topography and vegetation cover (Keijsers *et al.*, 2015). The largest amount of sediment is deposited on the seaward edge of the dunes, decreasing with distance inland (Petersen *et al.*, 2011). However, this is highly dependent on the vegetation cover. Rates of sediment supply, deposition and erosion are determining factors of vegetation density and community composition (Darke *et al*., 2016). Stallins (2005) identified three important sand dune plants: dune builders, burial tolerant stabilizers and burial intolerant stabilizers.

2.5.1 Adaptations to the coastal environment

Sand is a coarse and porous sediment, therefore, the soil is unable to store large amounts of water, resulting in low water availability for plants (Tsoar, 2005). Big pore spaces also lead to high rates of leaching, therefore, dune sand is nutrient limited. Out of all soil types, sandy soils have the lowest threshold velocity for aeolian sediment transport (Pye and Tsoar, 1990). Subsequently, sand dunes can be easily eroded during high winds or wave energy. However, coastal plants have adapted specific traits to be able to establish communities and survive in these conditions.

The adaptations dune-specific species have developed range from the stages of germination and seedling growth, through to the development of root systems and uptake of nutrients. There is a very high mortality rate of seedlings during their first few days and weeks in the coastal environment, however, this varies between different plant species (Maun, 1994). For seeds to germinate, they require small amounts of burial to increase surrounding soil contact and relative humidity (Maun, 1998). This could be through wind, rain, sedimentation or activity of other organisms in the dunes, such as insects and rodents. If conditions are unfavourable for survival, these plant species have varying responses where they are able to become dormant until conditions improve by delaying germination (Ievinsh, 2006). These seeds remain viable and form a seed bank that acts as an important reserve for the species, particularly following disturbances such as erosion (Luzuriaga *et al.*, 2005). *A. arenaria* seeds accumulate in seed banks as they are buried and can remain viable for at least 21 years (Hilton *et al.*, 2019).

2.5.2 Coastal ecological communities

Once plants establish, ecological communities develop. Succession is the change in species composition over time and is integral to the development of coastal dune

ecosystems (McIntosh, 1980). Maun (2009) stated the importance of pioneer plant species in colonizing to initiate the establishment of an ecological community, allowing other species to then colonize through stages of succession. These species enhance soil development, allowing for the build-up of vital nutrients, creating ideal conditions for other plant species to grow. Pioneer species may first colonize the dune crest or at the toe of the stoss face of the foredune and grow up, as they trap sediment, causing the dune ridge to build (Martínez and Psuty, 2004).

The process of succession is integral to maintaining the natural character and variation within dune systems (Everard *et al.*, 2010). Various stages of succession can exist simultaneously on mobile dune systems if geomorphological processes permit (Arens *et al.*, 2013a). Vegetation can recover from disturbances such as storms through short-term succession (Miller *et al.*, 2010). Over long periods of time, the dune morphology evolves as a result of stages of succession (Miller *et al.*, 2010). Eventually, the dune systems become stabilized as perennial plants develop, resulting in an accumulation of nutrients, promoting the establishment of other species (Bird *et al.*, 2020). Invasion of non-native species largely accelerates this process (Wiedemann and Pickart, 1996).

Ecological communities develop in sand dunes and vary depending on the conditions of the coastal environment. This is because different environmental conditions favour different species, including rates of burial, abrasion, exposure or moisture. The adaptations of plants and the range of habitats within coastal dunes, often leads to high levels of endemism, particularly evident in dynamic dune systems (Lomba *et al.*, 2008). Feedback between vegetation and the morphology of the dune system is a driving factor that determines the spatial distribution of plant species from the foredune, to the hinterland (Miller *et al.*, 2010). Therefore, sand dune stability is important in determining plant community composition (Musila *et al.*, 2001; Garcia-Mora *et al*., 1999). Plant species present in mobile sand dunes are generally psammophilic, adapted to dry conditions and form unique communities (Bird *et al*., 2020).

There is a strong relationship between disturbance and plant community composition in sand dunes. Dynamic processes such as erosion are integral to the development of vegetation on coastal dunes (Maun, 2009). This results in a release of resources, such as nutrients, previously immobilized by established individuals, making these available for

other species to establish (Bakker and Olff, 2003). High rates of aeolian sediment transport have been linked to reduced N-deposition, limiting plant growth (Ejrnaes *et al.*, 2006). This leads to an increase in bare spaces and subsequently, opportunities for pioneer plant species to establish. Brunbjerg *et al.* (2014) found there was an increase in species richness and a reduction in biomass following an increase in disturbance in Danish dunes. Species assemblages changed towards more annuals and stress tolerant species and the species were less closely related phylogenetically than in undisturbed areas. Therefore, disturbed environments increase ecosystem resilience.

Dynamic geomorphic processes produce a range of microenvironmental conditions in sand dunes, and therefore, there are a number of habitats within coastal dunes where diverse plant communities develop (Hesp *et al.*, 2011; Maun, 1998). Plants that inhabit the foredune are exposed to high wind abrasion, salt spray, erosion and burial (Hesp, 1991). Foredune species often require certain levels of burial to survive (Maun, 1998). In New Zealand, the primary native sand binding species can tolerate high rates of burial (dm per year); *F. spiralis*, a sedge and *S. sericeus*, a grass (Sykes and Wilson, 1990). The deflation surface habitat is not suitable for primary sand binding species, such as *F. spiralis*, due to the lower rates of activity in this environment, including low levels of sand deposition. In contrast to stable landscapes, dynamic, dunal landscapes experience high rates of aeolian activity, including erosion and deposition. As a result, mobile dune systems often provide habitat for rare, specialist plant species, that are adapted to survive in these environments (Barchyn and Hugenholtz, 2013; Konlechner *et al.*, 2014).

2.5.3 Plant response to burial

Maun (1998) discussed burial by sand as one of the key abiotic stresses placed on plants living in coastal sand dunes. Burial influences the characteristics of the soil including moisture, temperature and aeration. Maun (1998, p. 717) identified three classifications of plants related to their tolerance to burial '(i) nontolerant, restricted to inland community types where there is no sand deposition; (ii) sand tolerant, occurring in both sand accreting and nonaccreting areas; and (iii) sand dependent, found only in areas with regular sand deposition'. Burial effectively eliminates species from the coastal environment that are intolerant, thus, resulting in only highly specialized species where deposition rates are high. Adaptation to burial has resulted in some plants, such as *A.*

arenaria, becoming so dependent on burial that they require certain rates of sand accretion to survive and maintain a dense population (Marshall, 1965). Therefore, tolerance to burial is one of the primary factors that determines the spatial distribution of plant species in the coastal environment (Maun, 1998).

Maun (1998) identified three plant responses to burial; i) a negative response, whereby a plant is unable to withstand burial; ii) a neutral and then negative response, in which the plant is tolerant to the initial levels of burial and does not show a response, however, dies soon after burial levels become too great; and iii) a positive response, whereby burial stimulates plant growth (Fig. 2.5). However, eventually the rate of burial becomes too great for plants to withstand, resulting in a negative response.

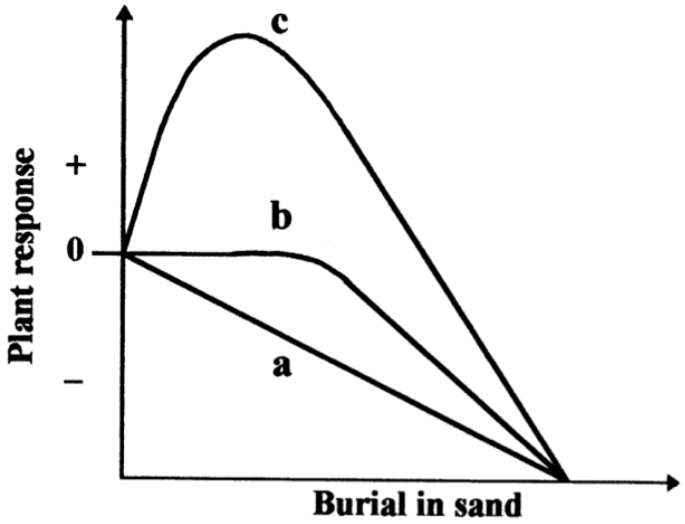

Figure 2.5: Three potential responses of coastal dune plants to burial by sand; a) a negative response; b) a neutral and then negative response; c) a positive response (from Maun, 1998).

Sykes and Wilson (1990) studied the burial tolerance of 30 plant species found in New Zealand sand dunes. They found the native sand binding sedge *F. spiralis* showed a decrease in leaf:stem ratio following partial burial, the same response of *A. arenaria*. Furthermore, creeping herbs such as *Centella uniflora* were able to keep up with high burial rates. However, the exact rate of burial hinterland plants at Mason Bay are tolerant to is unknown, which leads to the question, will these species be able to keep up with the

expected rates of deposition that are expected to occur in the parabolic dune deflation surfaces downwind of the devegetated foredune at Mason Bay?

2.6 Dynamic dune restoration

Dynamic dune restoration aims to re-establish processes which favour disturbance such as wind erosion, abrasion and burial, to provide environments that support natural ecological communities and resilience (Walker *et al.*, 2013). More energy is required to destabilize a dune system compared to stabilising or maintaining an active state (Tsoar, 2005). One of the main methods to restore active dune systems is through devegetation, particularly of the foredune environment (Arens *et al.*, 2013b). There are a range of methods to achieve this including, mechanical or manual removal, the use of herbicide and grazing pressure from animals (Arens *et al.*, 2013b; Hilton and Konlechner *et al.*, 2010). Intervention at the foredune is more effective in promoting aeolian processes and long-term development of the dune systems compared to the hinterland (Arens *et al*., 2013b). This is due to the higher exposure of the foredune which leads to increased erosion (Arens *et al.*, 2013b). If there is a constant supply of sediment from the beach, foredune destabilization can result in the development towards a transgressive dune system (Durán and Moore, 2013).

The interaction between the foredune and downwind environment influences the rate of erosion, sediment supply, deposition and the extent of sediment transport (Bauer and Davidson-Arnott, 2002). Introduction of invasive species, such as *A. arenaria*, impacts the sediment exchange between the beach and hinterland as most of the sediment accumulates in the foredune (Petersen *et al.,* 2011). These changes influence vegetation through altering habitats, such as increasing the deflation surface area and reducing the available habitat for species that are specialized to open dunal environments (Konlechner *et al.*, 2016; Barchyn and Hugenholtz, 2013).

Promoting ecological resilience through dune restoration requires the return of dynamic geomorphic processes such as wind erosion, abrasion and burial which favour early pioneer species (Walker *et al.*, 2013; Nordstrom *et al.*, 2008). Walker *et al*. (2013) developed a series of indicators based on results from the mechanical removal of *A. arenaria* from sections of a foredune in Canada, that can be used to assess the

effectiveness of dynamic dune restoration. These included increased aeolian activity, positive sediment budgets, increased active sand surface area, enhanced morphodynamcis, geomorphic diversity and resilience. These factors are required to re-establish optimal conditions to stimulate ecological processes in order to assist the return of resilient ecosystems, composed of native, dune-specific species.

Globally, the number of dynamic restoration projects have increased in recent years. A number of dune restoration projects in Europe have achieved at least partial success in restoring dune mobility through the removal of vegetation (Bird *et al*., 2020). For example, large scale dune destabilization has occurred in the Netherlands where dunes were previously stabilised for canals. Arens *et al.* (2013b) provided a review of these projects aiming to remobilise dune systems in North Holland which have been destabilized, mainly through the mechanical extraction of vegetation from the dunes. The scale of restoration at these sites has ranged from a few hundred metres to 13 ha. These projects have found varying results, at one site, within eight years following foredune devegetation, increases in aeolian activity, shadow dune and blowout development and changes in plant communities were observed (Arens *et al.*, 2004; Arens and Geelen, 2006). In Van Limburg Stirum the removal of vegetation was linked to small-scale features like blowouts, sand patches and small deflation zones (Arens *et al*., 2013b). Van Boxel *et al.* (1997) found the reactivation of blowouts following the removal of vegetation led to poorer nutrient conditions which stimulated plant diversity.

Other locations where devegetation has occurred include California, Israel and New Zealand (Pickart *et al.*, 1998; Hilton and Konlechner, 2010; Bar, 2013). Pickart *et al.* (1998) described the impact of removing the non-native yellow bush lupine from dunes in Northern California. Lupine alters soil characteristics by increasing the amount of nitrogen and other nutrients present which promotes the establishment of other weeds and invasive grasses that would otherwise not be able to survive in this environment. Four years following removal of lupine, it was found native species, particularly those less influenced by the presence of lupine, significantly increased in abundance, especially where the duff and litter was also removed. Therefore, removing invasive vegetation can restore the natural characteristics of the soil, aiding the re-establishment of native species.

Bar (2013) reviewed dynamic restoration in Israel, focussed on protecting the endemic biodiversity of the dune systems on the Mediterranean coast. Woody vegetation which resulted in large-scale stabilization of the dune systems was mechanically removed either completely or partly from seven dunes along this coast. Two years following devegetation there was significantly more sand movement occurring on these dunes compared to the dunes where intervention did not occur (Tsoar and Blumberg, 2002). However, five years after removal, there was regrowth of woody vegetation and transition to an active dune landscape did not occur. Bird *et al.* (2020) analysed the effects of the restoration of these dunes on the dune ecology. They found there was no significant change in ecology following devegetation of fixed dunes and this was largely attributed to the effects invasive vegetation had on changing the natural soil characteristics, thus making it more difficult for only natives to re-establish. A stronger response was observed on the semi-fixed dunes where there was recolonization of mobile dune indicator species a few years following devegetation.

The removal of *A. arenaria* has been a focus of many dynamic restoration projects due to its widespread distribution and role in the stabilization of dune systems worldwide. The removal of *A. arenaria* has resulted in a number of changes to dune systems. In British Columbia in Canada, *A. arenaria* was mechanically removed from approximately 200 m at a number of sites along a 3 km section of the foredune following displacement of native species, described by Eamer *et al.* (2013). Six years following devegetation they found there was increased aeolian activity, including deposition and erosion, the foredune crest lowered, blowouts developed and migration of the transverse and parabolic dunes was observed. There was also a net positive gain in sediment volumes to dune systems and the re-establishment of the stoss profile (Eamer *et al.*, 2013; Walker*, et al.*, 2013).

There are several complexities involved in dynamic restoration, particularly the removal of invasive vegetation, such as *A. arenaria.* A notable challenge is the extensive seed bank these species can develop (Hilton *et al.*, 2019). Remnant roots can result in significant regrowth and seeds germinate as they become exposed (Hilton and Konlechner, 2010; French *et al.*, 2011). Consequently, initial eradication of a species does not lead to immediate and effective remobilization of the dune system. Once erosion occurs, there are a number of factors which can slow this process, including the

establishment of vegetation or changes to the sediment supply. Therefore, a long-term management strategy is required to achieve complete activation.

There has been extensive effort into the restoration of dune systems on Rakiura/Stewart Island, New Zealand. For example, restoration at Doughboy Bay, located to the south of Mason Bay, on the west coast of Rakiura/Stewart Island, was focussed on the removal of *A. arenaria*, described by Konlechner *et al.* (2014). Initially active sand transport was minimal and small blowouts developed. The transition to a pre-*A. arenaria* landscape was halted by regrowth from the extensive seed bank which had developed. However, once this was removed, activation of the dune system occurred mainly through erosion of the stoss face and activation of the inland barrier surface about three years after the initial application of herbicide.

Following re-mobilisation of the Doughboy Bay dune system, native vegetation was planted or re-colonized the dune system (Konlechner *et al.*, 2014). In particular, *F. spiralis* was planted and replaced *A. arenaria* as the primary sand-binding species present. As a result of the increase in sand movement, the cover of vegetation was a lot more sparse compared to the *A. arenaria*-dominated landscape. Species richness also declined as only species tolerant to high rates of burial were able to survive in this dynamic environment (Konlechner *et al.*, 2014). Species composition at this site now resembles a mobile dune system and is similar to nearby mobile dune systems that have not been invaded by *A. arenaria.* Restoration at Doughboy Bay has not resulted in the return of the pre-*A. arenaria* landscape, however, it has transformed the dune system into a more dynamic landscape, providing habitat for native and threatened plant species adapted to this environment. Although there are differences between the landscape at this site and Mason Bay, results from restoration at Doughboy Bay provide an important comparison to what can be expected at Mason Bay, including the development of the plant communities.

2.7 Conclusion

Transgressive dune systems are naturally dynamic environments that have historically been managed towards stabilization. Awareness of the importance of mobile dune

systems for the conservation of native flora and fauna has increased in recent years, globally, and in New Zealand. This has resulted in a number of dynamic dune restoration projects of varying scales and methods around the world. However, the response of transgressive dune systems to the removal of vegetation, particularly foredune restoration, is variable at different locations. This is particularly a result of the different scale and methods of devegetation. Restoration has been more successful following devegetation from larger sections of the foredune and following consistent monitoring to prevent regrowth.

There is a strong connection between aeolian sediment transport, plant community composition and the dynamism of dune systems. Therefore, when considering the development of dune systems following restoration it is important to understand these processes. However, the consequences of dune destabilization, particularly foredune evolution, the rate and patterns of landform development and the implications for hinterland plant communities are unknown. The dynamic dune restoration project at Mason Bay is one of the largest in the world. Long-term monitoring at this site, including the implications of the introduction of *A. arenaria* on the dune system, as well as how the landscape has evolved following devegetation, provides an exceptional opportunity to understand species and plant community response to *A. arenaria* removal.

Chapter 3

Foredune devegetation, sedimentation and dune system morphodynamics

3.1 Introduction

The Department of Conservation has undertaken one of the largest dynamic dune restoration projects in the world at Mason Bay, Rakiura/Stewart Island. The aim of the dune restoration project is to remove the invasive *A. arenaria* from the dune system to restore dynamic geomorphic processes that are imperative to the natural character of the dune system (Hilton and Konlechner, 2010). *A. arenaria* eradication commenced at Mason Bay in 2000 and initial spraying was primarily focussed on the hinterland, inland from the parabolic dunes (Hilton and Konlechner, 2010). Foredune devegetation commenced in 2010 with the spraying of the foredune upwind of P6 (P6 FD), while the foredune upwind of P4 and P5 (P4 FD; P5 FD), was not sprayed until 2015 (Fig. 1.4). Therefore, the spray history of P4 and P5 varies from P6, providing a unique comparison to understand the processes following foredune devegetation.

This chapter describes the spatio-temporal patterns of sand erosion and deposition following foredune devegetation at Mason Bay. It examines how the landscape has evolved since the commencement of foredune devegetation in 2010. In particular, this chapter aims to understand the rate of foredune erosion at Mason Bay and where sediment has been redistributed following devegetation. This chapter is primarily focussed on the period between 2015 and 2020 because initially, the rate of change in foredune morphology was slow and large rates of erosion did not occur until 2017.

The introduction of *A. arenaria* to Mason Bay has altered the natural dynamics and morphology of the dune system, described by Hart *et al.* (2012). The pre-*A. arenaria* landscape consisted of a low-lying, discontinuous, *F. spiralis*-dominated foredune (Cockayne, 1909). Following the invasion of *A. arenaria,* the foredune transformed from a sparsely vegetated Type 5 foredune (after Hesp, 1988), to a densely vegetated and continuous, Type I foredune. This had implications for the wider dune system. The foredune acted as a barrier, preventing the transfer of sediment from the beach to the hinterland. This resulted in an area of sand deficit and formation of deflation surfaces behind the foredune. Subsequently, between 1989 and 2002, the size of the P6 deflation surface increased at a rate of 15.60 m/year and the depositional lobe of P6 accreted vertically (Hart *et al*., 2012).

A. arenaria eradication on Rakiura/Stewart Island was initially undertaken at Doughboy Bay, located to the south of Mason Bay. Following the removal of *A. arenaria* in Doughboy Bay, the foredune lowered and eroded (Konlechner *et al.*, 2014). However, the rate of foredune decay was slow as a result of the extensive seed bank *A. arenaria* had developed, which led to regrowth, continuing to stabilise the foredune. Therefore, erosion did not occur for up to five years following the initial application of herbicide (Konlechner *et al.*, 2014). Due to the similarity in site conditions and method of devegetation, it is expected the Mason Bay foredune will display a similar response to devegetation.

The methods used to monitor and quantify the changes in the morphology of the central dune system at Mason Bay will be outlined in this chapter. The results will then be analysed, to show how the morphology has changed following devegetation by comparing the three parabolic dunes. This is followed by a discussion of the processes that have occurred at Mason Bay, following the removal of *A. arenaria,* to explain the changes that have occurred.

3.2 Methods

3.2.1 Surveying

Due to the dynamism of coastal environments, frequent monitoring is required to understand morphological changes and to be able to relate these changes to other processes occurring, for effective management (Morton *et al*., 1993; Moloney *et al*., 2018). Surveying methods have been utilised to monitor the dune system at Mason Bay throughout the duration of the dune restoration project, providing a rare, detailed record of how the morphology of the dune system has changed following foredune devegetation.

Real-time kinematic global positioning system (RTK-GPS)

The RTK-GPS consists of a static receiver (the base station), a mobile receiver (the rover), and a communication link (for example a radio link using an antenna) which connects the base and the rover (Pardo-Pascual *et al.*, 2005). The base station is set up over a point, where the co-ordinates are already known, and the receivers communicate with satellites to determine the position of the rover. The RTK-GPS has a horizontal accuracy of several millimetres and a vertical accuracy of 4-9 cm (Lee *et al*., 2013).

A Trimble R10 was used to survey the profile and ground control points in the study area. The base station was set up over a LINZ benchmark on the top of Big Sandhill, relative to the New Zealand Geodetic Datum 2000, using the New Zealand Transverse Mercator 2000 co-ordinate system. The RTK-GPS recorded x, y, z points and the occupation time for the rover was two seconds.

Topographical profiles

A transect along the axis of P6 has been maintained since 1999 and surveyed regularly since the restoration project began at Mason Bay (Fig. 3.1). A transect along the axis of P5 has also been maintained since 2012 (Fig. 3.1). These two profiles have been surveyed annually using a range of methods including a total station and RTK-GPS. These profiles typically comprise of about 130 points of x, y, z data. The data collected was transferred into x, y data using ArcGIS™ to provide the elevation and distance from the beach relative to the NZTM2000 co-ordinate system.

The topographical profile of the foredune upwind of P6 was used to calculate the volume of erosion and accretion on the foredune for every year between 2010 and 2020. The area of erosion was calculated for the stoss face of the foredune, and accretion was calculated for the lee of the foredune, up to 290 m inland, where sediment from the foredune has been deposited. The area calculated was in m^2 as the profile is 2-dimensional. The area was converted into m^3 by multiplying the area by 1, to produce a value of volume change for a 1 m cross-section of the profile. The same method was used to calculate the volume of erosion of the erosional face of the depositional lobe and accretion in the lee of the depositional lobe using the topographical profiles obtained in 2004 and 2020.

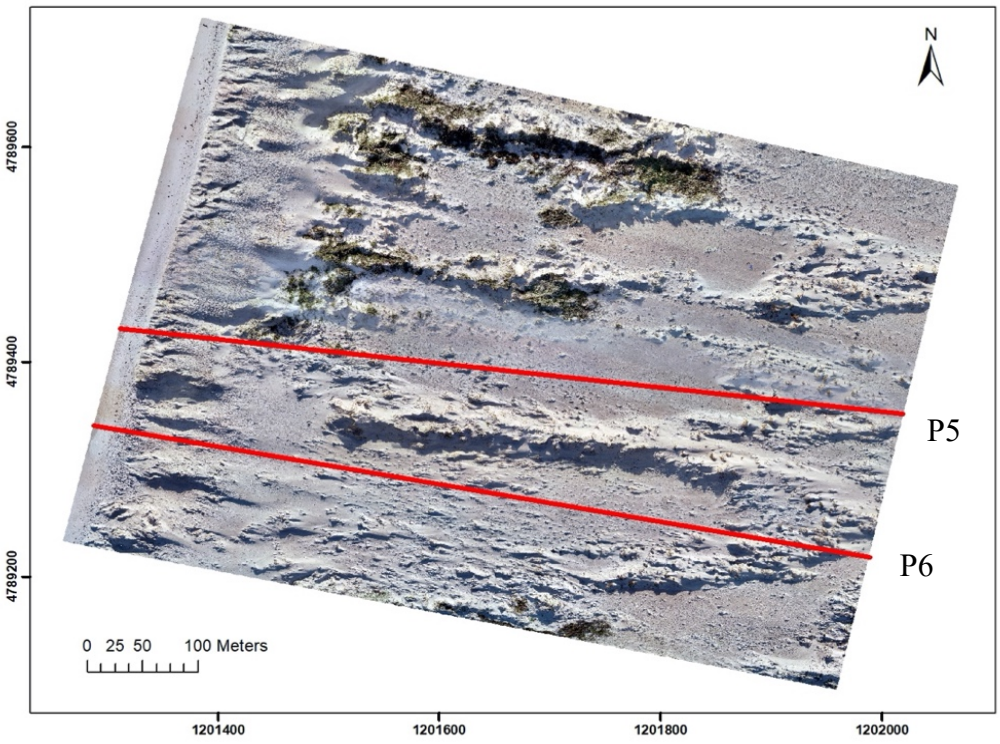

Figure 3.1: Location of the transect lines surveyed in P5 (top) and P6 (bottom). These have been maintained prior to the commencement of the restoration project and surveyed annually to provide a timeseries of the parabolic dune profiles.

Unmanned aerial vehicles (UAVs)

UAV technology are highly effective for monitoring changes in the coastal environment (Ierodiaconou *et al.*, 2016). UAVs allow for a digital surface model to be obtained over a small time period, producing DEM accuracy of ~5 cm (Moloney *et al.*, 2018; Casella

et al., 2020). In recent years, UAVs have become common tools used to survey coastal environments (Moloney *et al.*, 2018).

The first UAV survey at Mason Bay was completed in November 2015 using a Trimble UX5 fixed wing UAV. This survey was completed by Dr Pascale Sirguey. The survey covered the parabolic dune system at Mason Bay, including P4, P5 and P6. In June 2020, a Phantom 4 drone was used to resurvey of the same area. Drone Deploy™ was used to set the flightpath of the drone to fly in parallel lines over the survey area. The frontal and side overlap of the photos taken in these surveys was 70%. The altitude the drone flew at was 70 m. These were used to create an orthomosaic and digital elevation model of the survey area.

A profile from the P6 transect line (Fig. 3.2) was extracted from the UAV survey in June 2020 and compared with the RTK-GPS survey along the same line, also completed in June 2020, to cross-validate these methods. The RTK-GPS profile is a lot smoother compared to the UAV profile, because fewer points were used to construct the RTK-based profile; 140 points for the RTK-GPS survey, compared to 43,700 points from the UAV survey. The profiles from both surveys are very similar. Discrepancies occur mostly on the stoss face of the foredune and the depositional lobe, from about 670 m. This is likely due to a location error, being off the profile line, when completing the RTK-based survey.

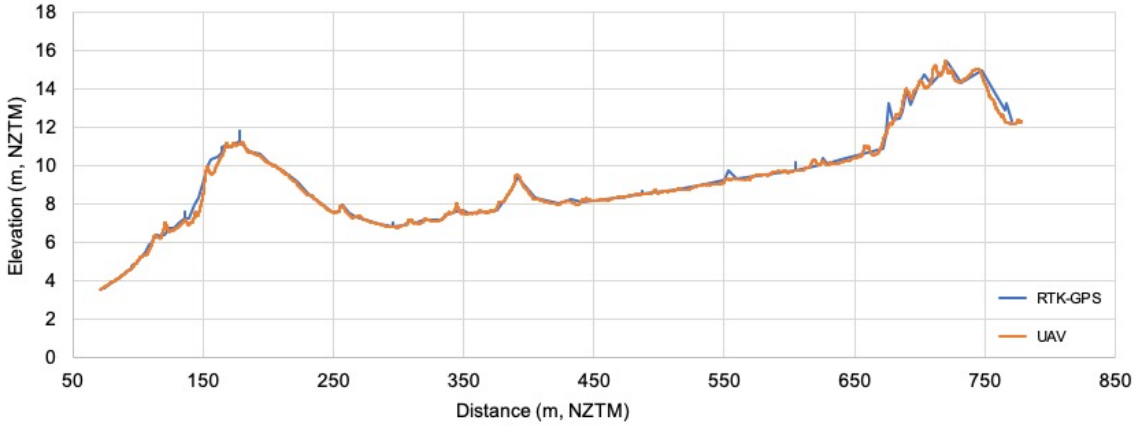

Figure 3.2: Topographical profile from the RTK-GPS and UAV survey along the P6 transect line completed in June 2020. The similarity between both surveys validates the use of these surveying methods.

Ground control points (GCPs)

GCPs are markers of known location and elevation, which are distributed throughout a UAV survey area. They are used to indirectly georeference an aerial survey to create a digital elevation model (Sanz-Ablando *et al.*, 2018). GCPs are required because the internal GPS of the UAV does not obtain co-ordinates of sufficient accuracy. Therefore, the number and distribution of GCPs is the greatest contributor to the accuracy of the DEM and orthophoto produced from UAV surveys (Martinez-Carricondo *et al.*, 2018; Gonçalves and Henriques, 2015). To obtain high accuracy that is representative of the survey area, GCPs should be distributed around the edge of the survey area and stratified throughout the centre, to account for variations in height, to enhance vertical accuracy (Martinez-Carricondo *et al.*, 2018).

Before the UAV surveys were completed in Mason Bay, GCPs were distributed throughout the survey area. The GCPs used were square tiles, composed of black and white squares, to make them easily visible by the UAV. These were distributed in a pre-determined layout, which included areas of high and low points, as well as the border of the survey area (Fig. 3.3). They were then surveyed with the RTK-GPS to obtain their x, y, z co-ordinates.

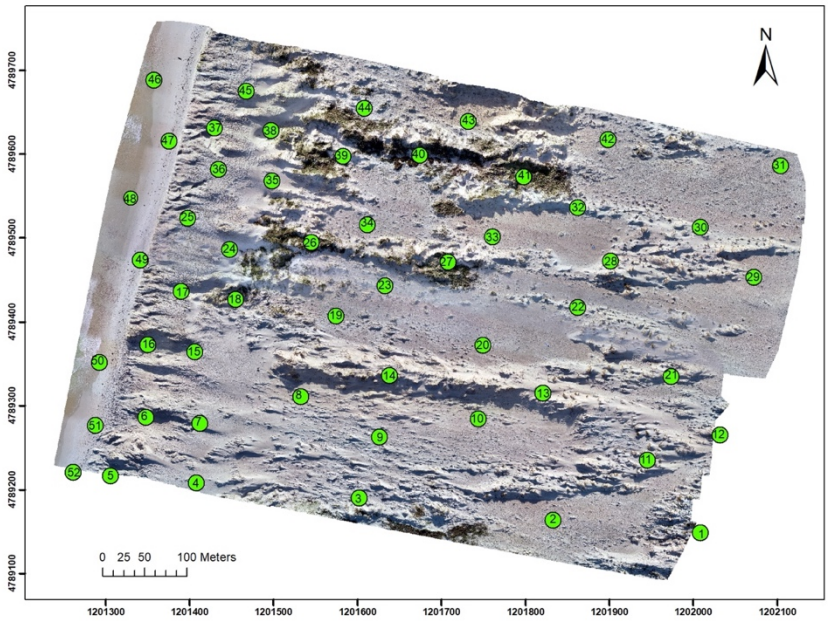

Figure 3.3: Layout of the ground control points at Mason Bay used for the UAV survey in June 2020. GCPs were distributed around the edge of the survey area as well as on the deflation surfaces and trailing arms of the parabolic dunes.

Digital elevation models

Data collected from UAVs can be converted into a digital elevation model (DEM), showing the variations in elevation over the survey area. GIS software determines the elevation for points throughout the survey area. Through interpolation of the point cloud produced, elevations for the unknown areas are calculated and the result is a raster surface where all cells are assigned an elevation (Gallay *et al.*, 2013). This can then be used to monitor and compare changes in morphology overtime (Casella *et al.*, 2020; Gonçlaves and Henriques, 2015).

Data collected from the UAV surveys was used to produce a series of DEMs. The images from the UAV surveys were imported into Pix4Dmapper software. The co-ordinates for the GCPs were also imported and each GCP was manually marked. The quality report produced was reviewed to ensure the mean RMS error was low (<0.05), and thus, the GCP co-ordinates used were accurate. The outputs following this process included a DEM and orthomosaic image for each of the surveys. This process was completed for surveys carried out in November 2015 and June 2020.

To understand changes in the morphology of the dune system from 2015-2020, the DEMs from each of these surveys were compared using ArcGIS™. The Raster Calculator tool was used, to compare the 2015 DEM with the 2020 DEM, to calculate the change in elevation for the survey area over this period of time.

The Cut Fill tool was used to calculate areas where volume had been lost or gained in ArcGIS™. Volume change calculations were made for the whole area surveyed, including P4, P5 and P6; the area of P6, from the foredune to the apex of the parabolic; and the foredune adjoining P6. To understand the areas within P6 that have eroded or accreted, P6 was split into eight sections, 80 m in length and 160 m in width, and the volume change for each of these sections was calculated (Fig. 3.4). The total change in volume was calculated for each location/section. The total change in volume was also divided by the total area to calculate the change per square metre.

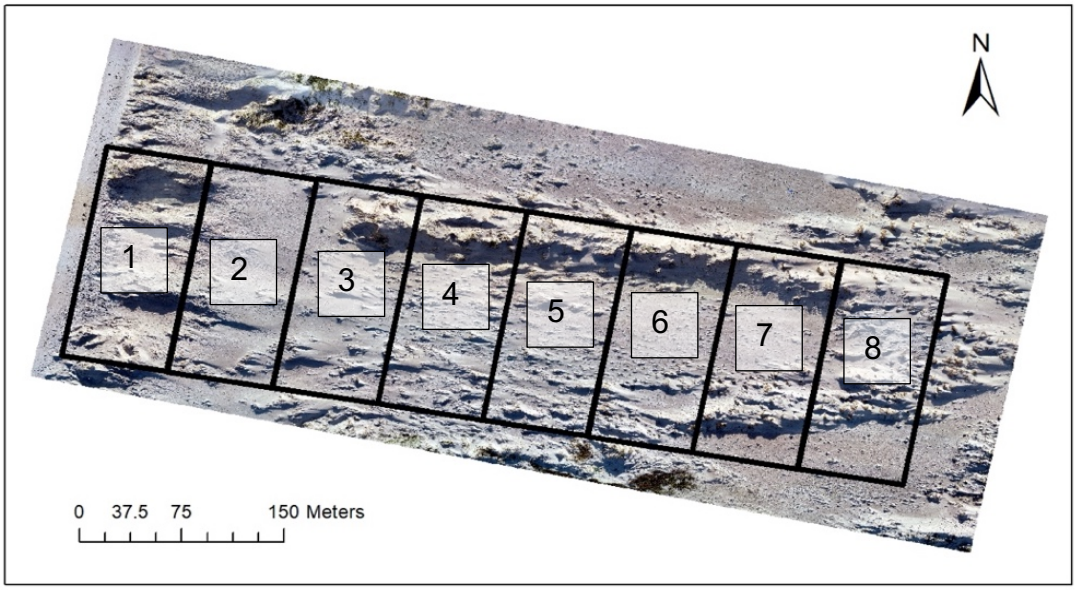

Figure 3.4: Volume change between 2015 and 2020 was calculated for eight sections of P6 using the Cut Fill tool in ArcGIS™. Section 1 is the western-most section, closest to the beach and section 8 is the eastern-most section, closest to the apex of the parabolic.

3.2.2 Soil profiles

Paleosols can indicate patterns and rates of sediment accumulation and support reconstruction of past climates (Kraus, 1999; Goble *et al.*, 2004). Patterns of soil stratigraphy can be identified through the excavation of soil pits. Soil profiles were dug in the deflation surface of P4, P5 and P6 in June 2020 to record the rates of deposition downwind of the foredune since the restoration project began, in 2010. A predetermined layout of 7 rows, containing 7 pits, 10 m apart, was established for the deflation surface of P5 and P6 (Fig. 3.5). The rows were separated by 30 m. The soil pits in P4 consisted of 11 rows, 20 m apart, of 2-8 pits, dependent on the width of the deflation surface. The location of the pits was marked with a hand-held GPS in the field. The stony deflation surface was used as an indication of the pre-restoration surface. The depth from the surface to this layer was measured (Fig. 3.6). There was a distinct colour change between the sandy layer and the deflation surface. The deflation surface was darker in colour and composed of small stones and gravel as well as plant roots, making it a rougher texture compared to the sandy layer. The data from the soil profiles was input into ArcGIS™. The Inverse Distance Weighted tool was used to interpolate between the sample points

obtained to create a choropleth map showing the depth of deposition that has occurred in the deflation surface of the parabolics since the implementation of the restoration project.

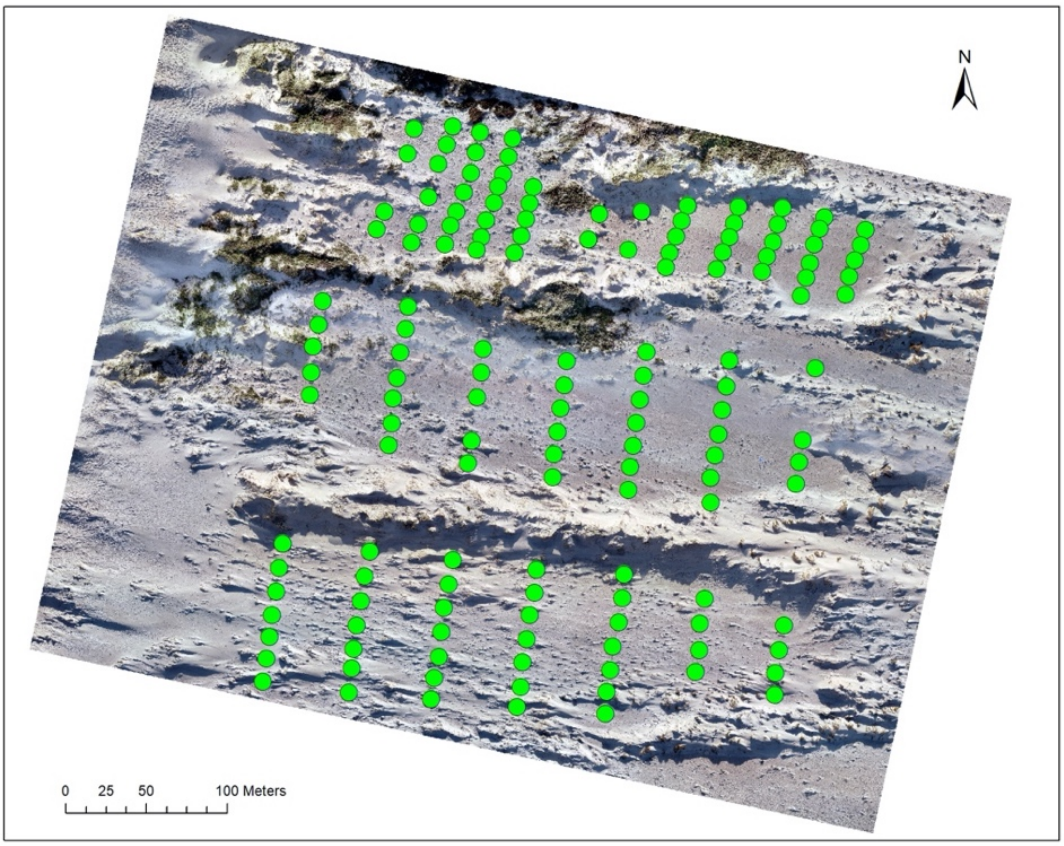

Figure 3.5: The locations of the soil pits dug in P4, P5 and P6 in June 2020.

Figure 3.6: Soil profile which displays the stratigraphy of the soil in the deflation surface of the parabolic dunes. The arrow is pointing to the former deflation surface (indicated by a layer of coarse granules and gravel, comprised of degraded granite). The depth from the surface to this layer was measured for each pit in P4, P5 and P6.

In addition, a series of pits were excavated in August 2019 along a 360 m transect in P6 (Fig. 3.7). Pits were dug every 5 m along this transect and the depth from the surface to the former deflation surface was recorded.

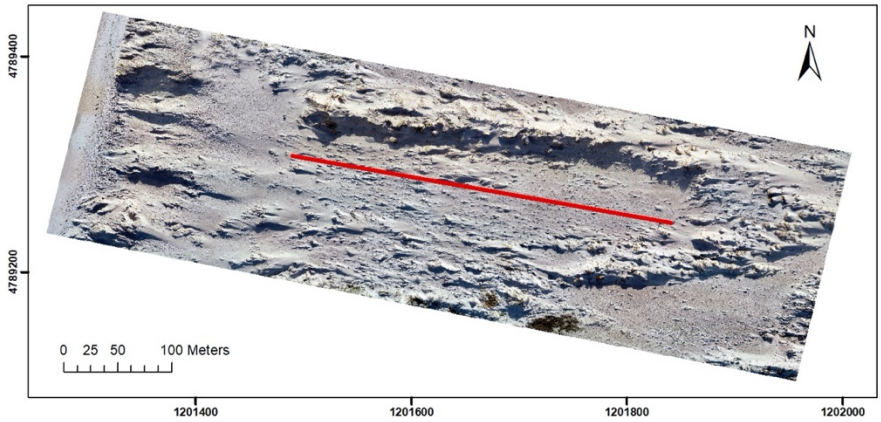

Figure 3.7: Soil pits were dug every 5 m along this transect in the P6 deflation surface in August 2019. The depth of the sand layer above the deflation surface was measured.

There were limitations to the excavation of soil pits. It was not possible to manually dig to the deflation surface at some points in the western end of P6 due to the deposition of sediment that had occurred. Therefore, these data points were not included, resulting in an underestimation of the actual depth of sand accumulation here.

3.3 Results

3.3.1 Foredune-parabolic dune complex morphology

The orthomosaic derived from a UAV survey completed in June 2020 shows the study area of the foredune-parabolic dune complex at Mason Bay, including P6 the furthest south, P5 in the centre and P4, the northern-most parabolic dune (Fig. 3.8). Blowouts have formed in the foredune of P6, as well as nabkha in the P6 deflation surface. The parabolic dunes consist of a deflation surface, trailing arms and depositional lobe.

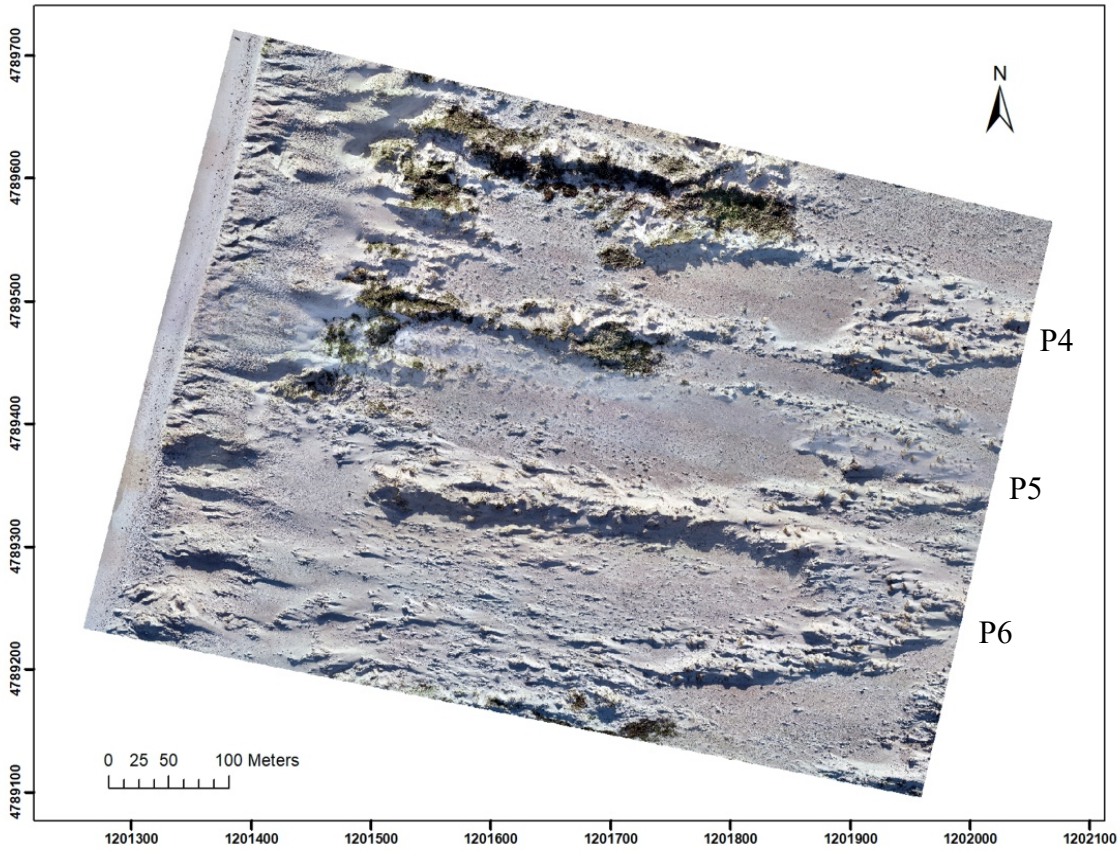

Figure 3.8: Orthomosaic of the study site at Mason Bay, June 2020. The image displays the study site, including the foredune and three parabolic dunes, P4, P5 and P6.

The oblique image displays similar patterns to those observed in the orthomosaic image (Fig. 3.9). The foredune upwind of P6 has a lower elevation and the difference in the colour of the deflation surface can also be observed. P6 is much lighter in colour compared to the other parabolics showing more sand has been deposited in the deflation surface. The depositional lobe of P4 is most prominent in the image and it shows *F. spiralis* has colonised here.

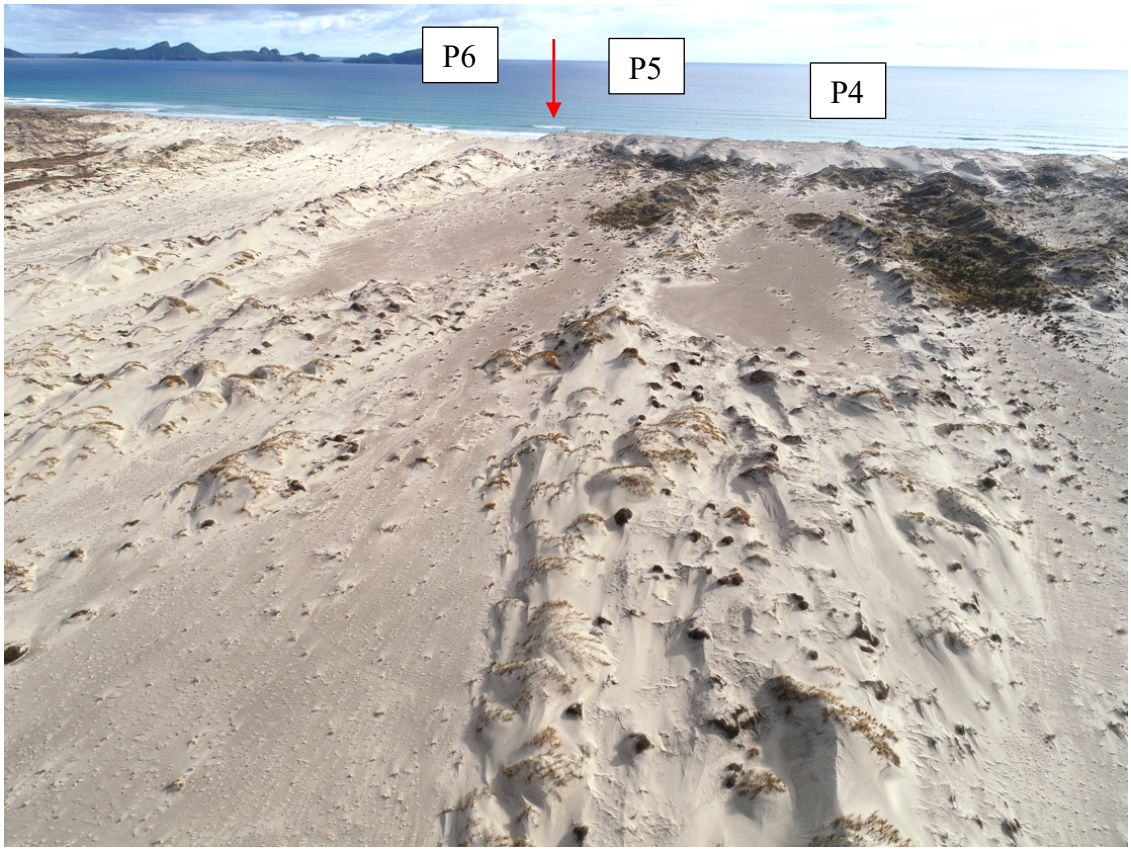

Figure 3.9: Oblique image of P6 (left), P5 (centre) and P4 (right), in Mason Bay, August 2020, oriented towards the west. The difference between the height of the foredune (marked by the arrow) and colour of the deflation surfaces is clear.

3.3.2 Foredune morphology following devegetation

The progressive eradication of *A. arenaria* from the foredune upwind of P6 is evident in ground photos (Fig. 3.10). Following the application of herbicide in 2010, the dense cover of *A. arenaria* was significantly reduced by 2015. *A. arenaria* present in 2015 was either regrowth from the seed bank which had developed in the foredune, or decaying roots. By 2019, blowouts had changed the morphology of the foredune, and the cover of vegetation was minimal, with only a few *A. arenaria* plants remaining. The different treatment histories of the foredune are indicated through the differences in vegetation cover. The vegetation cover on the foredune upwind of P4 and P5 was considerably denser, particularly up to 2015, compared to the foredune upwind of P6, as this section was sprayed 5 years later.

Figure 3.10: Ground photos showing the breakdown of the foredune upwind of P6 in 2012, 2015 and 2019. The photos were taken on the foredune and are oriented towards the north (source: Mike Hilton).

Following the removal of *A. arenaria* from the foredune upwind of P6 in 2010, it has eroded. The profile shows a high proportion of the sand eroded from the stoss face of the foredune (65%) has been deposited directly in the lee of the foredune (Fig. 3.11). The foredune has become lower and wider. The foredune crest has lowered by about 6 m and the lee slope has extended an additional 100 m inland. The rate of change on the foredune has also increased (Fig. 3.12). There was little change between 2010 and 2017. Since 2017, erosion of the stoss face has increased and the change that has occurred each year following 2017 is greater than what occurred between 2010 and 2017. The rate of erosion has also become greater than the rate of accretion in the lee of the foredune. Between August 2017 and August 2018, 149 m^3 of sediment eroded from the stoss face of the foredune profile, compared to 65 m^3 of accretion. This shows that since 2017, more sediment has been transported beyond the lee of the foredune, primarily into the seaward half of the deflation surface and the P6 depositional lobe.

The topographical change in the foredune upwind of P6, is contrasting to the foredune upwind of P5, where there has been little change in the morphology of the foredune since 2012 (Fig. 3.13). The stoss face of the foredune is steep and has not changed. A small amount of sand has been deposited in the lee of the foredune since 2018, however, there has not been a large change in the profile of foredune in comparison to the foredune upwind of P6.

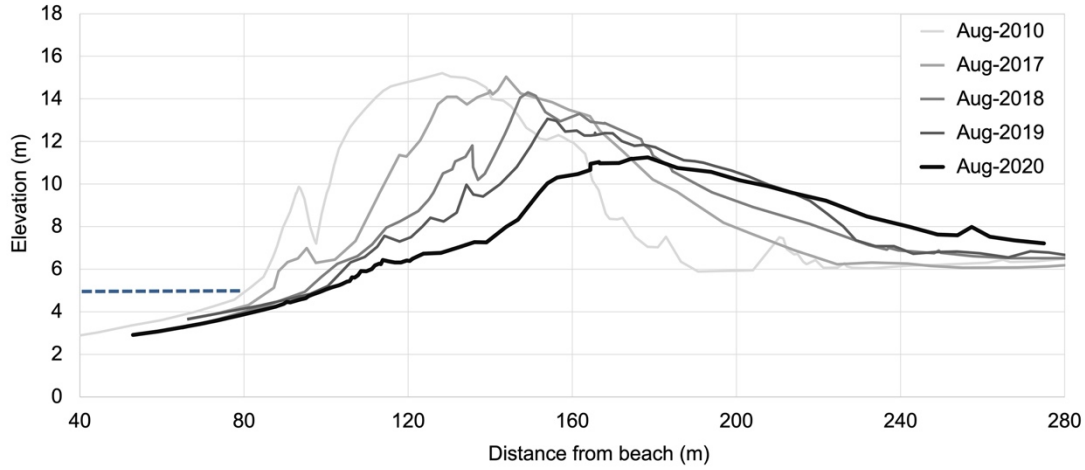

Figure 3.11: Profile showing the decay of the foredune upwind of P6 between 2010 and 2020. Profiles were surveyed in 2010, 2017, 2018, 2019 and 2020. The dotted line represents the high-water mark. The profile is relative to the NZGD2000 datum.

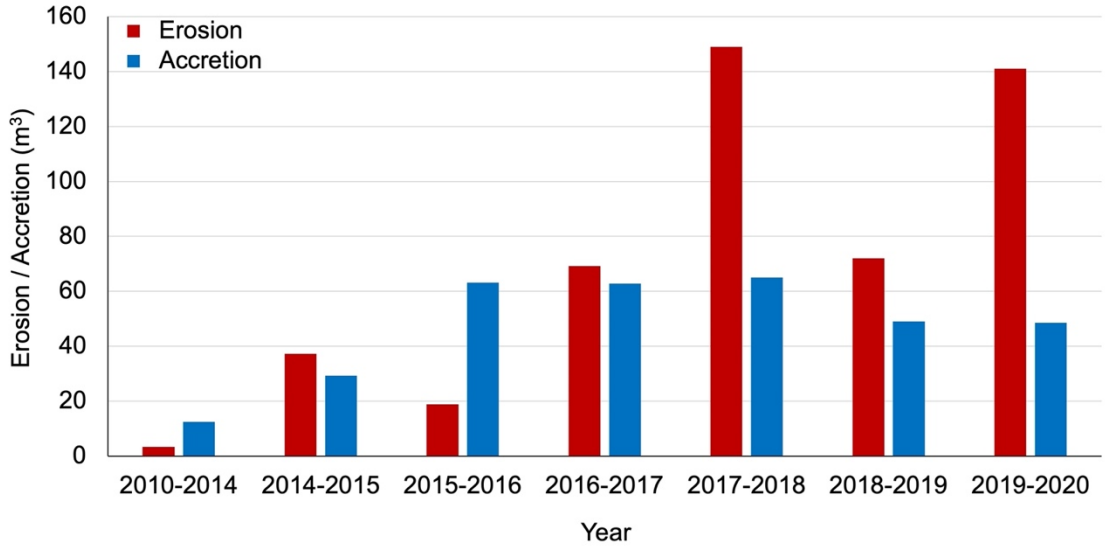

Figure 3.12: Rate of erosion and accretion on the foredune upwind of P6. Erosion was calculated for the sediment eroded on the stoss face of the foredune (m^3) and accretion was calculated for the lee of the foredune (m^3) for every year between 2010 and 2020. Rates were calculated from the profile in Fig. 3.11.

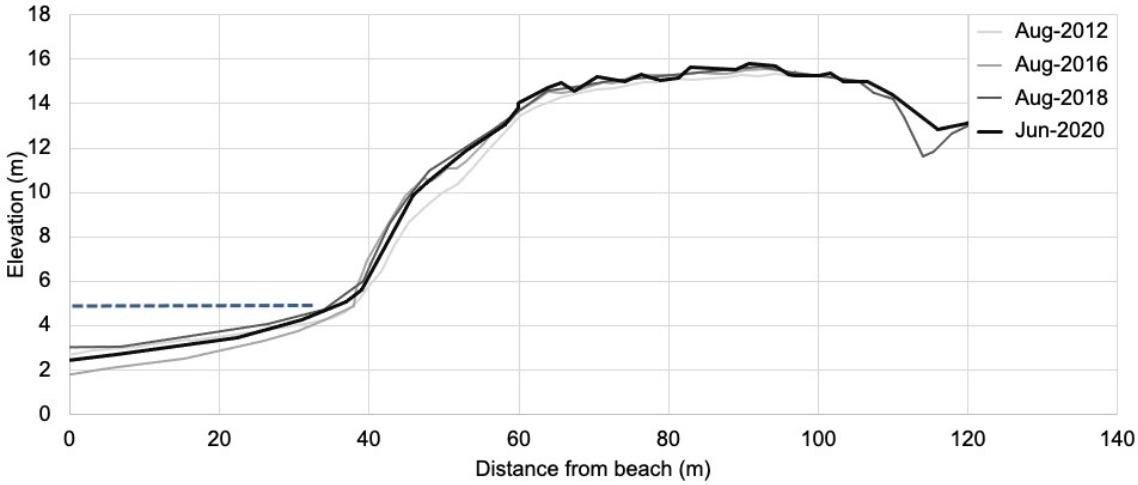

Figure 3.13: Profile of the foredune upwind of P5 between 2012 and 2020. Vegetation was removed in 2015. Profiles were recorded in August 2012, August 2016, August 2018 and June 2020. The profile is relative to the NZGD2000 datum.

3.3.3 Deflation surface morphology following devegetation

In 2007, the P6 deflation surface was dominated by nabkha associated with *A. arenaria* (Fig. 3.14). Following foredune devegetation, nabkha that had formed in the deflation surface, are now primarily associated with the presence of *F. spiralis* and a number of these nabkha have reached over 3 m in height. These have promoted the deposition of sediment in the deflation surface, which has been highest in the lee of the foredune and decreased with distance inland.

Figure 3.14: Ground photos oriented towards the east, looking landward of the P6 foredune in 2007 and 2021. The trailing arms, deflation surface and depositional lobe of P6 are shown in the images (source, top: Mike Hilton; bottom: Campbell McCusker).

3.3.4 Depositional lobe morphology following devegetation

Since 2004, the depositional lobe of P6 has eroded and a high proportion of this sediment has been deposited directly in the lee (Fig. 3.15). The depositional lobe pictured in Fig 3.14 was small and did not extend very far inland, compared to the current depositional lobe. *F. spiralis* has established in the depositional lobe and it has formed a more hummocky, dunal shape (Fig. 3.16). The movement of the depositional lobe inland has coincided with the erosion and widening of the foredune. Sediment eroded from the erosional face of the depositional lobe between 2004 and 2020 (85.6 m^3) is smaller than sediment that has accreted in the lee of the depositional lobe (236 m^3). This shows that a high proportion of sediment transported downwind of the foredune, has been trapped within the depositional lobe.

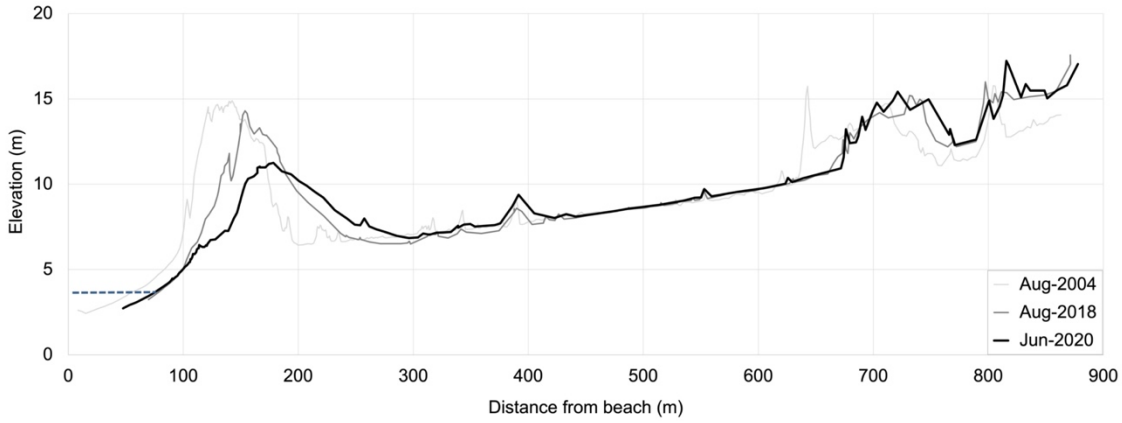

Figure 3.15: Profile showing the topographic development of P6, from the beach to beyond the depositional lobe. Profiles were recorded in August 2004, August 2018 and June 2020. The dotted blue line represents the high-water mark. The profile is relative to the NZGD2000 datum.

Figure 3.16: Oblique image of P6, June 2020. The depositional lobe of P6 dominates the image and the growth of *F. spiralis* has resulted in the development of a hummocky shape.

3.3.5 Morphological change in the landscape following devegetation

The DEMs derived from UAV photogrammetry record the topographic change that has occurred across the parabolic landscape between 2015 and 2020, when the rate of devegetation and erosion accelerated (Fig. 3.17). The foredune is represented clearly by the blue colour on the left of the DEMs. The greatest change has occurred on the foredune upwind of P6. In 2020, there was a clear difference between the foredune upwind of P6 and the foredune upwind of P4 and P5. The foredune upwind of P6 has shifted further inland, whereas the foredune upwind of P4 and P5 is much more uniform in elevation.

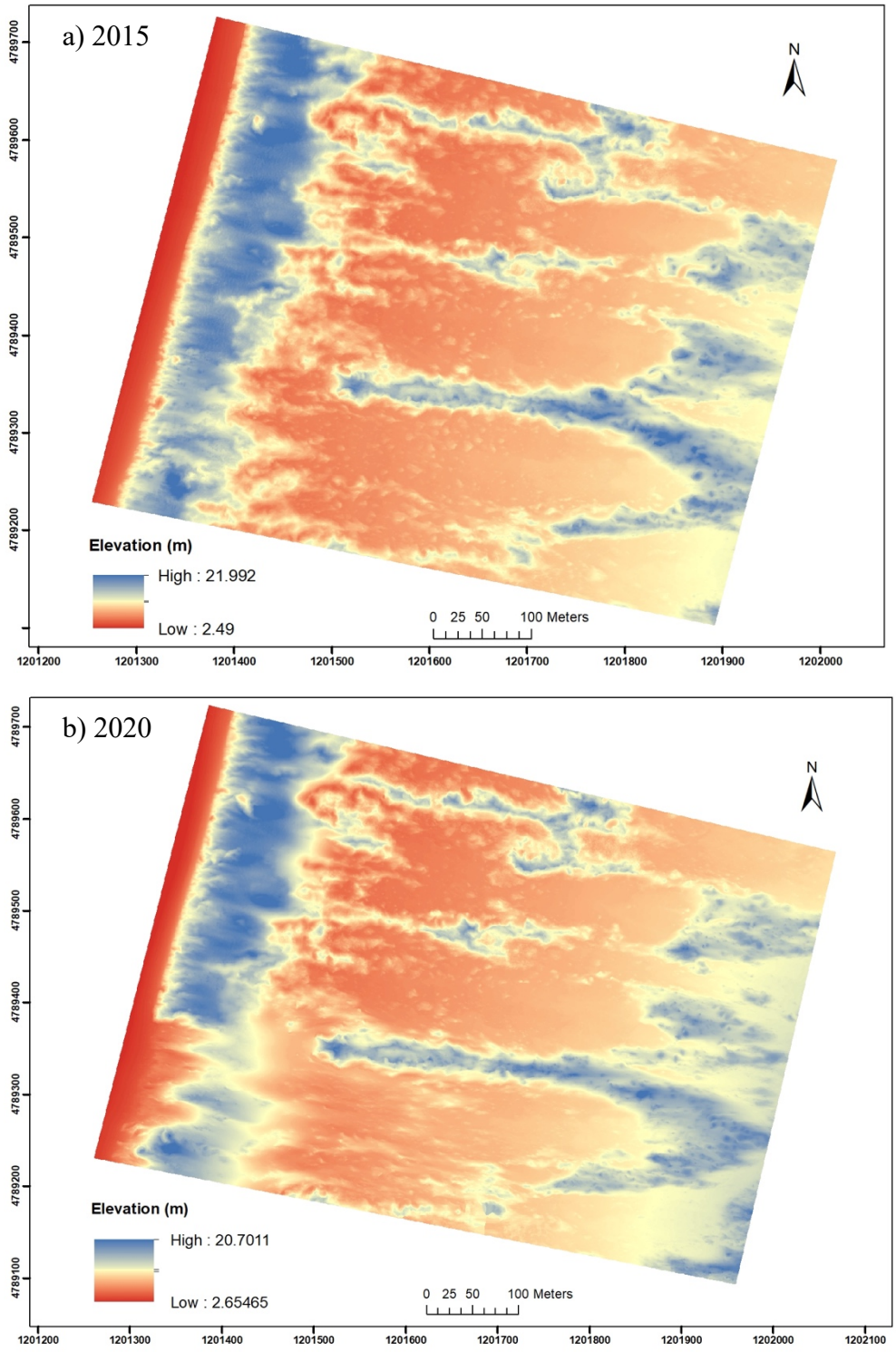

Figure 3.17: Digital elevation model of the study site at Mason Bay in a) November 2015 and b) June 2020. Blue represents high elevation and red represents low elevation. The image includes P4, P5 and P6. The 2020 DEM extends further inland than the 2015 DEM. The greatest change is observed in P6, particularly the adjacent foredune, which has lowered in elevation.

The DEM of the study site provided a more detailed representation of the morphological changes that have occurred at Mason Bay (Fig. 3.18). There has been a large amount of change in the morphology of the dune system since the removal of *A. arenaria.* This is evident in the net elevation change of the study site from 2015 to 2020. P6 stands out as the area where there has clearly been the largest amount of change. The foredune upwind of P6 has lowered in elevation, by up to 10 m in some areas. As was shown in the topographical profile of P6, most of this sediment has been deposited in the lee of the foredune, where the elevation has increased by up to 7 m. In comparison, the foredune upwind of P4 and P5 has had much less change. There has also been a lot of change in the depositional lobes of P4, P5 and P6. The front face of the depositional lobes of all parabolics have eroded, with a lot of this sediment being deposited in the lee, where there has been an increase in elevation.

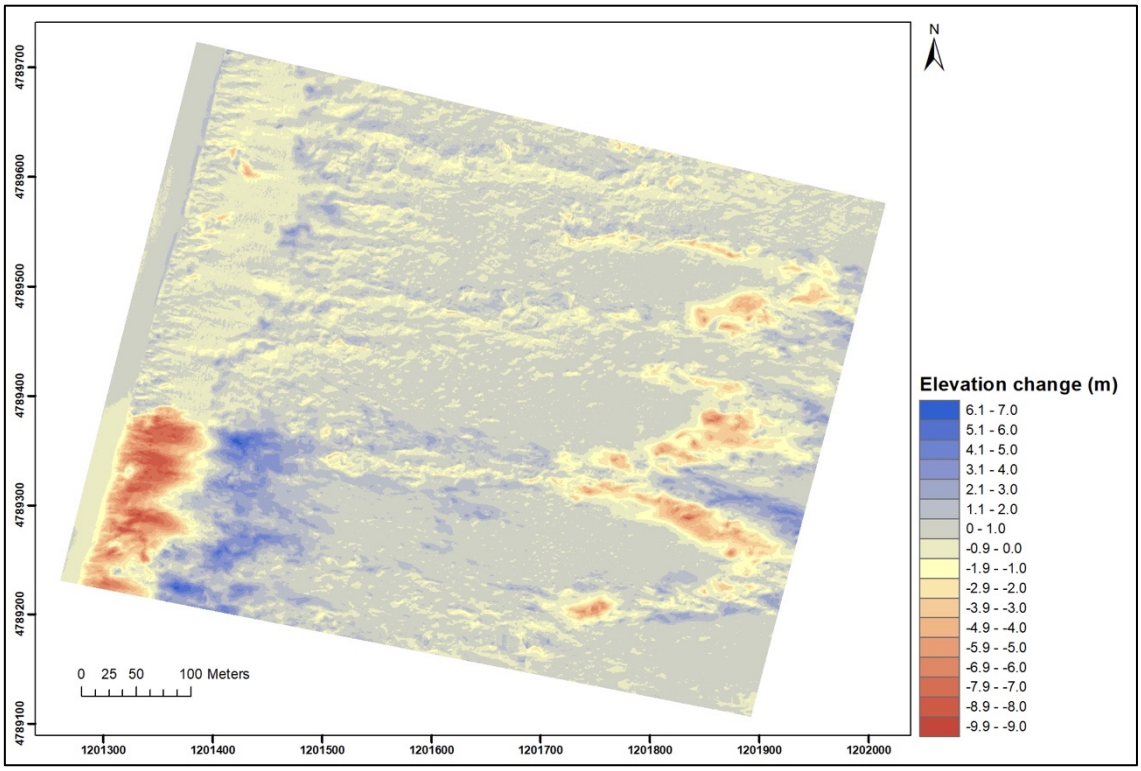

Figure 3.18: Digital elevation model of the study site showing the change in elevation (m) from November 2015 to June 2020. The area includes P4, P5 and P6. Blue represents a gain in elevation while red represents a decrease in elevation. The co-ordinate system is NZGD2000 New Zealand Transverse Mercator.

Change in foredune morphology

There has been a large decrease in elevation of the foredune upwind of P6 between 2015 and 2020 (Fig. 3.19b). There has also been an increase in elevation in the lee of the foredune. The red colour represents the stoss face of the foredune, while the blue represents the lee. These observations are similar to the topographical profiles, showing the foredune is becoming lower and wider, shifting landward. There was a lot of variation in the elevation change over this area, due to the blowouts that have established in the foredune, seen in the orthomosaic (Fig. 3.19a).

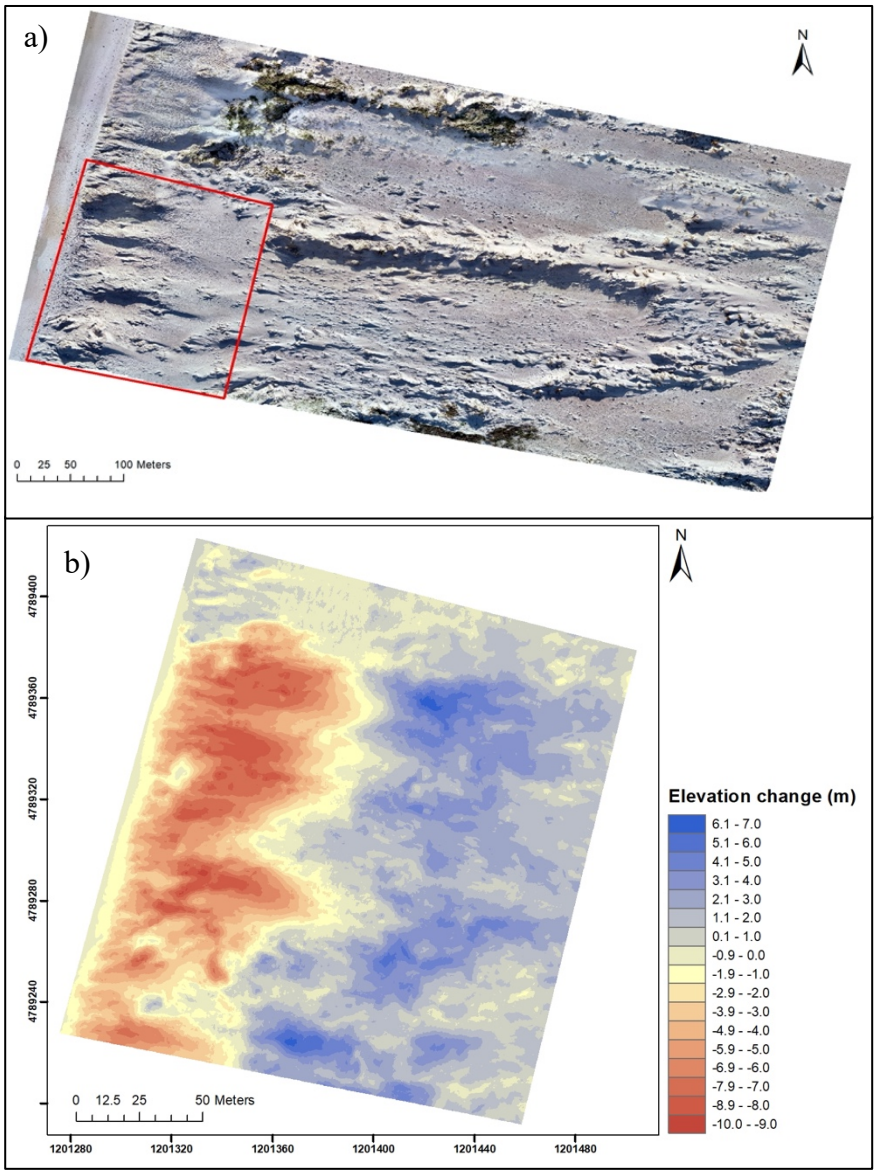

Figure 3.19: a) Location of the foredune upwind of P6 used to calculate the change in elevation and volume b) Digital elevation model of the foredune upwind of P6, showing the change in elevation from 2015 to 2020. Blue represents a gain in elevation while red represents a decrease in elevation.

Sediment volume change

Since 2015, areas of P6 have eroded and accreted. Erosion has primarily occurred in the foredune and depositional lobes while accretion has occurred in the lee of both of these zones (Fig. 3.20). P6 was split into eight sections and the volume change was calculated for each of these (Fig. 3.4).

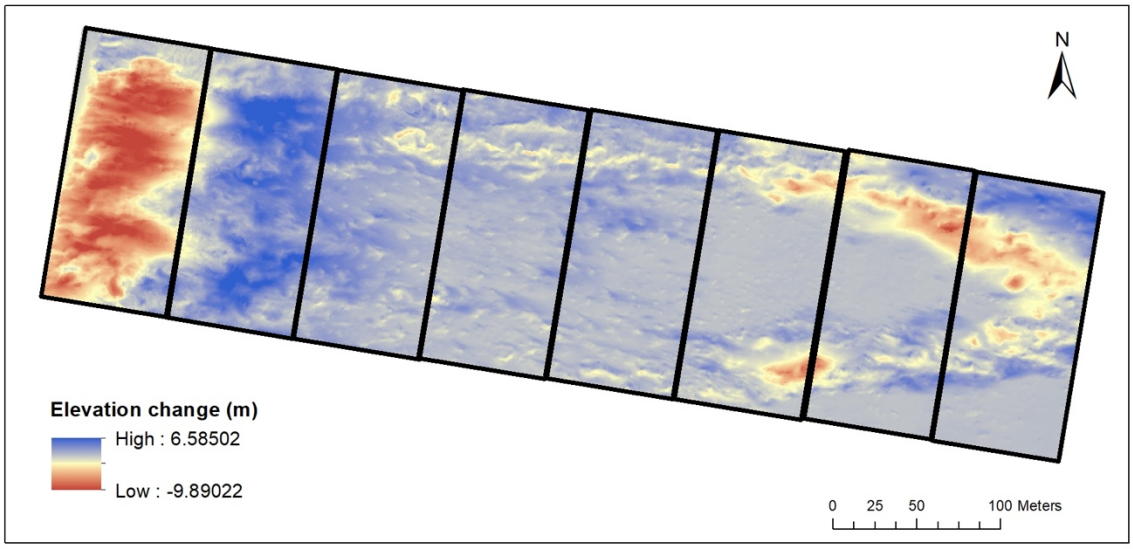

Figure 3.20: Change in elevation of the foredune and P6 between 2015 and 2020. The foredune-parabolic dune complex was split into eight sections to show where accretion and erosion has occurred within the parabolic and the volume change for each of these sections was calculated.

Table 3.1: Volume change calculations from 2015-2020 for the UAV analysis, P4, P5, P6 (Fig. 3.18) (including the adjacent foredune) and the foredune adjacent to P6 (P6 FD) (Fig. 3.19). The accretion, erosion and net volume change for the area was calculated, as well as the volume change per m^2. A negative value represents a loss in volume and a positive value represents a gain in volume (m^3).

Location	Area (m^2)	Accretion (m^3)	Erosion (m^3)	Net volume change (m^3)	Volume change per m^2 (m^3)
P4, P5 and P6	321,077	119,216	-131.074	-11,859	-0.037
P4	90,185	20,026	25,903	-5,877	-0.065
P5	87,206	21,393	24,051	-2,658	-0.030
P6	117,604	69,870	-77,087	-7,217	-0.061
P6 FD	37,492	39,546	-57,975	-18,429	-0.492

Table 3.2: Volume change calculations for sections of P6. Section 1 is the closest to the beach and section 8 is the furthest inland, at the apex of the parabolic dune (Fig. 3.20). Each section is 80 m in length and 160 m in width. The accretion, erosion and net volume change for the area was calculated, as well as the volume change per m^2. A negative value represents a loss in volume and a positive value represents a gain in volume (m^3). Erosion has occurred on the stoss face of the foredune, and depositional lobes and accretion has occurred in the lee of the foredune and deflation surface.

Section	Area (m^2)	Accretion (m^3)	Erosion (m^3)	Net volume change (m^3)	Volume change per m^2 (m^3)
1	12,594	1,075	-49,142	-48,067	-3.817
2	12,594	24,746	-680	24,066	1.911
3	12,594	10,960	-906	10,053	0.798
4	12,594	7,075	-755	6,320	0.502
5	12,594	6,591	-678	5,914	0.470
6	12,594	2,040	-6,206	-4,166	-0.331
7	12,594	4,101	-7,336	-3,236	-0.257
8	12,594	7,706	-7,386	-320	-0.026

Sand has been redistributed within the Mason Bay foredune-parabolic dune complex between 2015 and 2020 (Table 3.1). The total area that was surveyed, including P4, P5 and P6 lost 11,859 m^3. Almost half of this sand, 7,217 m^3, has been lost from P6, with the majority of this being eroded from the foredune, 18,429 m^3.

The stoss face of the foredune, section 1 and the depositional lobes, section 6, 7 and 8 have eroded (Table 3.2). A large proportion of this sand had been deposited in the lee of the foredune (section 2), where 24,746 m^3 of accretion has occurred, as well as in the seaward (western) half of the deflation surface, closest to the foredune (sections 3, 4, 5). Section 8 had the smallest net volume change. This is because sediment has eroded from the erosional face of the depositional lobe but has also been deposited in the lee. The profile data in Fig 3.15 shows that if the DEM extended further inland, accretion would be observed in the lee of the depositional lobe, where a lot of sand has been trapped by *F. spiralis* present here (Fig. 3.16). Therefore, the overall net volume change for all

parabolics would show less erosion has occurred, as the depositional lobes have accreted in the lee, beyond the 2015 survey area.

3.3.6 Sedimentation in the deflation surfaces

In conjunction with the results in Section 3.3.5, soil pits dug in the deflation surface show there is a clear difference in the level of deposition of sand in the deflation surfaces of P4, P5 and P6 (Fig. 3.21). Relatively high levels of deposition have occurred in P6. As the foredune has shifted eastwards, there has been between 1-6 m of deposition in the seaward half of the deflation surface (Figs. 3.18 and 3.21c). Deposition in P5 has been concentrated in the lee of the foredune, where there has been up to 70 cm of deposition. The lowest levels have occurred in P4, where the highest level of accretion recorded was 22 cm. The deposition in P4 has been concentrated near the apex of the parabolic (Fig. 3.21a). Contrarily, in P5 and P6, deposition has primarily occurred directly behind the foredune. In P5, the highest rates of accretion are concentrated here, as well as closer to the trailing arms of the parabolic dune which, as shown in Fig 3.18, are eroding. This is because sediment that is released from the foredune upwind of P6 is being transported around the P5/P6 trailing arm, into the P5 deflation surface.

There was a clear difference in accretion between the parabolic dunes (Fig. 3.22). Most of the deflation surface in P4 and P5 have had less than 30 cm of accretion, whereas more accretion has occurred in P6. All three parabolics showed small levels of accretion near the apex of the deflation surface.

Maximum accretion in the P6 deflation surface occurred close to the foredune (Fig. 3.23). The greatest rates of accretion in the deflation surface are associated with the presence of nabkha. These nabkha established because of *A. arenaria* that was either not sprayed or survived spraying. In more recent years, these have transformed to nabkha associated with *F. spiralis*. The presence of these shadow dunes has promoted the deposition of sand in the deflation surface and a number of these have grown in size as a result. These results are similar to what was found in the topographical profiles displayed in Section 3.3.4.

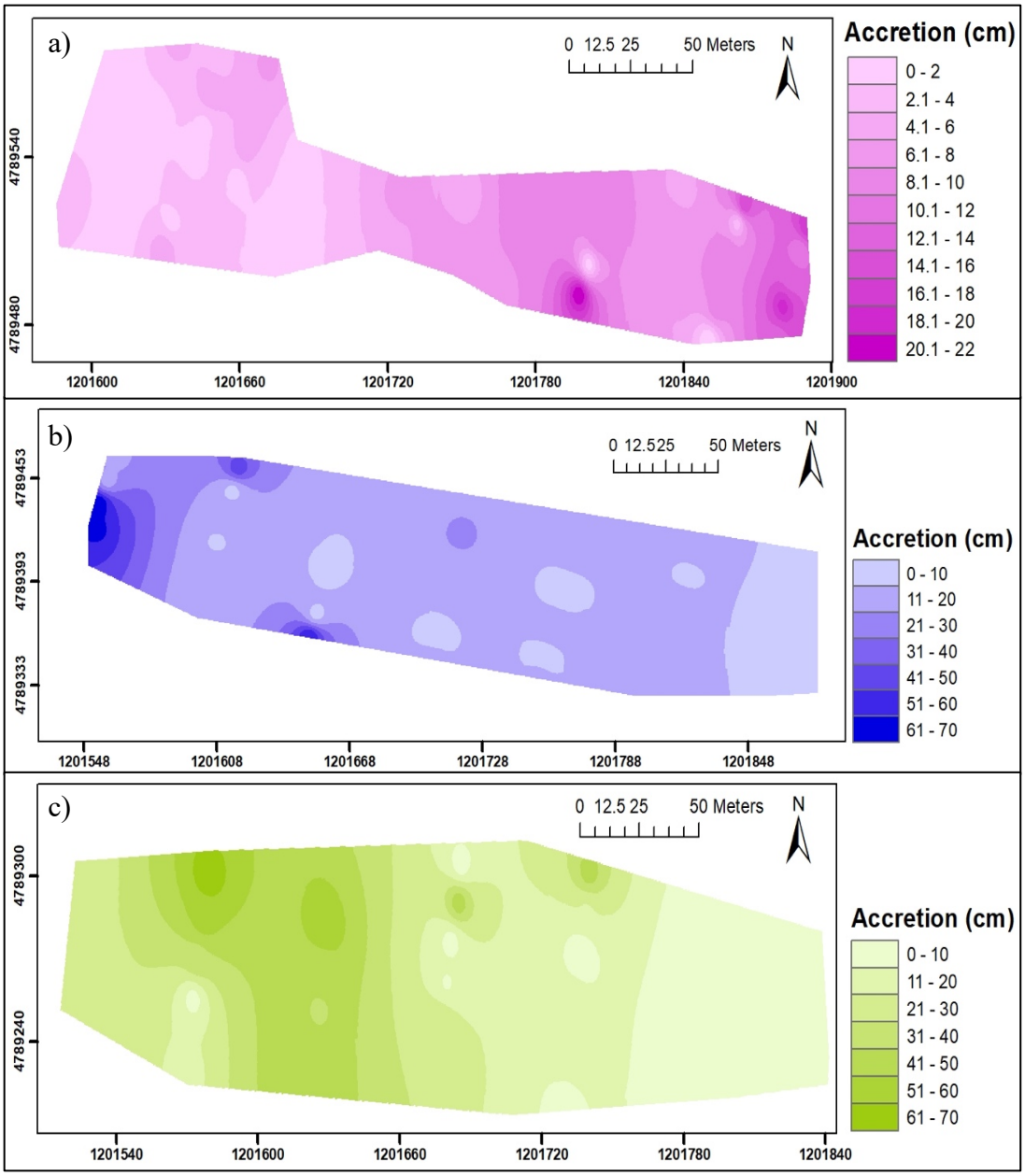

Figure 3.21: Choropleth map showing accretion (cm) of sand measured in the soil pits dug in a) P4, b) P5 and c) P6 in June 2020. Note the difference in scales for the three maps.

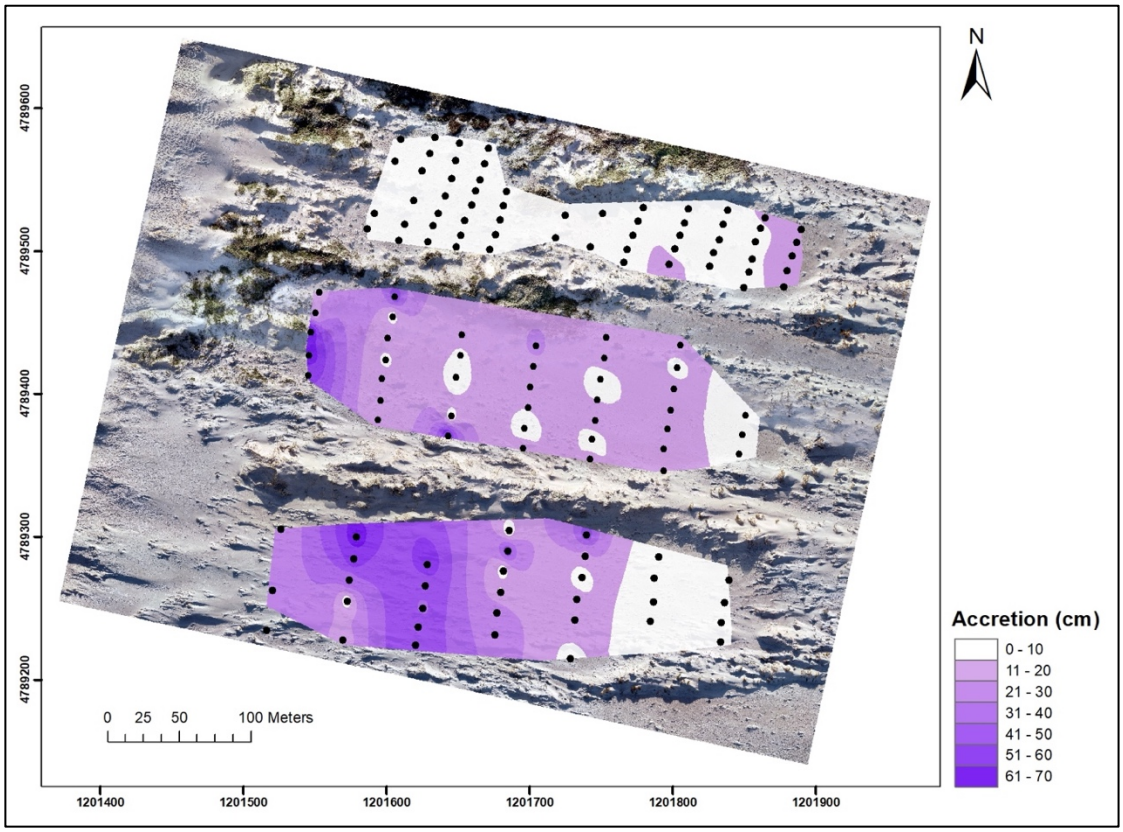

Figure 3.22: Choropleth map showing accretion (cm) of sand measured in the soil pits dug in P4, P5 and P6 in June 2020. The black dots identify the location of the soil pits.

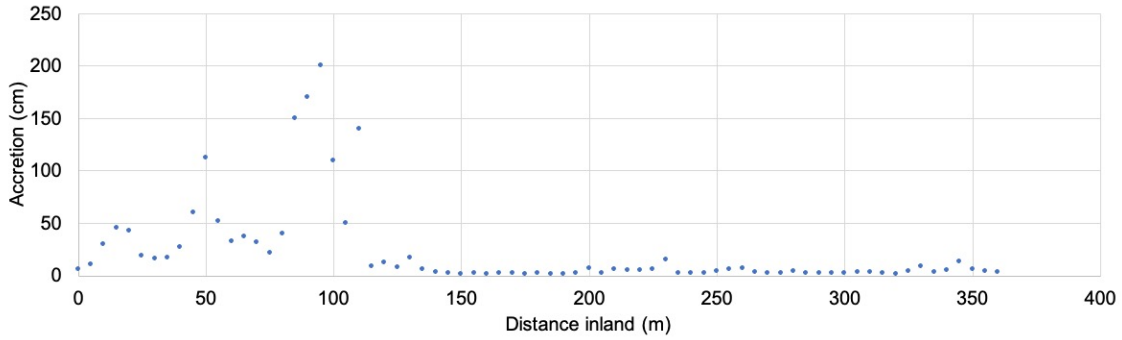

Figure 3.23: Scatterplot along the historic P6 profile line (Fig. 3.1) showing accretion in the deflation surface of P6. Soil pits were dug in August 2019 in the deflation surface. The depth of burial from the surface to the former deflation surface was measured. A pit was dug every 5 m along the transect. The highest accretion levels were associated with the presence of nabkha.

3.4 Discussion

The introduction of *A. arenaria* at Mason Bay led to the development of a stable, Type 1 foredune, 11-12 m high, extending 150 m inland from the spring high tide line (Hart *et al.*, 2012). This had a major effect on aeolian processes and dune dynamics, described by Petersen *et al.* (2011), where they found only 2% of sand blown from the beach was transported beyond the foredune. Aeolian sediment transport patterns have changed following the removal of *A. arenaria*, influencing the morphology of the landscape. Parts of the Mason Bay dune system have eroded, while others have accreted following re-activation. The largest change has been observed in P6 and the upwind foredune, where *A. arenaria* was first removed in 2010. The foredune is breaking down, resulting in the transport of sand into the hinterland. This is influencing sedimentation patterns and the morphology of the deflation surface and depositional lobe of the parabolic.

The morphology of the foredune upwind of P6 has changed following the eradication of *A. arenaria*. It has progressively become lower and wider, resulting in the transport and deposition of more sand inland. The initial breakdown of the foredune was slow, with little change observed between 2010 and 2017 (Fig. 3.11). This was a result of remnant *A. arenaria* roots, which prevented sand from being released. Decaying plant matter, the regrowth of roots and buried seeds prolong erosion following devegetation, resulting in a lag response (Pickart, 2013; Arens *et al.*, 2013b; Hilton *et al.*, 2019). By 2017, most of the vegetation on the foredune had been removed. This resulted in an increase in the rate of stoss face erosion, leading to rapid change in the morphology of the foredune.

About half of the sediment eroded from the foredune upwind of P6 has been deposited in the lee of the foredune and into the seaward half of the former P6 deflation surface (Fig. 3.20). Topography impacts airflow, including reducing wind speeds and causing separation of flow. This pattern of deposition is explained by the 'lee-eddy effect' (Walker and Hesp, 2013). As air flows over the foredune crest, a separation cell develops in the immediate lee of the foredune. This results in the formation of an eddy, reversing flow back to the foredune, resulting in the deposition of sediment here (Fig. 3.24). At Mason Bay there was an average increase of 1.911 m^3 of sand per square metre in the lee of the foredune, the largest rate of accretion in any section of P6 (Section 2 in Fig. 3.20).

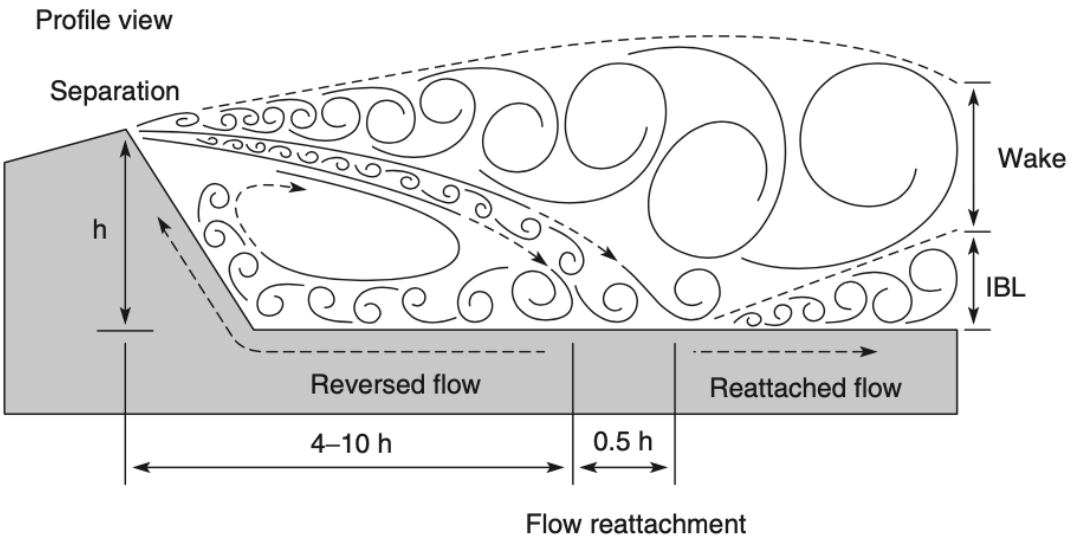

Figure 3.24: Conceptual model of airflow over a transverse dune. As air flows over the crest of the foredune, separation occurs on the lee side, leading to the formation of eddies (from Walker and Hesp, 2013).

The removal of *A. arenaria* from the foredune occurred progressively due to a number of factors and this has also likely contributed to the deposition of sediment in the lee of the foredune. These factors include, sections of *A. arenaria* on the foredune survived the initial spray, regrowth occurred as a result of inconsistencies with the application of herbicide and decaying roots were present on the foredune for years following the initial spray. The continued presence of *A. arenaria* resulted in an increase in surface roughness, leading to a reduction in wind speed flowing over the foredune and subsequently, deposition of sediment in the lee of the foredune.

Foredune erosion has also been observed following devegetation and remobilisation of foredunes in Canada and the Netherlands (Darke *et al.*, 2016; Arens *et al.*, 2013b; Ruessink *et al.*, 2018). Following foredune devegetation in Canada, erosion occurred rapidly, enhancing aeolian sediment transport and the foredune transformed into a lower, more hummocky shape (Darke *et al.*, 2016). In the Netherlands, Ruessink *et al.* (2018) described the development of depositional lobes downwind, following the construction of notches in a foredune by the mechanical removal of vegetation. The lobes that formed were between 3-8 m in depth and grew up to 125 m in length.

The most notable change in the deflation surfaces is in P6, where the adjacent foredune was sprayed the earliest. Deposition in the P6 deflation surface was most concentrated in the seaward half and decreased with distance inland. This could be because the influence of the foredune on airflow is reduced with distance inland, as the deflation surface slopes upwards. Therefore, the deflation surface closer to the apex of the parabolic is more exposed to stronger winds, leading to the transport of sediment right through the parabolic. An increase in wind speed with distance along the deflation surface axis has been observed in other locations (Smyth *et al.*, 2020). Areas in the deflation surface where the greatest levels of accretion have occurred are associated with nabkha, which are efficient at trapping sand (Hesp and Martinez, 2007). A number of the large nabkha present in the deflation surface were existent in the pre-restoration landscape, as they formed with *A. arenaria.* Sections of *A. arenaria* present in the deflation surfaces were either not sprayed or survived spray and a number of nabkha remained. These nabkha are now primarily associated with *F. spiralis*, which re-colonised the dunes following the removal of *A. arenaria* and have continued to promote the deposition of sediment.

The P6 depositional lobe is returning to a more dynamic state. In 1958, before *A. arenaria* had established a dense population at Mason Bay, the depositional lobe had not completely formed and was low-lying, with a sparse cover of vegetation (Hart *et al.*, 2012). The depositional lobe grew alongside the invasion of *A. arenaria* and became a more stable feature that accreted vertically (Hart *et al.*, 2012). In active dune systems, depositional lobes naturally migrate along the prevailing wind direction (Duran *et al.*, 2008; Hesp and Martinez, 2007). Wind causes the front face to erode and sediment is transported to the lee slope (Hesp and Walker, 2013). The morphological development and migration of parabolic dunes are primarily controlled by sand supply and the presence of vegetation (Hugenholtz, 2010). The lack of a consistent supply of sediment causes vegetation to colonize the head of the depositional lobe, resulting in stabilization, as occurred at Mason Bay following the invasion of *A. arenaria* (Hugenholtz, 2010; Hart *et al.*, 2012).

Following the removal of *A. arenaria* from the dune system and the subsequent increase in sand flux downwind of the foredune, the depositional lobe has moved landward, similar to what occurred on the foredune. The shape of the depositional lobe has transitioned from a vegetated and stabilized V-shape, to a more dynamic and sparsely

vegetated, U-shape. The topographical profile between 2004 and 2020 showed the rate of accretion on the lee slope of the depositional lobe (236 m^3), was higher than the rate of erosion on the erosional face (85.6 m^3). This shows there has been a net gain in accretion in the depositional lobe as sediment eroded from the foredune has been trapped within the *F. spiralis* in the depositional lobe. The topographical profiles showed the combined sediment eroded from the stoss face of the foredune and erosional face of the depositional lobe (576.2 m^3) was slightly greater than the sediment that has accreted in the lee of the foredune and depositional lobe (566.3 m^3). This indicates that less than 2% of the sediment eroded from the foredune and depositional lobes has been transported further inland, beyond the parabolic dune. This shows that a high proportion of the sediment eroded from the foredune and depositional lobe has been retained within the foredune-parabolic dune complex.

The landward extension of the depositional lobe can be attributed to the growth of *F. spiralis* alongside the increased rate of sand flux. Although *F. spiralis* was not replanted here, an extensive seed bank may have been retained within the depositional lobe, which has subsequently been exposed following the erosion of the front face. Seed has also likely been transported inland from *F. spiralis* present in the deflation surface. There is now an abundance of *F. spiralis* on the depositional lobes, forming a number of nabkha (Fig. 3.16). The presence of *F. spiralis*, in addition to the lee eddy effect, is resulting in a high rate of deposition of sand here. This process is most pronounced in P6, however, has also occurred in P4 and P5. This is because the depositional lobes of all parabolics were sprayed at the same time, in 2006. Following the mechanical removal of vegetation from a foredune in Canada, Darke *et al.* (2016) also found there was a growth and landward migration of the depositional lobe due to the increase in aeolian sediment supply.

There has been a change in the morphology of the foredune-parabolic dune complex at Mason Bay as a result of the redistribution of sediment within the system. However, due to the fact this is not a closed system, the erosion and deposition of sediment has not been equal. Sediment is not only entering the system from the beach and eroding foredune but is also entering the parabolic dunes from the east, during offshore winds. Therefore, the devegetated foredune is not the only source of sediment for the dune system, adding an

additional complexity to understanding the redistribution of sediment within the dune system.

3.5 Conclusion

This chapter has examined the change in the foredune and parabolic dune morphology following deliberate devegetation at Mason Bay. A range of methods have been utilised to document the subsequent morphological changes to understand the processes that occur following foredune devegetation.

Foredune erosion following devegetation at Mason Bay was not rapid. There was little change in foredune morphology for five years following the initial spray application. However, following the decay of remnant *A. arenaria* roots, since 2017, the rate of change has been rapid, resulting in a lower and wider foredune. The stratigraphic analysis of soil pits in the deflation surface revealed the largest amount of deposition has occurred in P6 and there has been a reduction in the rate of deposition with distance inland. The depositional lobes of the parabolics are returning to an active state of landward migration.

The response to foredune devegetation at Mason Bay was similar to that which occurred at Doughboy Bay, where there was a delay in the erosion of the foredune following *A. arenaria* necrosis. Maximum sand mobility occurred 4-8 years following the initial application of herbicide at Doughboy Bay (Konlechner *et al.*, 2014). The destabilisation of the foredune at Mason Bay has changed the morphology of the dune system and the dune system is transitioning towards a more active state. This impacts aeolian sediment transport processes and the downwind plant communities.

Chapter 4

Rates and processes of aeolian sediment transport at Mason Bay

4.1 Introduction

Coastal dune systems are characterized by the frequent movement of sand (Willis, 1989). The transport of sediment from the beach to the dune system, via aeolian processes, is the primary input of sediment into the dune system (Nickling and Davidson-Arnott, 1990). Prior to the devegetation of the foredune at Mason Bay, commencing in 2010, virtually all sand was trapped in the foredune (Petersen *et al.*, 2011). Chapter 3 established that removing the dense cover of *A. arenaria* from the foredune has promoted the release and inland transport of sediment from the foredune. About half of the sand eroded from the foredune has been deposited in the former P6 deflation surface, predominantly in the seaward (western) half.

Understanding aeolian sediment transport is important for understanding dune dynamics (Andreotti *et al.*, 2010). This chapter aims to quantify the rates and patterns of sedimentation in the parabolic dunes at Mason Bay. In particular, to compare the rate of sediment transport downwind of vegetated (P5) and devegetated (P6) sections of the foredune and to determine the source of transported sediment through a devegetated parabolic dune. The wind regime is one of the primary controls of aeolian sediment transport and dune type in coastal dunes (Lancaster, 2009). This includes wind direction, which is key in determining where sediment is transported to and wind speed, which determines the rate of sediment transport (Bauer *et al.*, 2012). It is known that wind events play an integral role in the transport of sediment in coastal dunes (Delgado-

Fernandez and Davidson-Arnott, 2011). This chapter also aims to identify the relative importance of winds of different strength and direction at Mason Bay.

Topography impacts airflow over the foredune. This includes influencing wind speed, wind direction and subsequently, the erosion and deposition of sediment. As air flows up the stoss face of the foredune, acceleration occurs as streamlines are compressed due to the formation of a negative pressure gradient (Lancaster 2009; Walker and Hesp, 2013). Wind velocity then decreases as it flows over the lee of the foredune crest, as a result of flow expansion and separation. These patterns of airflow influence erosion and deposition. Due to flow acceleration on the stoss slope, there is an exponential increase in sediment transport towards the foredune crest, leading to increased erosion of the stoss slope. As wind speeds reduce in the lee of the foredune, deposition is increased here (Lancaster, 2009).

There is large spatial and temporal variation in aeolian sediment transport (Barchyn *et al.*, 2014). Sediment transport can vary spatially due to wind gusts, variation in direction and topographical variability (Bauer and Davidson-Arnott, 2014). Smyth *et al.* (2014) found that sediment flux rates on a deflation basin within a blowout varied in traps that were spaced less than 0.5 m apart. There is also an exponential decrease in sediment transport with height above the surface (Bagnold, 1941; Ni *et al.*, 2002). Temporal variability of aeolian sediment transport can range from seconds to years (Alcántara-Carrió and Alonso, 2002). At the micro-scale (seconds-minutes), strong wind gusts result in an increase in sediment transport and turbulence in airflow, resulting in high temporal variability (Bauer and Davidson-Arnott, 2014). Furthermore, wind events (meso-scale, hour-day) have a significant role in the transport of sediment and dune development (Delgado-Fernandez and Davidson-Arnott, 2011; Poortinga *et al.*, 2015). Consequently, it is difficult to model and predict sediment transport in coastal environments.

Empirical data on aeolian sediment transport is difficult to obtain, therefore, data on airflow and sediment transport through parabolic dunes is limited (Delgado-Fernandez *et al.*, 2018). Connecting microscale processes, such as wind speed, to mesoscale landforms, such as sand dunes, is challenging due to the spatial variation in topography and vegetation (Nordstrom *et al.*, 2007). Mason Bay is situated on the west coast of Rakiura/Stewart Island, a high energy coast, that is frequently exposed to strong winds, and thus, has a high potential for aeolian sediment transport. The predominant wind

direction at Mason Bay is onshore, from the west, however, there is also a strong north-easterly component. The dynamic dune restoration project at Mason Bay provides an exceptional opportunity to understand the implications of foredune devegetation on sedimentation processes. The difference in treatment histories of the foredune adjacent to P5 and P6 offers a rare comparison of the sedimentation patterns downwind of a devegetated and vegetated foredune. Understanding the transport of sediment within the dune system is important for understanding how the landscape functions and predicting how it might evolve in the future. Unvegetated areas on sand dunes provide a source for the entrainment and transport of sediment (Jackson and Nordstrom, 2013). Therefore, it is expected that following foredune devegetation, sediment transport will increase.

This chapter outlines the results of an empirical study of rates and patterns of sedimentation downwind of a foredune at Mason Bay. Two aeolian sediment transport experiments completed at Mason Bay in 2019 and 2020 are described. The results of these experiments are then analysed to understand the processes of aeolian sediment transport in the Mason Bay dune system. This includes determining the influence of foredune devegetation on sedimentation and identifying the source of transported sediment.

4.2 Methods

Dynamic dune restoration at Mason Bay has resulted in the progressive erosion of the foredune and redistribution of sediment inland (Chapter 3). The vegetation cover on the foredune upwind of P6 has been removed and the foredune is lower and wider. In contrast, the foredune upwind of P5 was sprayed with herbicide five years after the foredune upwind of P6. Therefore, the foredune upwind of P5 is similar to its pre-restoration morphology and retains some *A. arenaria* cover. This provides an ideal comparison of the influence of foredune devegetation on downwind sediment transport.

Two sediment transport experiments were completed during strong onshore wind events (15-20 ms^{-1}). The first experiment compared sediment transport rates downwind of a vegetated (P5) and devegetated (P6) foredune and the second experiment focussed on sediment transport through a devegetated parabolic dune (P6). During these experiments, transported sediment was collected concurrently with data on wind speed and direction. Self-orienting, swinging sand traps, described in Hilton *et al.* (2017) were used to collect transported sediment during the experiments. The sand traps were attached to a fibre glass pole at 0.05 m, 0.18 m and 0.68 m above the surface. These heights were selected due to the anticipated exponential decrease in sediment transport with height above the surface (Bagnold, 1941; Ni *et al.*, 2002).

4.2.1 Experiment one

Experiment one was completed in August 2019. The aim of this experiment was to compare sediment transport in the centre of the P5 and P6 deflation surfaces, downwind of a section of a vegetated and devegetated foredune at Mason Bay. Chapter 3 established the foredune adjacent to P6 has lowered and widened following devegetation. In contrast, the foredune adjacent to P5 is higher and has a greater cover of vegetation. It is expected that these differences in morphology and vegetation will influence the rates of downwind aeolian sediment transport.

Data on wind speed and direction were collected simultaneously with the sand trap experiments to relate the rates of aeolian sediment transport to wind conditions. A 2 m mast was deployed in the centre of the P5 and P6 deflation surfaces at an equal distance

from the foredune (Fig. 4.1). Four Gill 2D windsonic anemometers were attached to the masts at 0.05 m, 0.18 m, 0.68 m and 2 m above the surface. (Fig. 4.2). They were logarithmically spaced at the same heights as the three sand traps. The anemometers were aligned to magnetic north. A 5 m mast was deployed on the highest section of the foredune crest, upwind of P5, with a Lufft anemometer attached to the top of the mast to indicate the incident wind speed and direction. The anemometers were connected to a Campbell data logger and recorded at 1-second intervals in the deflation surface and 8-second intervals on the foredune.

Rates of sand flux were estimated on eight occasions over three days. Two fibre glass poles were deployed at each site during each run, with three sand traps attached at 0.05 m, 0.18 m and 0.68 m above the surface (Fig. 4.3). Each run was typically 10 minutes in length, however, varied depending on the time it took for the sand traps to almost fill. The runs were repeated at least two times for each day they were completed to account for variation between experiments.

Six runs were completed comparing sediment transport in the centre of the deflation surfaces in P5 and P6 (Fig. 4.1). These runs were completed under W-NW winds, with wind speeds recorded on the foredune crest ranging between 15-20 ms^{-1}. The sand traps were deployed in P5 and P6 simultaneously and placed on each side of the anemometer masts so the rates of sand flux could be directly compared with the wind speed and wind direction recorded (Fig. 4.2). Two runs were also completed on the foredune crest to compare sediment transport over the foredune upwind of P5 and P6. This provided an additional comparison to determine whether the differences in sediment transport observed in the deflation surfaces were similar to on the foredune. Two sand traps were deployed on the foredune upwind of P5 and two deployed on the foredune upwind of P6.

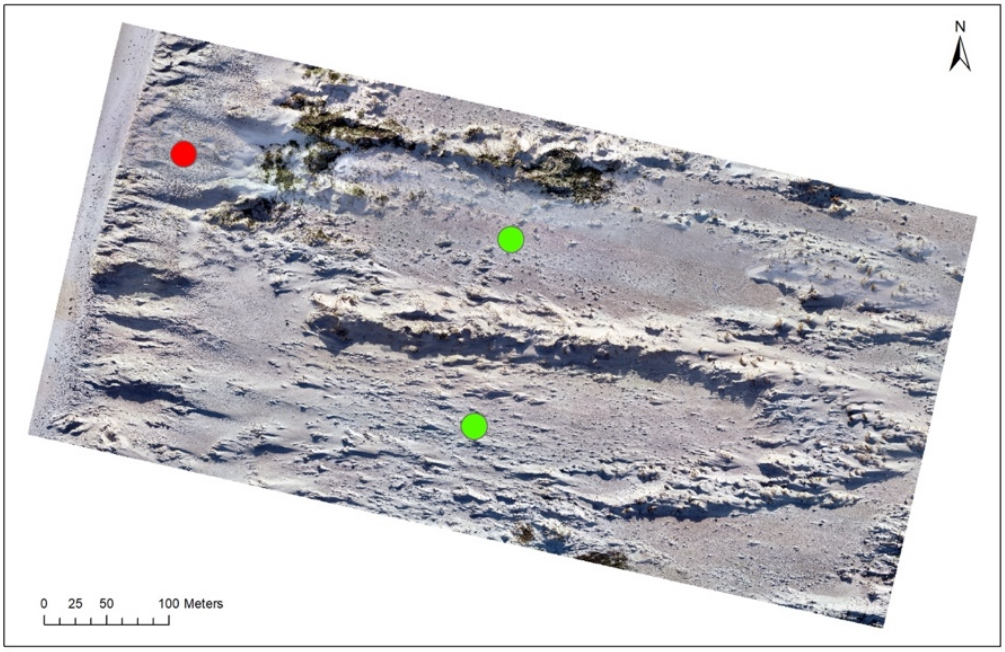

Figure 4.1: The green dots represent the location of the anemometers deployed in the P5 and P6 deflation surface in August 2019. The red dot shows the location of the anemometer deployed on the foredune to indicate the incident wind speed and direction. The sand traps comparing sediment transport in the deflation surfaces were also deployed by the green dots.

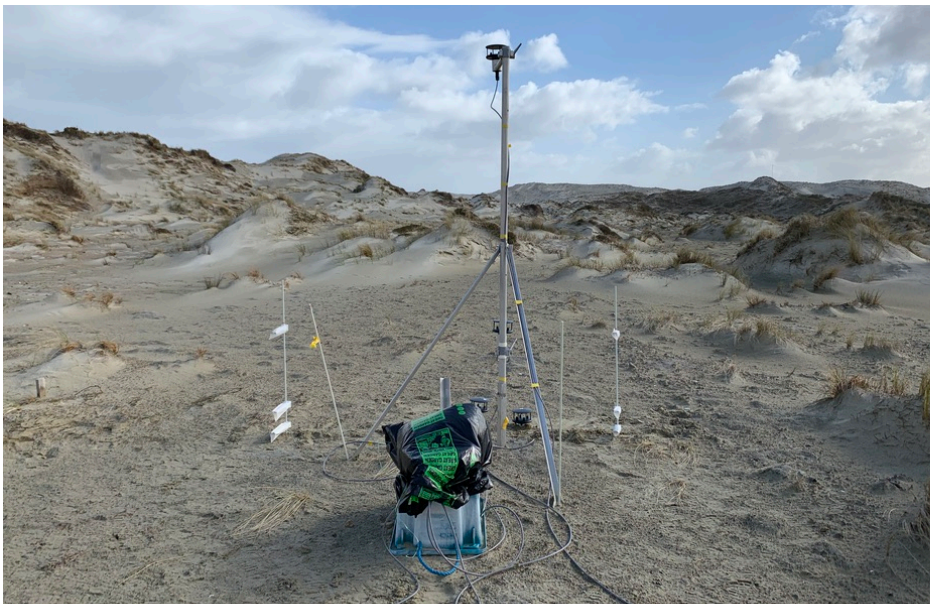

Figure 4.2: The anemometer deployed in the deflation surface in P5 in August 2019. Four anemometers were attached to the 2 m mast at 0.05 m; 0.18 m; 0.68 m and 2 m. The sand traps were deployed on both sides of the anemometer mast. The anemometers and sand traps were set up in the same arrangement in the P6 deflation surface.

Figure 4.3: The array of swinging sand traps deployed during sediment transport experiments. A sand trap was placed at 0.05 m, 0.18 m and 0.68 m. The sediment trapped at each height was used to calculate the sediment flux.

4.2.2 Experiment two

The second sediment transport experiment was completed in August 2020. The purpose of this experiment was to understand how sediment moves through P6 to determine the source of transported sediment. This involved establishing whether the main input of sediment into the wider dune system was from the beach or the devegetated foredune. A 5 m mast was deployed on the foredune upwind of P5, with a 2D windsonic anemometer attached to the top to indicate the incident wind speed and direction, recording at 1-second intervals.

Four locations between the beach and the apex of P6 were selected to deploy sand traps. The sampling locations were selected to represent the key features in the landscape to understand the change in aeolian sediment transport through the parabolic dune. These were at the rear of the beach, above the high tide mark, at the foredune toe; the crest of the foredune upwind of P6; the P6 deflation surface; and the P6 depositional lobe (Fig. 4.4). Four runs were completed on the same day (29/08/2020) during W-NW winds that averaged 20 ms^{-1}. The sand traps were deployed at the same height as experiment one. Three fibre glass poles, each with three sand traps, were deployed at each location, to

account for the spatial variation in sediment transport. They were separated by 10 m, covering a total width of 20 m (Fig. 4.5). The sand traps were deployed at each location simultaneously and collected the same way they were deployed; thus, all traps collected sand for an equal period of time. The experiments lasted between 5 and 10 minutes. The length of the experiments was limited by the time it took for the sand traps to almost fill. Data was not collected on the beach during run 4 because of limitations in the number of sand traps.

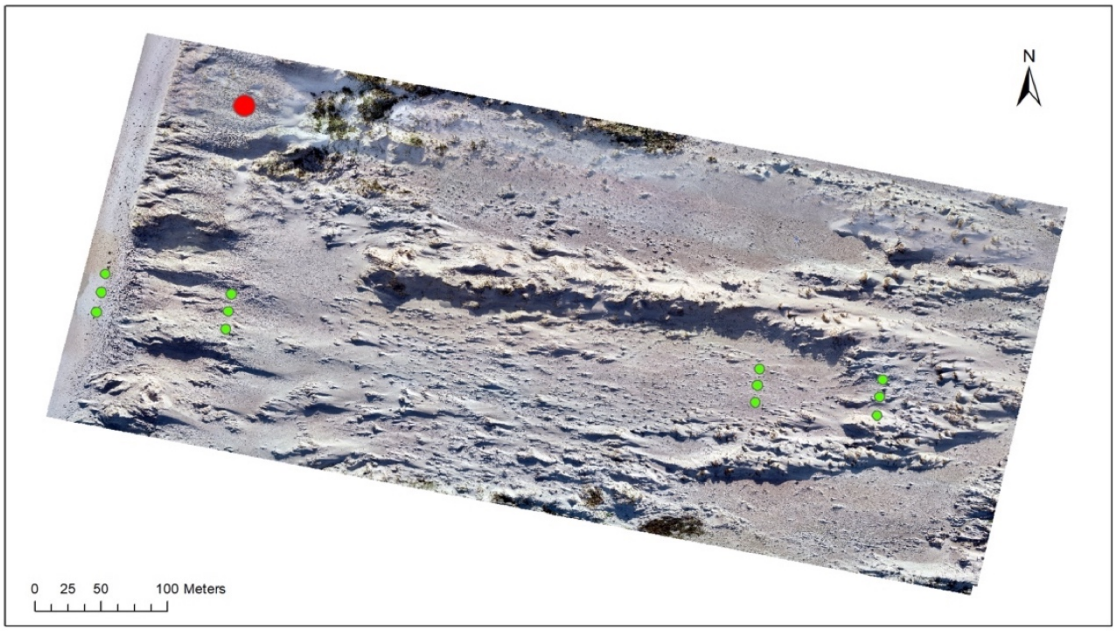

Figure 4.4: The location of sand traps deployed during experiment two in August 2020. Three sand traps were deployed at each location, at the rear of the beach, at the foredune toe, the foredune crest upwind of P6, the deflation surface and depositional lobe of P6. The sand traps were separated by 10 m.

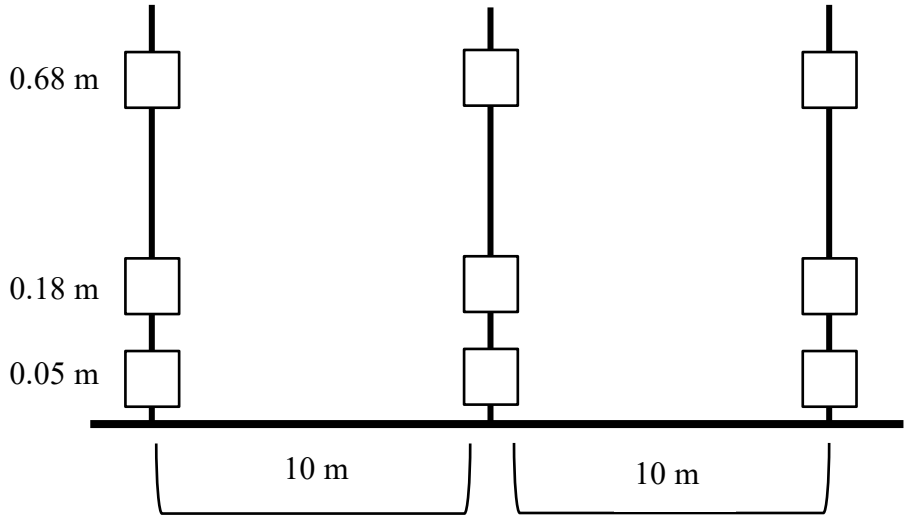

Figure 4.5: Array of sediment traps deployed at each location in August 2020. Three traps were deployed on each mast at 0.05 m, 0.18 m and 0.68 m above the surface. Each set of traps were separated by 10 m.

4.2.3 Limitations of aeolian sediment transport experiments

There were a number of limitations to the sediment transport experiments. These include the number of people that were available to complete the experiments. Mason Bay is a remote location so there were only four people present for the experiments completed in 2019 and 2020. Therefore, the number of sand traps that could be deployed and the number of locations that could be sampled were limited by the number of people that were present.

There is large spatial and temporal variation in sediment transport within coastal sand dunes (Barchyn *et al.*, 2014). Rates of sediment transport can vary due to topography and wind strength, as stronger gusts of wind will cause greater transport of sediment (Anderson and Walker, 2006). Therefore, it is acknowledged the sand traps only provide an indication of sediment transport for the specific point in time the experiments were completed. To account for this variation in sediment transport, multiple runs were completed at each location. Furthermore, due to the wind conditions that occurred during fieldtrips completed, sediment transport experiments were only completed under W-NW winds. Therefore, data during offshore, NE winds, that are also a strong component of the Mason Bay wind regime, was not able to be obtained.

Collection of aeolian sediment transport data in the field was further limited by the design of the sand traps used. As these traps self-orientate in the direction of the wind, they cannot be deployed on the surface of the bed. Consequently, the lowest trap was installed at 0.05 m above the surface and sediment transport along the bed was missed.

4.2.4 Data analysis

Wind data analysis

The wind speed and direction data were analysed in Microsoft Excel and Grapher. Microsoft Excel was used to create time-series graphs of wind speed and direction. The average wind speed and direction was calculated for each run completed in 2019 and 2020. The wind directions recorded were adjusted to true north by adding the magnetic declination of Mason Bay. Grapher was used to create a wind rose for each day sediment transport experiments were completed and for the long-term data set on the Mason Bay foredune and South West Cape weather station. Data for the South West Cape weather station was provided by the Meteorological Service of New Zealand Limited.

Aeolian sediment flux

The sediment trapped during the sediment transport experiments was dried and weighed to an accuracy of 0.001 g. This data was then analysed to calculate the sediment flux and related to the results from the wind analysis. Estimates of sediment flux are important for determining the rate of sand transport (Butterfield, 1999).

The weight of sand caught in each trap was first divided by the duration of each run, to produce a value of g/min at each height. This was then plotted on a graph for each run and the points were fitted with an exponential trendline. The integral was calculated from the equation of the line, to obtain the sediment flux for the vertical column, equal to the height of the highest trap (0.68 m) and the width of the sand traps (38 mm) (Fig. 4.2). The 2020 sand flux estimates were extrapolated to produce a value of g/min for the 10 m distance between each sampling point at each location. This was the distance, 10 m, divided by the width of the trap, 38 mm. This value was then used to calculate an estimate of sand flux for the distance between the sampling points, which had an area of 6.99 m^2 (10 m multiplied by the height of the highest trap, 0.699 m). The sand flux for the total

area was then converted into a value of kg/m^2/min by dividing the calculated sediment flux by the area (6.99 m^2). The same method was used for the 2019 values.

The sediment flux from the two sampling stations collected in 2019 and 2020 were averaged and extrapolated for the 70 m width of the deflation surface to produce an estimate of sediment flux through a cross-section of the deflation surface. This transect had an area of 48.93 m^2 (the width of the deflation surface multiplied by the height of the highest trap). It is acknowledged that these are only estimates based on a small number of sampling points at each location and in reality, due to the large temporal and spatial variability of sediment transport, these estimates would be different. However, they provide a good indication of the quantity of sediment that was moving through each location at the point in time sediment was sampled.

The sediment flux was also normalised using the method dscribed in Ellis *et al.* (2009). This method provides a comparison of vertical flux profiles obtained under different environmental conditions.

Long-term wind analysis

An automatic weather station recording wind speed and direction was deployed on the foredune upwind of P5 from June 2011 - September 2016. This provided a long-term data set to characterise the incident wind conditions the dune system at Mason Bay experiences. This was also compared with data collected at the nearest weather station at South West Cape, Stewart Island. A wind rose was created for Mason Bay and South West Cape to compare the frequency of wind speed and direction at these two locations. The wind data collected at Mason Bay was also used to create a histogram of the frequency of wind speeds during onshore winds (between 225° and 315°). The frequency the minimum threshold for sediment transport is reached at Mason Bay (8 ms^{-1}) was calculated, as well as the occurrence of strong onshore wind events (>15 ms^{-1}), observed during the experiments.

4.3 Results

4.3.1 Aeolian sediment transport downwind of a vegetated and devegetated foredune

Topographical profiles of the foredune upwind of P5 and P6 show the different morphologies, as previously established in Chapter 3 (Fig. 4.6). The stoss face of the foredune upwind of P5 is steeper than the foredune upwind of P6, which is lower and wider. The foredune upwind of P5 is about 5 m higher than the foredune upwind of P6, while the lee slope of the foredune adjacent to P6 extends further inland. The P5 and P6 deflation surface have a similar morphology, both sloping upwards with distance inland. At the time of experiment one, in August 2019, the foredune upwind of P6 was unvegetated, as this section of the foredune had been sprayed repeatedly over five years prior to the foredune adjoining P5. The foredune upwind of P5 had a greater cover of vegetation, as it was first sprayed in 2015. This was predominantly *A. arenaria* that had survived the annual herbicide applications and decaying plant roots. These differences in morphology and vegetation cover influence sediment transport over the foredune.

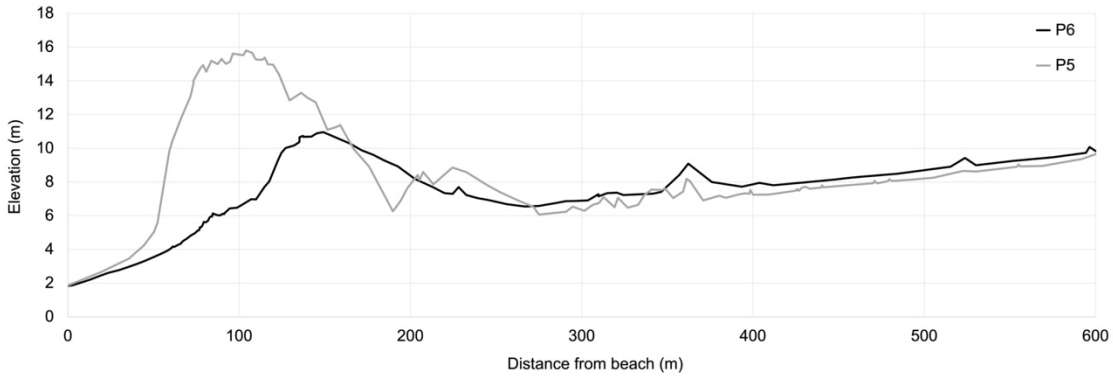

Figure 4.6: Topographical profile of the foredune upwind to P5 and P6 and the P5 and P6 deflation surface recorded in June 2020. The profile is relative to the NZGD2000 datum.

Despite the differences in upwind topographies, wind speeds recorded in the deflation surfaces were similar (Figs. 4.7-4.9). Wind speed in the P6 deflation surface were only about 1 ms^{-1} higher than the P5 deflation surface. The surface friction caused by the topography between the foredune and centre of the deflation surface likely has a strong influence on reducing wind speeds, regardless of the cover of vegetation. This also resulted in a decrease in wind speed between the foredune and the deflation surfaces. Wind speed on the foredune was about 5 ms^{-1} greater than in the deflation surfaces. Wind speed in the deflation surfaces also exhibited large temporal variability, indicated by the wide range of scatter points on each graph. Wind speed ranged between 5-20 ms^{-1} over the experimental period; therefore, was over the threshold for sediment transport (8 ms^{-1}, Sherman and Lee, 2009; Davidson-Arnott and Bauer, 2009) for the majority of the study period. Wind direction on the foredune turned more W from NW, throughout the study period, generally ranging between 280° and 305°. The windiest day was the 28th of August 2019, when gusts on the foredune reached 24 ms^{-1}.

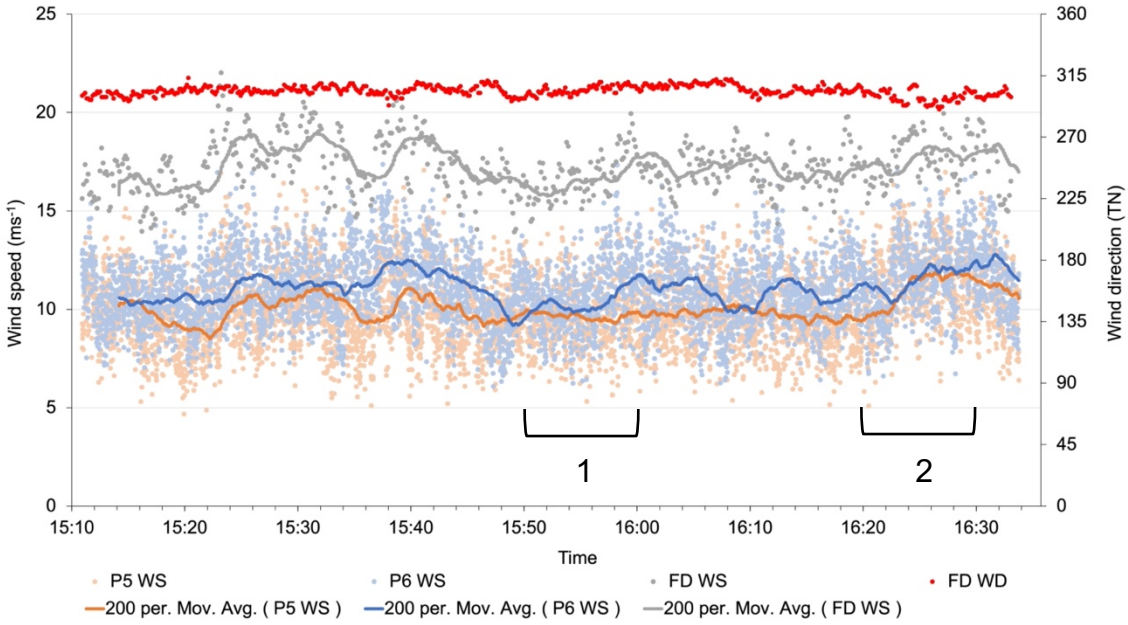

Figure 4.7: Wind speed (ms^{-1}) and direction (true north °) for 24/08/2019. Wind speed (WS) is displayed for the P5 and P6 deflation surfaces (1-second intervals) and the foredune (FD) adjacent to P5 (8-second intervals). The trend lines are 200 period moving averages. The wind direction (WD) was recorded on the foredune. The time and number of the sediment transport runs is also indicated.

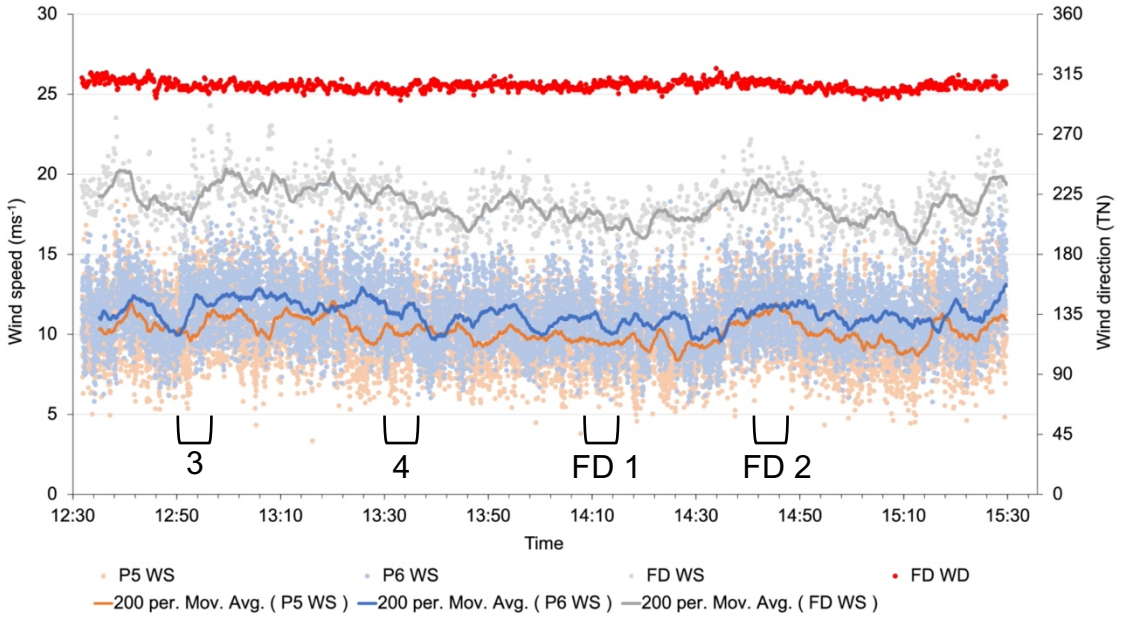

Figure 4.8: Wind speed (ms^{-1}) and direction (true north °) for 28/08/2019. Wind speed (WS) is displayed for the P5 and P6 deflation surfaces (1-second intervals) and the foredune (FD) upwind of P5 (8-second intervals). The trend lines are 200 period moving averages. The wind direction (WD) was recorded on the foredune. The time and number of the sediment transport runs is also indicated, including the runs on the foredune (FD).

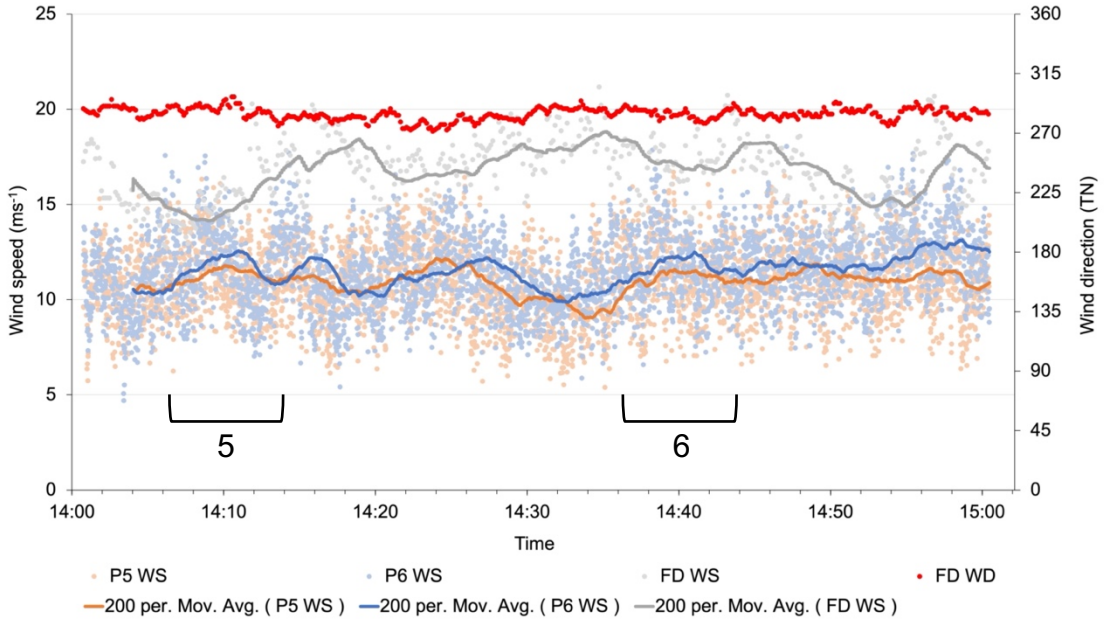

Figure 4.9: Wind speed (ms^{-1}) and direction (true north °) for 29/08/2019. Wind speed (WS) is displayed for the P5 and P6 deflation surfaces (1-second intervals) and the foredune (8-second intervals). The trend lines are 200 period moving averages. The wind direction (WD) was recorded on the foredune. The time and number of the sediment transport runs is also indicated.

Wind speed at the deflation surface masts increased exponentially with height (Fig. 4.10). Over a 20-minute period, recording at 1-second intervals, wind speeds recorded at the lowest height (0.05 m) averaged 5 ms^{-1} and at the highest height (2.0 m), averaged 10 ms^{-1}. The highest anemometer deployed in the deflation surface was not above the boundary layer since wind speed was still increasing with height. This means that wind speeds at this anemometer were still influenced by the surface, and likely, turbulent structures in the lee of the foredune.

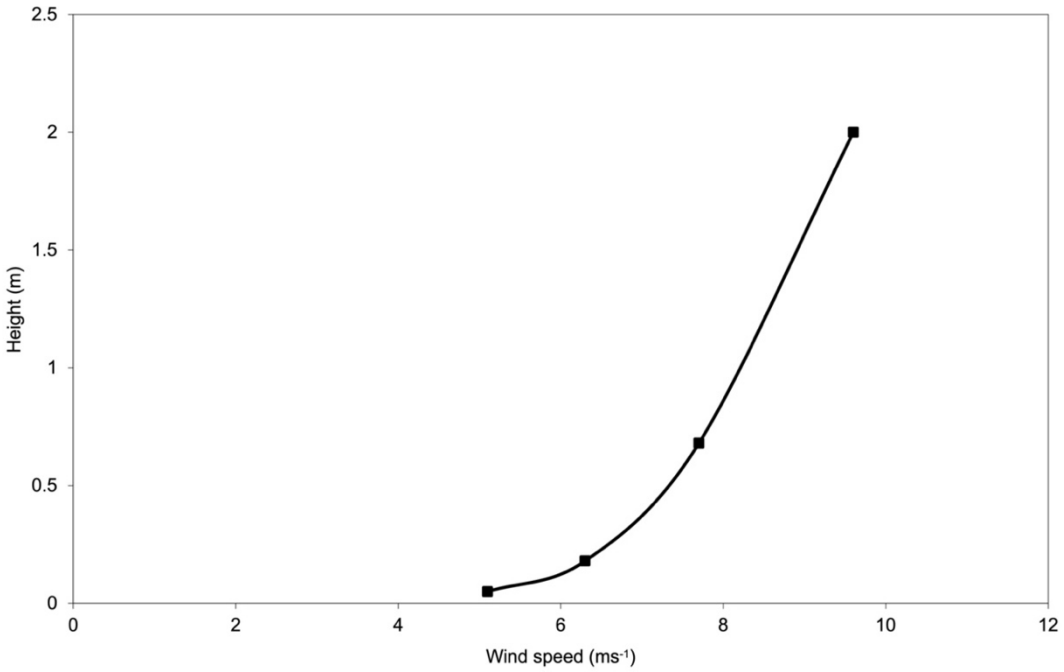

Figure 4.10: The average change in wind speed (ms^{-1}) with height (m) recorded over a 20-minute period of relatively consistent wind speeds. The wind speed was recorded by windsonic anemometers deployed on a mast in the P6 deflation surface, at 0.05 m; 0.18 m; 0.68 m; 2 m above the surface.

Wind roses were created for each day sediment transport runs were completed. They show there was a clear difference in the wind speed on the foredune (at 5 m) compared to the deflation surfaces (Fig. 4.11). Wind speeds on the foredune were consistently over 16 ms^{-1}, whereas in the deflation surfaces (at 2 m), mostly ranged between 8-16 ms^{-1}. The influence of topography on the wind direction is also evident as the wind direction was consistently oriented more westerly in the deflation surfaces than wind direction recorded on the foredune. This trend was observed in both P5 and P6. The long axis of P6 is oriented 275° and the axis of P5 is oriented 279°. This shows the wind direction is altered

as it is flows over the pre-restored foredune and is steered through the parabolic dunes. Larger variation in wind direction was recorded in the deflation surfaces compared to the foredune, showing the strong influence of topography on wind direction.

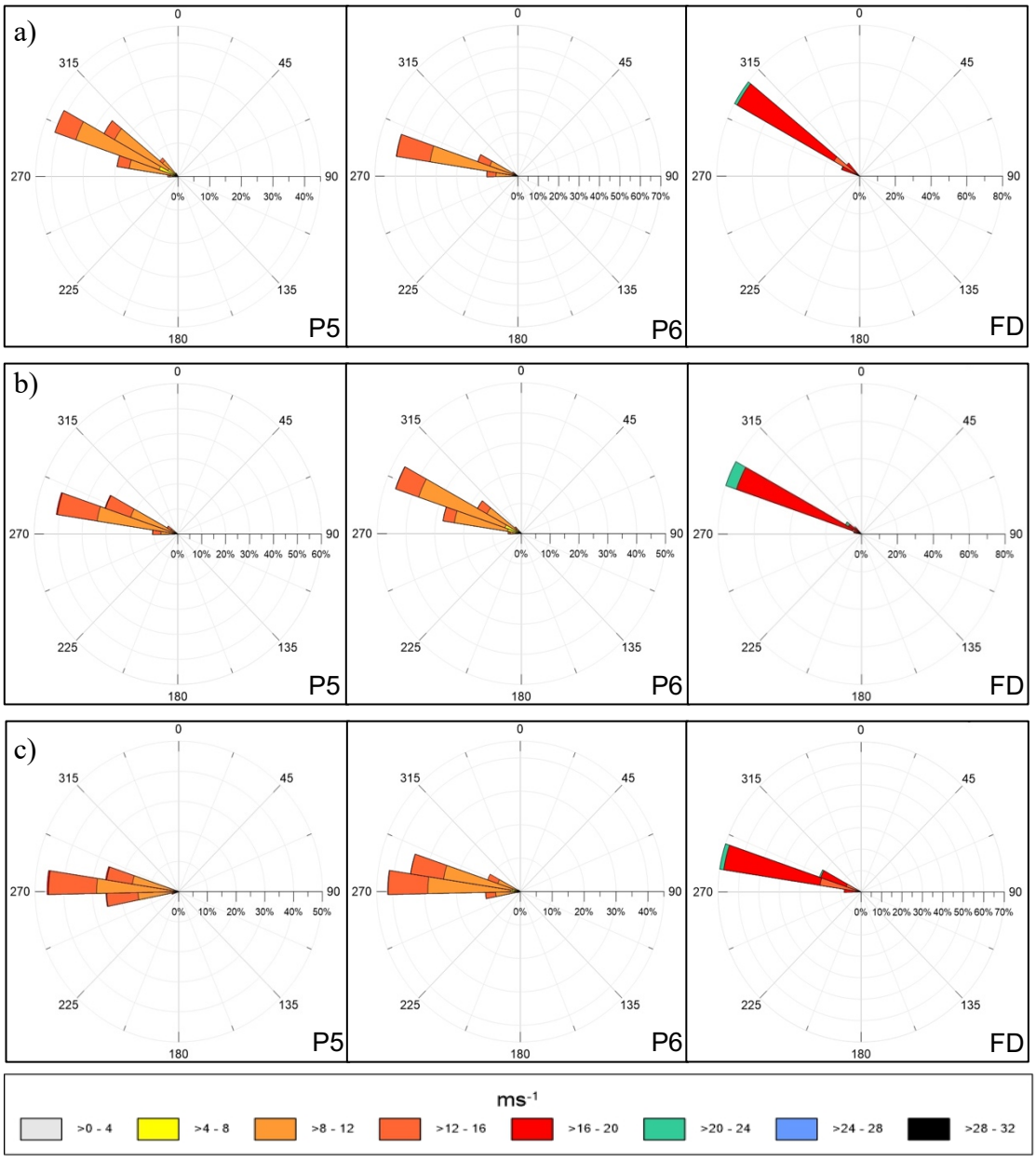

Figure 4.11: Wind rose for each day sediment transport runs were completed at Mason Bay in August 2019, a) 24/08/2019; b) 28/08/2019; c) 29/08/2019. The wind roses are from data collected in the P5 deflation surface (left); P6 deflation surface (centre) and the foredune (right). The wind rose displays the wind speed (ms^{-1}) and wind direction (°) relative to true north.

Table 4.1: The average wind speed (ms^{-1}) and wind direction (true north °) during each run of aeolian sediment transport experiments in the deflation surface of P5 and P6 and on the foredune. Run 1 and 2 were completed on 24/08/2019; Run 3 and 4 were completed on 28/08/2019; Run 5 and 6 were completed on 29/08/2019. The standard deviation for each value is displayed in brackets.

Run	P5 wind speed (ms^{-1})	P5 wind direction (TN°)	P6 wind speed (ms^{-1})	P6 wind direction (TN°)	FD wind speed (ms^{-1})	FD wind direction (TN°)
1	9.6 (1.66)	296 (4.84)	10.6 (1.61)	285 (3.98)	16.7 (1.11)	304 (3.36)
2	11.5 (1.85)	293 (4.42)	12 (1.84)	282 (3.0)	17.9 (1.04)	299 (4.40)
3	10 (1.93)	293 (4.23)	11.6 (2.12)	287 (4.24)	17.9 (1.75)	306 (2.16)
4	9.6 (1.83)	291 (3.58)	10.2 (1.61)	285 (3.38)	18.1 (1.17)	305 (3.16)
5	11.3 (1.73)	279 (5.07)	11.9 (2.07)	273 (3.71)	18.1 (1.16)	285 (4.14)
6	11.2 (2.0)	279 (4.87)	11.9 (1.82)	273 (3.60)	17.1 (1.55)	285 (2.88)

There was a difference in wind speed and direction in the deflation surfaces and foredune crest during the sediment transport runs completed in August 2019 (Table 4.1). The wind speed on the foredune were consistently about 6 ms^{-1} higher on average than in the deflation surfaces. Wind speeds in the P6 deflation surface were slightly higher, by about 1 ms^{-1}, compared to the P5 deflation surface. There was variability in the wind speeds recorded during the runs as shown by the standard deviations that ranged from 1.61-2.12 ms^{-1} in the deflation surfaces. There was more variability in the wind speeds recorded in the deflation surfaces compared to the foredune, where the standard deviation was consistently lower (1.04-1.75 ms^{-1}). As was observed in the previous figures, the wind direction was slightly more westerly in the deflation surfaces, and this was most pronounced in the P6 deflation surface during the runs.

There was an exponential decay in aeolian sediment transport with height in both P5 and P6 (Fig. 4.12). This was most pronounced in P6, where sand flux rates were 575 times greater than in P5. The low sediment flux at the lowest trap in P5 resulted in a less distinct

exponential decay, however, the trend of a reduction in sediment transport with height was still evident in most runs (Fig. 4.12a). Sediment transport below 0.1 g/min was recorded in the lowest traps in P5 during all runs. Whereas in P6, between 10-15 g/min was recorded in the lowest trap in most runs, excluding run 3, when the sediment transport in the lowest trap was over 20 g/min, almost double the sediment transport recorded in the other five runs completed.

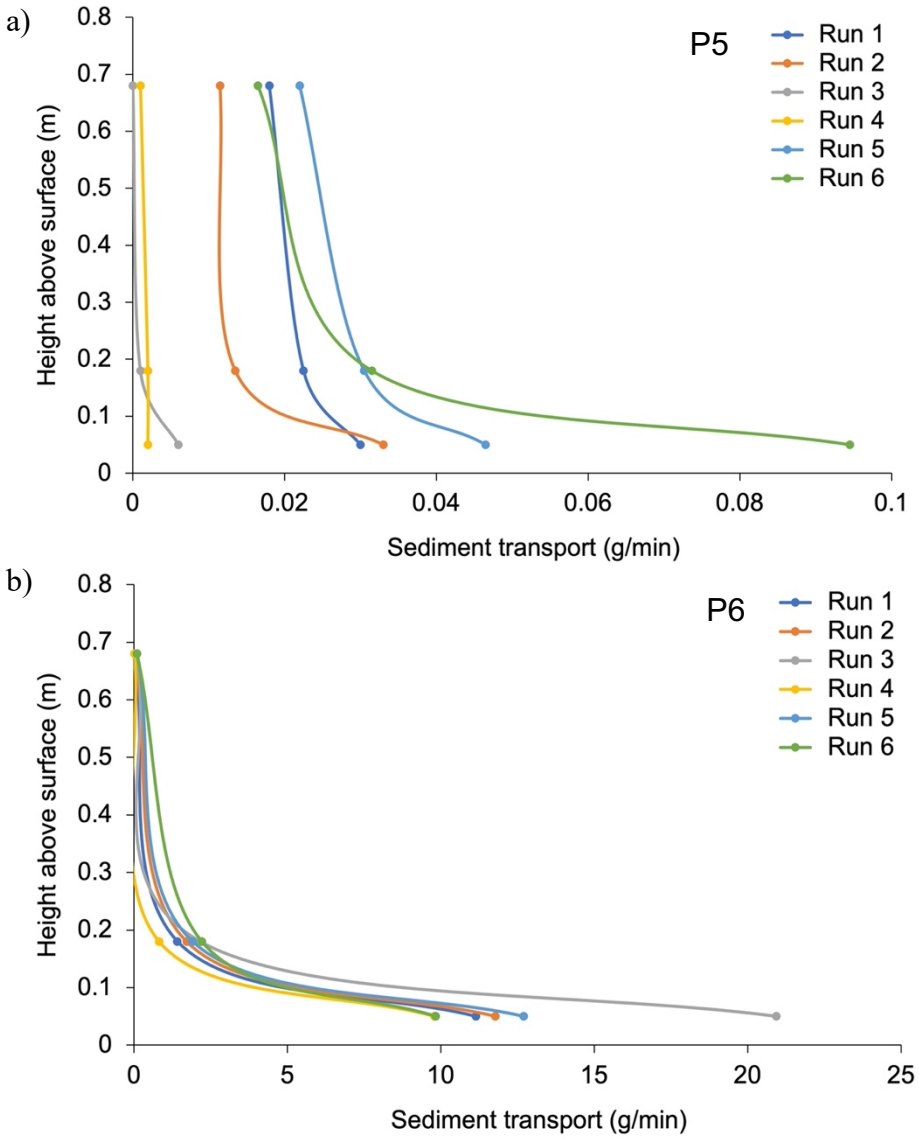

Figure 4.12: The change in sediment transport (g/min) with height (m) for each run completed in a) the P5 deflation surface and b) the P6 deflation surface in August 2019. Sediment flux was sampled at 0.05 m, 0.18 m and 0.68 m above the surface. A smoothed line was fitted to the points. Note the difference in scale on the x-axis.

Table 4.2: Percentage of sediment flux in each trap in the P6 deflation surface, 0.05 m; 0.18 m; 0.68 m above the surface, out of the total sediment flux of the vertical column sediment transport was sampled in (Fig. 4.4). The vertical column had an area of 258.4 cm^2.

Run	0.05 m	0.18 m	0.68 m
1	44.70%	5.68%	0.76%
2	43.97%	6.41%	0.12%
3	49.94%	5.14%	0.14%
4	53.21%	4.46%	0.09%
5	39.75%	5.98%	0.32%
6	35.37%	7.94%	0.36%

The largest proportion of sediment was trapped in the lowest trap, closest to the ground (0.05 m above the surface) (Table 4.2). Sediment trapped in the lowest trap was between 35-53% of the total sand flux. The middle trap (0.18 m) consisted of between 4-8% of transported sediment and the highest trap (0.68 m) consistently trapped less than 1% of sediment. These results indicate the trap array captured most of the column of sand transport, that is the highest trap was close to the top of the saltation layer.

The sediment flux rates were normalised using the method of Ellis *et al.* (2009) (Fig. 4.13). There was a stronger exponential trend of a decrease in sediment flux with height for the P6 flux rates compared to P5. This is likely due to the relatively low rates of flux in P5, resulting in a smaller difference in sediment transport with height. The normalised flux in P6 showed flux rates were highest closer to the surface and exponentially decreased with height. The normalised sediment flux in P6 is very similar across all 6 runs.

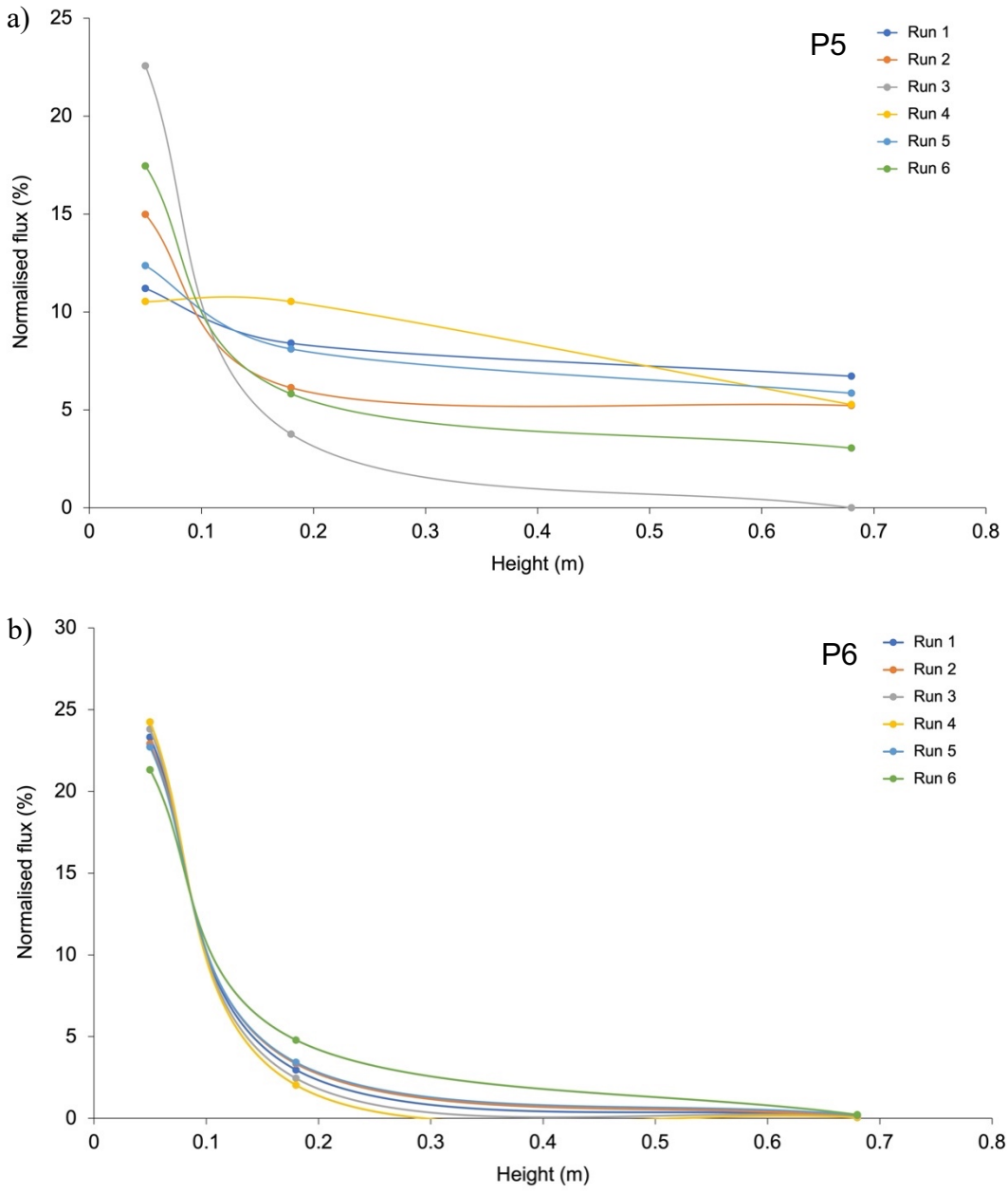

Figure 4.13: Normalised flux (%) for each run (n=6) completed in August 2019 in a) P5 deflation surface and b) P6 deflation surface using the method of Ellis *et al.* (2009). The flux rates were based on sediment transport data collected at 0.05 m, 0.18 m and 0.68 m above the surface.

Table 4.3: Sediment flux (kg/m^{2}min) sampled in P5 and P6 and sediment flux for a cross-section of the P5 and P6 deflation surface extrapolated from the vertical flux. The vertical flux (kg/m^2/min), sediment transport was sampled in, was multiplied by the width of the deflation surface (70 m, an area of 49 m^2), to estimate the amount of sediment moving through the deflation surfaces at a point in time.

Run	P5 sediment flux	P5 cross-section	P6 sediment flux	P6 cross-section
1	0.01	0.93	0.51	35.55
2	0.005	0.40	0.56	39.12
3	0.0008	0.10	0.44	61.02
4	0.0007	0.05	0.39	26.95
5	0.01	0.98	0.66	46.12
6	0.01	0.80	0.58	40.70

The devegetation and subsequent erosion of the foredune upwind of P6 has clearly influenced downwind sediment transport. Estimated sand flux was 575% greater on average in P6 compared to P5. Less than 0.01 kg/m^2/min of sediment was transported through P5. This contrasts with P6, where between 0.39-0.66 kg/m^2/min was being transported, extrapolated to 26.95-61.02 kg/m^2/min through the 70 m width of the deflation surface. The lowest sediment flux in P6 was in run 4. This coincides with the run with the lowest wind speed (Table 4.3). Run 3 had the highest sediment flux in P6 and during this run there were several strong gusts, above 15 ms^{-1}, which likely contributed to a higher rate of sediment transport. This shows that there is a relationship between wind speed and sediment flux rates.

4.3.2 Aeolian sediment transport on a vegetated and devegetated foredune

Table 4.4: Average wind speed (ms^{-1}) and direction (true north °) on the foredune and the average sediment flux ($kg/m^2/min$) for the vertical column sediment was sampled, for two aeolian sediment transport runs completed on the foredune upwind of P5 and P6 on the 28/08/2019.

Run	Duration (min)	Wind speed (ms^{-1})	Wind direction (TN°)	P5FD sediment flux ($kg/m^2/min$)	P6FD sediment flux ($kg/m^2/min$)
FD 1	3	19.1	296	0.004	0.43
FD 2	3	18.9	292	0.04	1.28

Two further runs were completed on the crest of the foredune upwind of P5 and P6, to compare the sediment transport over the foredune, measuring the sediment source from the beach and stoss face of the foredune. Wind speed on the foredune was similar between these runs, however, the sediment flux was much greater in the second run, 1.28 $kg/m^2/min$, on the foredune upwind of P6 compared to 0.43 $g/m^2/min$ in the first run (Table 4.4). This exhibits the high spatial and temporal variability of sediment transport and shows that rates of sediment transport are not always directly correlated with wind speed.

The differences in sediment flux on the foredune upwind of P5 and P6 was similar to what was observed in the deflation surfaces, as there was a lot more sediment being transported over the foredune upwind of P6 compared to P5. The amount of sediment trapped was slightly higher on the foredune compared to the deflation surface in both P5 and P6. This was particularly evident in the second run when sediment flux was 3 times greater than the first run. These results show the topography and vegetation cover of the foredune clearly influenced the amount of sediment that was transported over and beyond the foredune. The unvegetated stoss face of the foredune upwind of P6 was likely an important source of sediment transported into the deflation surface.

4.3.3 Aeolian sediment transport through P6

Experiment two was completed to determine the source of transported sediment through a devegetated parabolic dune, P6. A strong, onshore wind event occurred in August 2020 and four sediment transport runs were completed on the same day to show the change in sediment transport from the beach, through to the apex of P6 (Fig. 4.4). During the wind event the wind direction changed throughout the day from a NW direction to a more W direction (Fig. 4.14). The wind speed also fluctuated throughout the day, mainly ranging from 15-25 ms^{-1}. The wind speed was highest during run 2 and 3, with an average of 20.8 ms^{-1} and 20.9 ms^{-1} for these runs, compared to 19.8 ms^{-1} during run 1 and 19.1 ms^{-1} during run 4. The wind speeds during this event were higher than the event in August 2019.

The wind rose showed that during the wind event, the wind direction was predominantly 290°, W-NW (Fig. 4.15), but changed steadily as indicated in Fig. 4.14. Wind speeds were frequently above 15 ms^{-1} and were never below 8 ms^{-1}, thus, the threshold for sediment transport was reached for the entire day of this experiment.

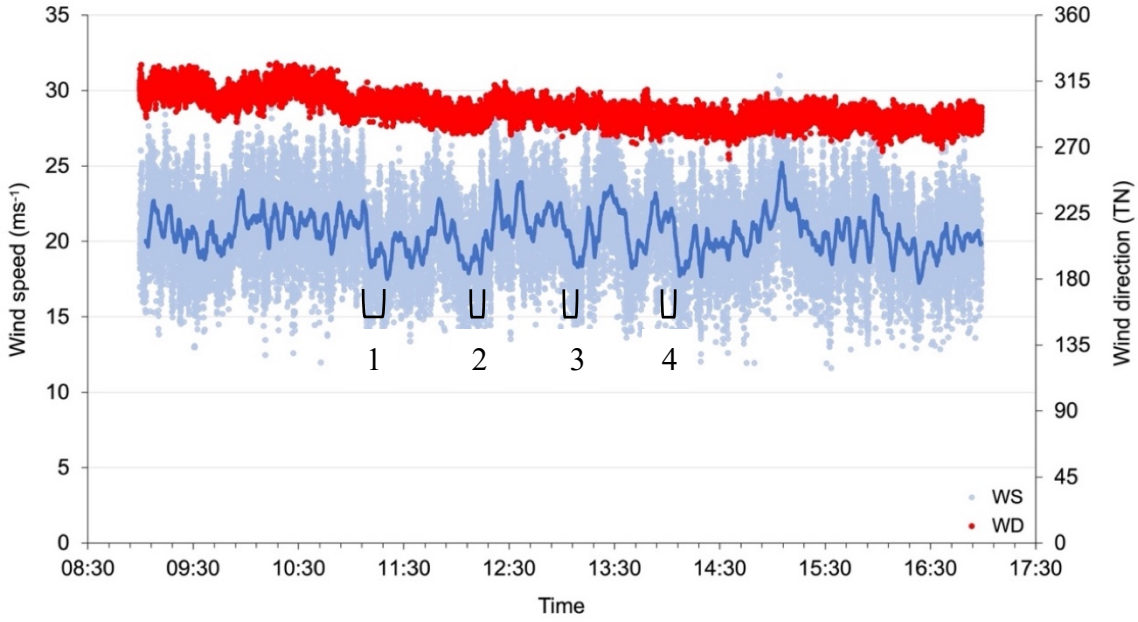

Figure 4.14: Wind speed (ms^{-1}) and direction (true north °) recorded at 1-second intervals on 29/08/2020 obtained from a 5 m mast deployed on the foredune at Mason Bay. The trendline is a 200-period moving average. Four runs were completed, and the time of each run is indicated.

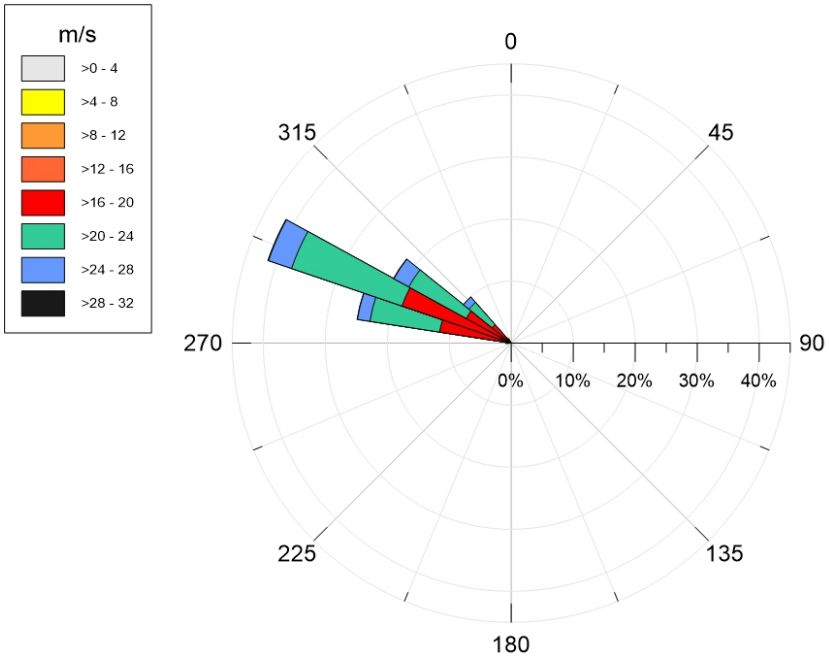

Figure 4.15: Wind rose for Mason Bay during the wind event on 29/08/2020. Wind data was obtained from a windsonic anemometer on a 5 m mast deployed on the foredune adjacent to P5.

Table 4.5: Average wind speed (ms^{-1}) and direction (true north °) for each run completed on 29th August 2020. Wind data was obtained from a windsonic anemometer on a 5 m mast deployed on the highest section of the foredune upwind P5.

Run	Duration (min)	Wind speed (ms^{-1})	Wind direction (TN°)
1	10	19.2	298
2	6	20.9	295
3	5	20.8	295
4	5	19.8	288

Wind speeds recorded on the foredune were similar in the four sediment transport runs completed in August 2020, ranging from 19.2-20.9 ms^{-1} (Table 4.5). The duration of the first run was the longest (10 mins), while the duration of the other three runs were 5-6 minutes. The length of the runs was determined by the time taken for the traps to almost fill.

There was a large difference in the sediment flux between the four locations (Fig. 4.16). Sediment transport was greatest near the apex of the parabolic. Sediment flux rates at the beach, near the foredune toe, were very low in every run, less than 0.2 g/min in the lowest trap, showing the beach was not a primary source of transported sediment within the parabolic during this event. Sediment transport on the foredune crest was greater than the beach and reached 10.35 g/min during run 3. The difference in sediment transport between the beach and foredune shows that sediment was being eroded from the stoss face of the foredune and transported inland. Estimates of sand flux on the foredune crest were lower than sand flux in the deflation surface and the depositional lobe of the parabolic dune. Sediment flux in the deflation surface and depositional lobe were similar across the four runs. In runs 2, 3 and 4, sediment transport in the lowest trap in these two locations was over 35 g/min. This shows that the source of a large proportion of the sediment transported through the parabolic was between the foredune crest and landward (eastern) half of the deflation surface. Furthermore, due to the similar values of sediment transport at these two locations, this shows that very little sediment was deposited in the deflation surface.

Despite the similarity in wind speed across the four runs, there was an increase in sediment transport between each run. This is likely due to changes in the moisture of the sediment. Rain in the early morning on the day of the experiment resulted in the sediment being damper earlier in the day and it progressively became drier throughout the day. This would have influenced the potential for sediment to be transported, as sediment that is wet requires stronger winds to be transported.

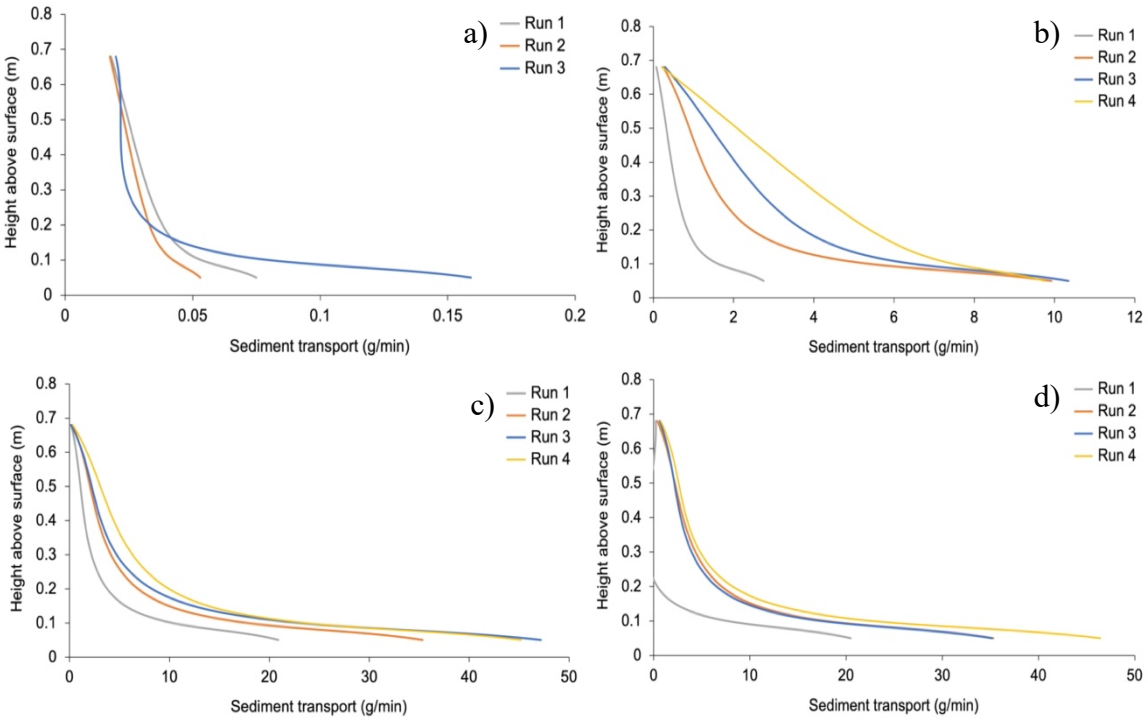

Figure 4.16: The sediment flux (g/min) for the vertical column sediment was sampled in the four locations in P6, a) the beach; b) the crest of the foredune; c) the deflation surface; d) the depositional lobe. Sand traps collected sediment at 0.05 m; 0.18 m; 0.68 m above the surface at three sampling points at each location and the weight of sediment at these three points was averaged. This data was used to calculate the sediment flux for the entire vertical column, with an area of 0.02584 m^2. Note the difference in scale on the x-axis.

Table 4.6: Sediment flux ($kg/m^2/min$) for the vertical column (VC) sediment was sampled in and extrapolated for the 70 m width of the deflation surface (DS) (area of 49 m^2) for the beach, foredune, deflation surface and depositional lobe of P6 in August 2020. The vertical flux ($kg/m^2/min$) was multiplied by the width of the deflation surface (70 m) to estimate the amount of sediment moving through the parabolic dune for each run completed.

Run	**Beach**		**Foredune**		**Deflation surface**		**Depositional lobe**	
	VC	**DS**	**VC**	**DS**	**VC**	**DS**	**VC**	**DS**
1	0.01	0.90	0.32	22.12	1.17	82.15	0.90	63.10
2	0.01	0.59	0.48	33.43	1.42	99.22	1.46	102.43
3	0.01	0.64	0.49	34.32	1.36	95.07	1.23	87.89
4	n/a	n/a	0.51	35.6	1.60	111.72	1.65	115.40

There was an increase in sediment transport through P6 with distance inland (Table 4.6). At the rear of the beach, sediment flux was less than 0.018 kg/m^2/min. The rate of sediment flux increased on the foredune, particularly in runs 2-4, where between 0.48-0.51 kg/m^2/min was transported. In the deflation surface and depositional lobe, transported sediment was three times greater than on the foredune, where between 0.90-1.65 kg/m^2/min was transported. The highest sediment flux was recorded during run 4 in the depositional lobe, 115.40 kg/m^2/min transported across the 70 m width of the deflation surface, although this run did not have the highest average wind speed. The wind direction had become more westerly by this run and the sediment had a longer time to dry throughout the day. This likely contributed to higher rates of sediment being transported. The rate of sediment transport recorded in the deflation surface in August 2020 was greater than the rate recorded in the first experiment in August 2019. This is a result of stronger winds, leading to an enhanced rate of sediment transport.

Ground photos taken during run 3 show the transport of sediment through P6 (Fig. 4.17). Sediment transport occurred as saltation streamers, as sediment was funnelled through the *F. spiralis* nabkha, identified as the white sand clouds in the images. Topographical variability on the surface resulted in spatial variability of sediment transport. A high rate of sediment was transported in the deflation surface near the apex of the parabolic and into the depositional lobe (Fig. 4.17b). These results are consistent with the results from the sand trap experiments.

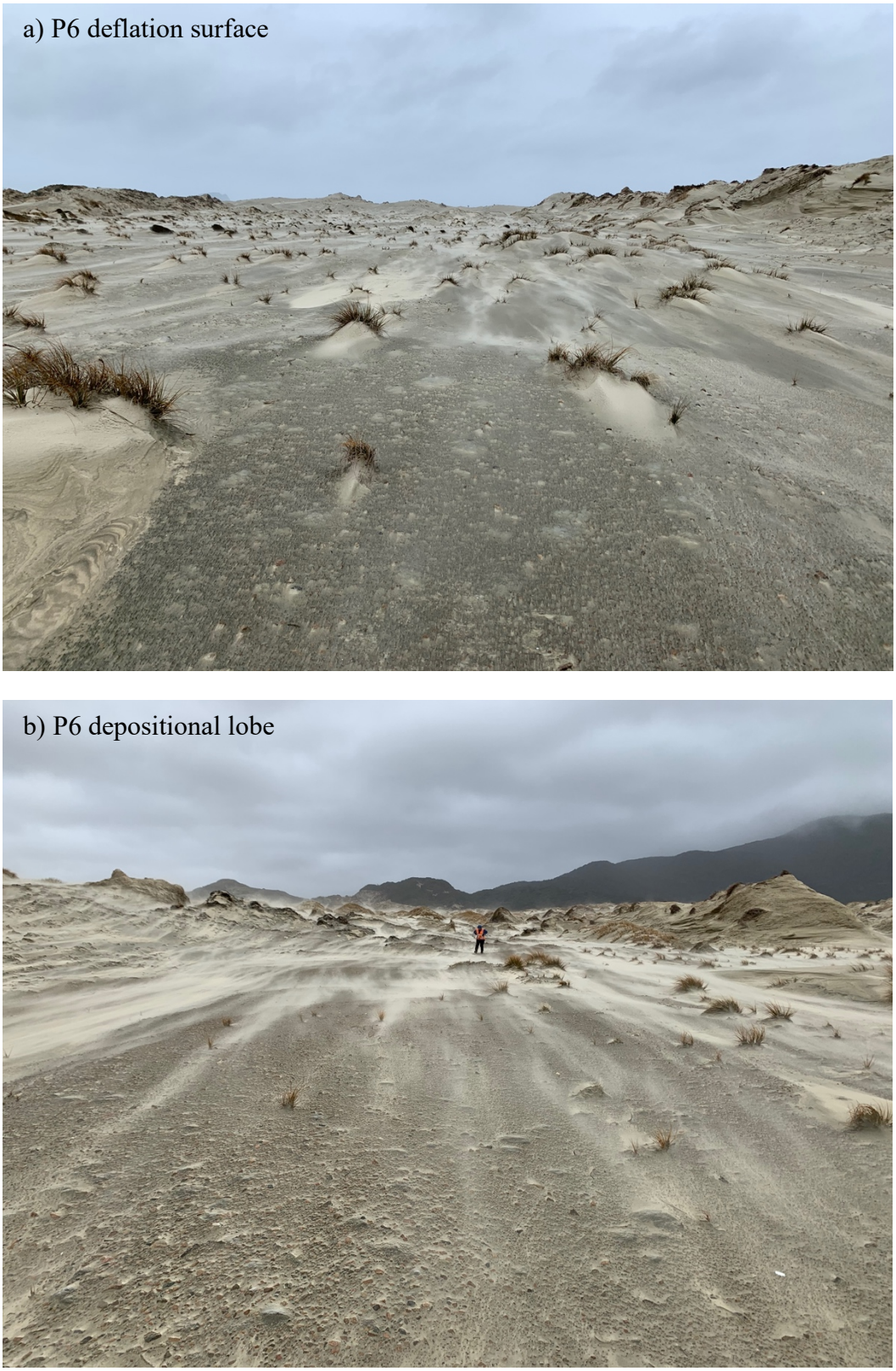

Figure 4.17: Ground photos of the P6 deflation surface during run 3 in August 2020, showing the sediment being transported through P6. a) looking towards the foredune upwind of P6 and b) looking inland, towards the P6 depositional lobe.

4.3.4 Frequency of wind events in Mason Bay

An AWS deployed on the foredune upwind of P5 recorded wind speed and direction between 2011 and 2016 (Fig. 4.18). This data was analysed to determine the frequency of strong wind events at Mason Bay, observed in the experiments described above. The average wind speed recorded was 6.77 ms^{-1} and the average wind direction was 213°. The AWS was located on the foredune upwind of P5 and was 2 m above the surface. Comparative experiments indicate the wind records at this site and elevation are influenced by the foredune topography. It was found that during SW winds, the wind direction recorded by the AWS was steered by about 12°, to a more westerly direction, between the intertidal beach and the AWS. The strong E component is a result of topographic steering as air flows over Rakiura/Stewart Island, generally from the NE. Therefore, the wind rose is not a perfect representation of the incident wind direction at Mason Bay, however, it provides the best indication of the wind conditions that this site experiences.

It was not possible to use longer term wind data since the AWS at Mason Bay was only deployed between 2011 and 2016. There is a difference in the wind regime experienced at Mason Bay compared to the nearest weather station on the South West Cape of Stewart Island. The prevailing winds at Mason Bay are from the west, however, there is also a strong easterly component (Fig. 4.18). This is in contrast to the South West Cape where the predominant wind direction is from the NW (Fig. 4.19). The South West Cape also experiences stronger wind speeds compared to Mason Bay. Wind speeds on the South West Cape are frequently above 20 ms^{-1}. The differences observed are likely due to the effect of local topography. The winds recorded at Mason Bay are steered in a more W direction due to the orientation of the coastline. The winds recorded at South West Cape are likely influenced by the orientation of Rakiura/Stewart Island. The NE component is not evident in the wind rose because this location is on the opposite side of the island and, therefore, these winds get steered in a more NW direction as air flows around the island. These results show the complexities of recording wind speed and direction due to the strong influence of topography and the importance of collecting localised wind data to relate wind conditions to sedimentation processes.

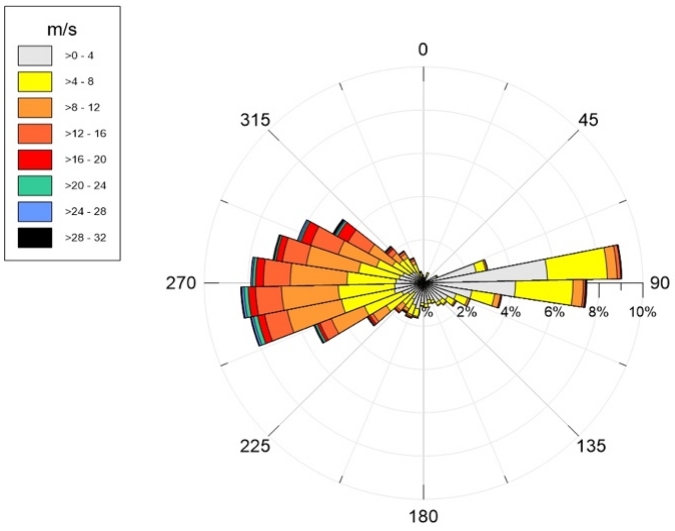

Figure 4.18: Wind rose derived from the foredune AWS at Mason Bay based (2011-2016). The prevailing winds are from the west, however, there is also a strong easterly component.

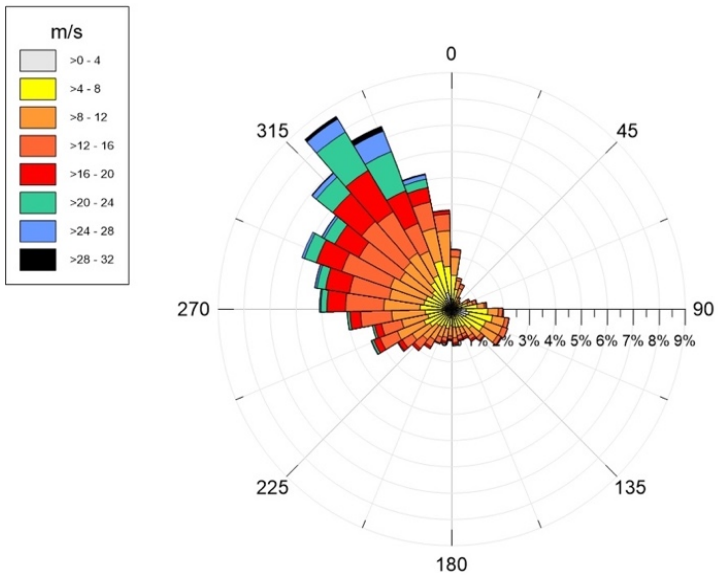

Figure 4.19: Wind rose for the South West Cape weather station based on a five-year data set (2011-2016) for the same period as the Mason Bay data (Fig. 4.18). The prevailing winds are predominantly from the northwest (data provided by the Meteorological Service of New Zealand).

Onshore winds at Mason Bay are frequently above the critical threshold for sediment transport (8 ms^{-1}) (Fig. 4.20). Between 2011 and 2016, the frequency of strong wind speeds (>15 ms^{-1}) observed in the experiments described above, occurred 10% of the time. Wind speeds that were above the threshold for sediment transport, 8 ms^{-1}, occurred 54% of the time. This shows onshore winds at Mason Bay play an important role in enhancing aeolian activity and promoting sediment transport. The strong wind events that were observed in the experiments are less frequent than smaller transport events.

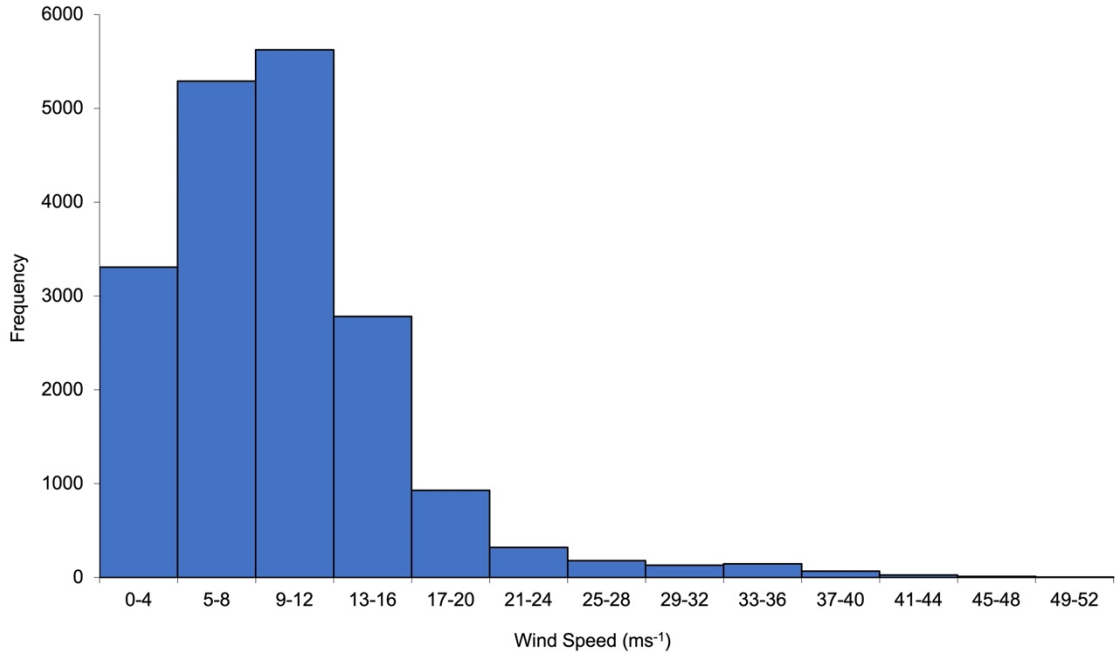

Figure 4.20: Frequency of wind speeds (ms^{-1}) at Mason Bay during onshore winds between June 2011 and September 2016. Data was recorded on the AWS located on the foredune upwind of P5. Wind speed frequencies were calculated for onshore winds, between 225° and 315°.

4.4 Discussion

The high *A. arenaria* foredune at Mason Bay trapped beach sand that would otherwise enter the wider dune system. Consequently, aeolian sediment transport beyond the foredune at Mason Bay was suppressed, resulting in a sediment deficit downwind of the foredune (Petersen *et al.*, 2011). Chapter 3 showed the removal of vegetation from the foredune upwind of P6 directly influenced sedimentation, leading to a redistribution of sediment within the foredune-parabolic dune complex and a positive sediment budget. This has implications for aeolian sediment transport.

Understanding sediment transport is important for understanding how dune systems function and will evolve in the future. The difference in foredune morphologies at Mason Bay provided a unique opportunity to study aeolian sediment transport downwind of these structures. This chapter aimed to determine the difference in the rate of sediment transport downwind of a vegetated (P5) and devegetated (P6) foredune to understand the implications of foredune devegetation on aeolian sediment transport. This chapter also aimed to establish the sources of sediment transported through a devegetated parabolic dune (P6) during a strong onshore wind event to derive a sediment budget for the dune system. The frequency of sediment transport events at Mason Bay was established to determine the importance of the observed wind events.

The data points to a change in direction as the incident wind crosses the foredune and enters the deflation surface of the parabolic dunes. This is likely a result of topographic steering. The mast on the foredune was 5 m above the surface, and thus, the influence of topography was not as great as the masts located in the centre of the deflation surfaces (2 m above the surface). The wind direction in the deflation surfaces was consistently more westerly than on the foredune. This is due to the airflow being funnelled through the parabolic dunes. P5 is oriented 279° and P6 is oriented 275°, therefore, the wind direction is steered to a more westerly direction as it flows through the parabolics. Topographic steering through blowouts and parabolic dunes has been observed in a number of locations under both onshore and oblique winds (Delgado-Fernandez *et al.*, 2018; Smyth *et al.*, 2014; Sun *et al.*, 2016; Hansen *et al.*, 2009). Smyth *et al.* (2014) found that within a trough blowout in County Donegal, Ireland, oblique winds

approaching at an angle of 100° from the orientation of the long axis of the deflation surface, were steered into the orientation of the deflation surface. Topographic steering of wind flow in parabolic dunes also contributes to the orientation of the parabolic being resistant to change (Hansen *et al.*, 2009).

Despite the differences in upwind foredune morphologies, wind speeds in the P5 and P6 deflation surfaces were relatively similar. During the runs, the wind speed in P6 was consistently about 1 ms^{-1} greater than in P5. The lower wind speeds in P5 could be due to the difference in vegetation cover. Vegetation increases surface roughness, which reduces wind speeds, and this subsequently decreases the sediment transport potential of the wind (Jackson and Nordstrom, 2013). However, the small difference in wind speeds between P5 and P6 indicates that regardless of vegetation cover, friction generated from surface topography has a strong influence on reducing near-surface wind speeds.

Wind speed has a direct influence on sand flux. Stronger winds result in a higher rate of sediment transport (Anderson and Walker, 2006; Hoonhout and de Vries, 2017; Bauer *et al.*, 2012). However, although the wind speeds in P5 and P6 were similar during the sediment transport runs, sand flux in P6 was on average 575 times greater than in P5. This can be attributed to the devegetated foredune upwind of P6, resulting in the release of sediment from the foredune. The higher vegetation cover on the foredune upwind of P5 reduces the rate of foredune erosion and as a result, minimal sediment was transported inland. As well as this, the large amount of sediment stored downwind of the foredune (Chapter 3) is an additional source of sediment that is not present in P5. Due to the large differences in sand flux recorded in the P5 and P6 deflation surfaces, it is clear foredune devegetation and the resultant differences in foredune morphologies has had a direct influence on aeolian sediment transport at Mason Bay. Walker *et al.* (2013) identified aeolian activity as a key indicator of mobile dune systems. Therefore, these results show foredune devegetation has increased the dynamism of the Mason Bay dune system.

Aeolian sediment transport is highly variable in space and time. This was exhibited by the variation between runs at Mason Bay. For example, the runs comparing sediment transport on the foredune upwind of P5 and P6 (Table 4.4). Although the wind speed during these two runs was similar, the rate of sediment flux was 3 times greater in the

second run. Furthermore, traps deployed at the same locations for the same runs, separated by 5-10 m, trapped different quantities of sand. These results are consistent with findings from previous research. Jackson *et al.* (2006) identified spatial variability in sediment transport rates of 200% over a distance of 4 m. Spatial variability of sediment transport is a result of a number of factors, including variation in wind speed, direction, vegetation, surface moisture, sediment properties and topography (Hesp, 1999; Jackson *et al.*, 2006; Nordstrom *et al.*, 2007). Temporal variability can be attributed to variations in wind, sediment and other environmental factors (Alcantara-Carrio and Alonso, 2002). There was large variability in wind speeds recorded in the deflation surfaces. Within a few seconds, wind speeds varied over 5 ms^{-1} and the standard deviations for the mean wind speeds during each run were higher in the deflation surfaces than the foredune. The higher variability in the deflation surfaces can be attributed to the influence of the topography between the foredune and centre of the deflation surface. Sediment flux is not continuous, and therefore, will not always be directly correlated with the strongest wind speeds (Smyth *et al.*, 2014). Consequently, the sediment flux recorded in the results are primarily indicative of the point in time the runs were completed. However, they provide a reasonable estimate of the amount of sediment transported through the parabolics during strong onshore wind events.

Aeolian sediment flux from the rear of the beach through to the apex of P6 was also analysed to identify the source of transported sediment during an onshore wind event. Sediment flux on the beach was minimal, less than 0.018 $kg/m^2/min$ was estimated to be transported. This shows the main source of sediment transported through the parabolic dune was not the beach. Sediment flux recorded on the foredune crest was higher than the beach (between 0.48-0.51 $kg/m^2/min$), showing the stoss face of the foredune was eroding during the event, consistent with the findings from Chapter 3. However, the sediment flux in the deflation surface and depositional lobe was almost 3 times greater than the foredune (between 0.90-1.65 $kg/m^2/min$ was transported). Smyth *et al.* (2014) investigated sediment transport within a blowout. They found sediment transport within the deflation basin was lowest at the throat of the basin and increased with distance inside the deflation basin. The increase in sediment transport with distance inland was attributed to a cascading saltation effect. Entrainment of sediment initiated in the deflation surface increases the rate of sediment transport and this process is enhanced with distance inland, as sand is entrained within the saltation cloud (Smyth *et al.*, 2014). At Mason Bay, it is

likely the sediment eroded from the stoss face of the foredune initiates further sand transport across the lee slopes of the foredune and into the deflation surface. This activates the sediment in the lee of the foredune and seaward half of the former deflation surface, which entrains sand as it is transported across the deflation surface, increasing saltation across the landward half of the deflation surface. Sun *et al.* (2016) found that sediment transport within a blowout was highest at the top of the depositional lobe. While there has been research of sediment transport within blowouts, very limited empirical data has been collected on sediment transport within a parabolic dune. Delgado-Fernandez *et al*. (2018) studied the sediment transport within a parabolic dune during a high wind event. They also found that sediment transport was largest along the deflation basin, where transport was large and continuous.

Chapter 3 established that about half of the sediment eroded from the foredune since 2010 has been deposited in the lee of the foredune and within the P6 deflation surface. However, the results from the experiments showed sediment transport increased with distance inland. Onshore winds of the strength observed during the experiments (> 15 ms^{-1}) occur 10% of the time at Mason Bay, whereas lesser wind events (8-12 ms^{-1}) occur more frequently (30% of the time) (Fig. 4.20). A two-staged model is proposed (Fig. 4.21). During lesser wind events, sand is eroded from the stoss face of the foredune and deposited in the lee of the foredune and into the seaward half of the P6 deflation surface. This is because winds of this magnitude are not strong enough to cause the cascading saltation effect described above. During stronger wind events (>15 ms^{-1}), the sand eroded from the stoss face of the foredune is transported across the lee slope of the foredune and activates the sediment deposited here, as it becomes entrained within the saltation cloud and transported downwind. This in turn increases saltation with distance inland as it is transported across the deflation surface. This sand is primarily deposited in the depositional lobe and a small proportion (2%) is transported further inland, beyond the parabolic dunes. In contrast, the *A. arenaria* foredune prevented sediment transport over the foredune and sand was primarily deposited within the foredune complex (Fig. 4.21).

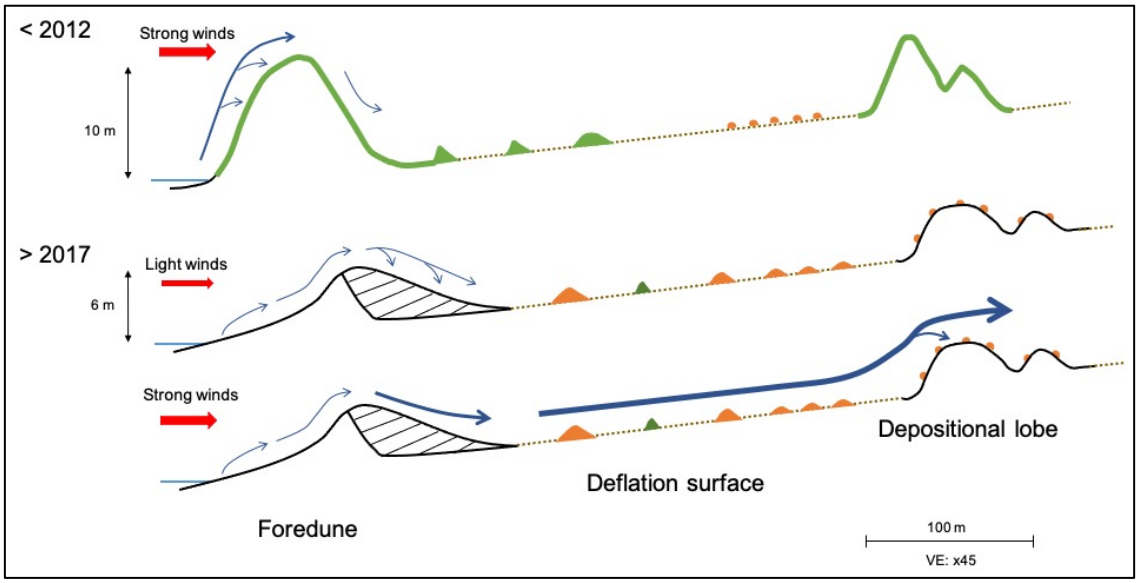

Figure 4.21: Conceptual diagram of aeolian sediment transport through a foredune-parabolic dune complex under different onshore wind conditions and foredune morphologies. a) an *A. arenaria* vegetated foredune during strong winds (> 15 ms^{-1}); b) a devegetated foredune during light winds (8-12 ms^{-1}); c) a devegetated foredune during strong winds (> 15 ms^{-1}). The wider the arrow, the higher the rate of sediment transport.

The rate of sediment transport through P6 at Mason Bay was similar to empirical data collected at other locations. Delgado-Fernandez *et al.* (2018) recorded sediment transport through a parabolic dune in the Sefton Dunes, North West England and found that the average rate of sediment transport was 0.732 kg/m/min. The values recorded at Mason Bay were higher, averaging between 1.17-1.596 kg/m/min in the deflation surface. However, wind speeds recorded during the runs were 4-8 ms^{-1} higher at Mason Bay, leading to higher rates of sediment transport. Smyth *et al.* (2014) recorded sediment flux in a number of traps through a blowout. Rates of sediment transport recorded in the traps were highly variable ranging from 7.20-30.17 g/min. Sediment transport recorded in the lowest trap in the deflation surface and depositional lobe in P6 ranged between 20-56 g/min. Therefore, sediment transport was greater at Mason Bay, however, as with the previous comparison, the wind speeds were also about 10 ms^{-1} higher at Mason Bay. The estimates of sediment transport rates at Mason Bay were also for a parabolic dune adjoining a devegetated foredune and this likely also contributed to the differences observed as the source of sediment in the lee of the foredune is greater (Fig. 4.21). However, these comparisons show that wind speeds do have a strong correlation with

rates of aeolian sediment transport and the importance of collecting empirical data to understand site-specific sedimentation processes.

Furthermore, the results showed that the rate of sediment transport was similar in the deflation surface and depositional lobe. This is consistent with findings from Chapter 3 that showed there has been little deposition in the landward half of the deflation surface of P6. This is likely because of the increased exposure with distance inland, as the deflation surface slopes upwards and the influence of the foredune on airflow is reduced. These results prove that sediment is being transported right through the parabolic dune during strong wind events, primarily deposited within the sparse cover of *F. spiralis* in the depositional lobe and a small proportion (2%) transported beyond this, into the wider dune system.

4.5 Conclusion

This chapter has discussed the rates and patterns of sedimentation at Mason Bay. Sediment transport experiments were completed during strong onshore incident wind events to compare sediment transport downwind of a vegetated and devegetated foredune and to understand the source of sediment transported within a devegetated parabolic dune.

Foredune devegetation has clearly influenced the rate of sediment transport at Mason Bay. The removal of *A. arenaria* from the foredune upwind of P6 has resulted in the release and downwind transport of sediment. The rate of sediment transport in the P6 deflation surface was considerably greater than in the P5 deflation surface. This shows *A. arenaria* has a strong influence on sedimentation processes at Mason Bay and the removal of *A. arenaria* is re-activating dynamic processes within the dune system.

Sediment transport from the beach through to the depositional lobe of P6 was also investigated during a strong onshore wind event. Sediment flux recorded at the rear of the beach was low (less than 0.018 kg/m^2/min). Sediment flux recorded on the foredune crest was higher, consistent with measured rates of foredune stoss erosion (0.48-0.51 kg/m^2/min). However, sediment transport within the deflation surface and depositional

lobe of P6 was much greater than the foredune (0.90-1.65 kg/m^2/min). Therefore, sediment eroded from the foredune during the experiments was not the primary source of sand captured in traps further inland during the experiments. This is due to a cascading saltation effect that leads to an increased entrainment of sediment with distance inland during strong winds. It was proposed that lower wind speed events (8-12 ms^{-1}) play an important role in depositing sediment in the lee of the foredune and within the deflation surface and during stronger wind events (>15 ms^{-1}), observed during the experiments, this sediment is transported further inland.

Chapter 5

Impact of foredune devegetation on deflation surface plant communities

5.1 Introduction

Chapter 3 demonstrated that foredune devegetation reactivates dynamic geomorphic processes, namely foredune erosion and downwind deposition. The development of the *A. arenaria* foredune at Mason Bay resulted in a sediment supply deficit downwind of the foredune and the development of dune slack plant communities in the deflation surfaces of the parabolic dunes (Petersen *et al.*, 2011; Konlechner *et al.*, 2016; Buckley *et al.*, 2016). Chapter 3 established there has been an increase in sediment deposition downwind of the destabilised foredune in P6. The impact this has had on deflation surface plant communities is examined in the current chapter.

The dynamic restoration project at Mason Bay provides a unique opportunity to understand the impact of foredune devegetation and increased downwind deposition on plant communities. The different treatment histories of the foredune have resulted in a difference in downwind sedimentation patterns as the deflation surface in P6 has received more sand compared to P4 and P5 (Chapter 3). This chapter describes the changes in the plant communities in the deflation surfaces of P4, P5 and P6 between 2015 and 2020 and relates these changes to patterns of sand accumulation.

The deflation surface habitat is less exposed than the foredune environment, experiences lower rates of accretion and is closer to the water table, where ponds and lakes can form, sometimes permanently (Wiedemann and Pickart, 2004). In Mason Bay, the deflation surfaces formed relatively recently, between 1958 and 1978, along with the formation of the parabolic dunes following the introduction of *A. arenaria* (Hesp *et al.*, 2012; Hart *et*

al., 2012). The deflation surfaces are relatively stable environments compared to the surrounding dunal landscapes, and thus, are associated with a greater species richness (Konlechner *et al.*, 2016). There are three functional groups present in the deflation surfaces at Mason Bay: primary dune builders, intermediate dune colonisers and dune slack species. The most common group present are the dune slack species. These species have the lowest tolerance to burial.

The aim of this chapter is to understand the influence of foredune devegetation and mobilisation on deflation surface plants and plant communities at Mason Bay. Foredune devegetation at Mason Bay has provided a rare opportunity to understand the implications on downwind plant communities, including how they respond to the transition from a deflation surface to dunal landscape. Following the devegetation of the foredune adjacent to P6, sand has slowly been released from the foredune complex and transported downwind. The findings in Chapter 3 showed that about 50% of this sediment has been deposited in the lee of the foredune and within the seaward half of the P6 deflation surface. Therefore, it is inevitable that the increase in sand accretion within the deflation surfaces following foredune devegetation will have an effect on the deflation surface plant communities, selecting for species that can tolerate higher levels of burial (Maun, 1998). The response of the deflation surface plant communities will provide an indication of the burial threshold these plants are able to tolerate and an understanding of the rate of change in the plant communities.

This chapter will address the following hypotheses to understand the impact of foredune devegetation on downwind plant communities:

i. The plant community composition in P6 will change in response to an increase in sand accumulation. It is expected that the type of species present in P6 will be different to those in P4 and P5. This includes a reduction in dune slack and herbaceous species in P6 and an increase in sand binding species, particularly *F. spiralis*. This is because it is expected the rate of burial that has occurred between 2015 and 2020 will be too great for the low-lying, dune slack species to survive (response (a) in Fig. 2.5). It is also predicted there will be a reduction in plant species diversity in P6, as this occurred following dynamic restoration at Doughboy Bay

(Konlechner *et al.*, 2014). It is expected there will be a difference in the plant community composition between the landward (eastern) and seaward (western) plots, as these plots are exposed to different environmental conditions.

ii. It is also hypothesised that there will be a change in the abundance of species present in P6. It is expected that the seaward plot in P6 will decrease in vegetation cover, as a large portion of sediment transported from the foredune has been deposited here. It is expected there will be no major change in vegetation cover in P4 and P5 as there has been less sediment deposited in these deflation surfaces (Chapter 3).

This chapter outlines methods used to survey vegetation in the deflation surfaces at Mason Bay between 2015 and 2020 and the methods used to analyse this data. The results will then be described to determine how the plant communities in the deflation surfaces have responded to foredune devegetation. These results will be discussed to explain the patterns identified.

5.2 Methods

Vegetation in the deflation surfaces of the parabolic dunes in Mason Bay have been monitored since 2015. Research completed for this thesis builds on this existing dataset to analyse the changes in plant communities in the deflation surfaces between 2015 and 2020. Due to the slow release of sediment from the foredune upwind of P6 (Chapter 3), the surveys included the deflation surface plant community composition before large quantities of sediment had been deposited in the P6 deflation surface. Therefore, this provided the opportunity to determine the impact of increased sand accumulation on deflation surface plant communities.

5.2.1 Vegetation surveying

In 2015, six plots were established in the deflation surfaces of P4, P5 and P6 (Fig. 5.1). In each deflation surface, one plot was located seaward, in the lee of the foredune and one plot was located landward, near the apex of the parabolic. The plots were aligned with the long axis of the deflation surfaces to only include deflation habitats. The seaward

and landward plots in the three parabolics were aligned so they could be compared directly, representing a similar distance from the foredune in each deflation surface. This provided consistency in the environmental conditions exposed to the seaward and landward plots, and therefore, the primary difference between the plots was patterns of sediment deposition. Each plot contained 25, 2x2 m quadrats, separated by 10 m, in an 80 m^2 grid (Fig. 5.2). As the foredune upwind of P4 and P5 was not sprayed at the same time as P6 (described in Chapter 1), the plots in P4 and P5 were used to represent the plant communities where the impacts of foredune destabilization have been minimal (i.e., a control). The plots in P6 were used to show the response of plant communities to increased sand accumulation due to the destabilization of the foredune (treatment unit).

The grid-point intercept method was used to survey the quadrats (Godínez-Alvarez *et al.*, 2009). This was completed using a 1x1 m frame, made of PVC pipe, with a 10 cm x 10 cm grid. There was a total of 81 intercept points in each 2x2 m quadrat. The total number of intercepts on the grid was recorded for each species. The presence of species within the quadrats was also recorded, regardless of whether they intercepted with a line on the grid. Five surveys were completed in August 2015, November 2016, August 2018, August 2019 and August 2020, covering a 6-year time period. The surveys were completed at a similar time of the year to achieve consistency in the environmental conditions across the surveys, to reduce the influence of factors other than sedimentation on plant species presence. The surveys in 2015, 2016 and 2018 were completed prior to the commencement of this thesis and the surveys in 2019 and 2020 were completed by the author. The survey completed in 2018 only recorded the presence of species in the quadrats.

The plots that were established in the deflation surfaces provide a representation of the plant communities in this environment. The seaward plots are closer to the foredune, and therefore, sedimentation processes have a greater influence on these plots. The landward plots are closer to the apex of the parabolic and are more exposed. The soil in the landward plots is predominantly a stony substrate, whereas the seaward plots are sandier and have a higher presence of nabkha, which predominantly formed with *A. arenaria.*

It was expected overtime the plant communities in the P6 plots would become increasingly different from the P4 and P5 plots. This is because the sand accumulation

that has occurred in the P6 deflation surface (described in Chapter 3) will select for dune flora rather than deflation surface species. Therefore, it is expected there will be a correlation with the changes in plant species and increased sand accumulation, due to the selective force of burial, described by Maun (1998).

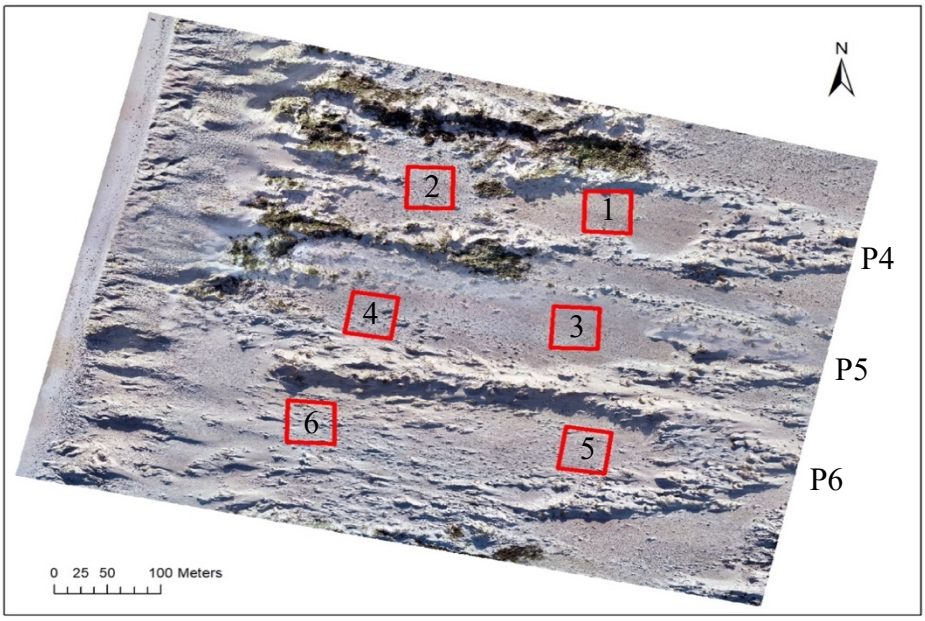

Figure 5.1: Location of the six plots in the deflation surfaces of P4, P5 and P6. The plots consist of 25, 4 m^2 quadrats, that were surveyed using the grid-point intercept method between 2015 and 2020. The plots are 80 m^2 in area. 1) landward P4; 2) seaward P4; 3) landward P5; 4) seaward P5; 5) landward P6; 6) seaward P6.

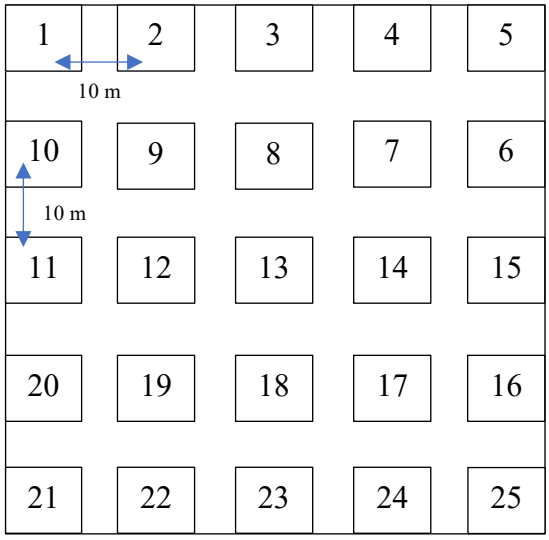

Figure 5.2: Grid layout of quadrats in each plot. There are 25, 2x2 m quadrats in each plot, separated by 10 m. Quadrat 1 is in the NE corner of the plot. The quadrats were surveyed using the grid-point intercept method.

5.2.2 Photographic timeseries

Ground photos of the plots were taken in 2015 and relocated in early 2021. The photos were taken at the same angle and scale to provide a comparison to identify visual changes in the plots over the study period.

5.2.3 Data analysis

Vegetation data analysis

The data collected between 2015 and 2020 was analysed and compared to identify changes in the plant communities across the six plots. Species richness, vegetation cover, the Shannon-Wiener diversity index and the Jaccard similarity index were calculated at the plot scale for each survey. Species richness was calculated by totalling the number of species present in each plot or quadrat. This included species that did not intercept with a point on the grid. The percentage of vegetation cover was established from the species abundance. The abundance was calculated from the number of intercepts for each species. The Shannon-Wiener diversity index, widely used to determine species diversity, was used to show the change in plant community diversity through time (Shannon, 1948; Magurran, 1988). This index accounts for the species richness and their relative abundance. It is calculated from the following equation:

$$H' = -\sum_{i=1}^{s} p_i \ln p_i$$

Where p_i = the proportion of individuals that belongs to species *i* and s = the total number of species.

The Jaccard similarity index was used to show the similarity in the plant communities between the years surveyed. This index is the proportion of species that are shared across the years surveyed, described by Real and Vargas (1996). Each year was compared with the previous year to calculate the similarity index over the study period (e.g., 2015 was compared with 2016, 2016 was compared with 2018 etc.). The equation used to calculate this similarity index is:

$$SJ = \frac{c}{(a + b + c)}$$

Where a and b are the number of species present in each year surveyed and c is the number of shared species present in both years surveyed.

The average abundance of each species in a quadrat was calculated for the 2015 and 2020 surveys. This was calculated by averaging the abundance across all of the quadrats surveyed (n=150). The Wilcoxon signed-rank test was used to determine whether there was a statistically significant difference between the abundance of each species in 2015 and 2020. This test was used because the data was not normally distributed and, therefore, a non-parametric test was required, as described in Shieh *et al.* (2007). The calculations were completed using IBM SPSS Statistics software. For species where the sample size was too small (below 5), a significant difference could not accurately be calculated.

The relative importance of the species in each plot in 2015 and 2020 was calculated. The relative importance is the ratio between the proportion of quadrats where species *i* occurs divided by the total number of quadrats (25) and the abundance of the species, calculated from the abundance of a species in a plot, divided by the total abundance of all species. This is described in Magurran (1988). The rank abundance graphs show which species are most dominant within the plots. The steeper the curve, the more dominant a species. The species were ranked, with 1 being the most dominant species present, then plotted on a logarithmic scale.

The species present in the plots were categorised into three functional groups: primary dune builders, intermediate dune colonisers and dune slack species, to show the change in vegetation cover of each of these groups between 2015 and 2020. This was based on their structural class. As *F. spiralis* is one of the primary native dune builders in New Zealand, it was placed in this category. The remaining sedges and shrubs were categorised as intermediate dune colonisers and the herbs, rushes and moss were classed as the dune slack species.

The vegetation cover of the three most common structural groups present in the deflation surfaces: herbs, shrubs and sedges was also calculated. This was based on the abundance data for each year vegetation was surveyed, 2015, 2016, 2019 and 2020. This was completed to determine the influence of increased sand accumulation on these three groups. Sedges have the highest tolerance to burial (cm-dm per year) whereas herbs have the lowest tolerance to burial (mm per year). Therefore, it was expected there would be a difference in the change in vegetation cover between the different groups over the survey period due to the differences in tolerance to burial.

The average species richness for each line of quadrats in each plot was also calculated for the 2015 and 2020 data by averaging the number of species present in each quadrat for each line. There were five lines in each plot, containing five quadrats (Fig. 5.2). These were plotted together, with the western-most line, closest to the sea in the plot (quadrat number 21-25) identified as line 1 and the eastern-most line, furthest from the sea (quadrat number 1-5) identified as line 5. This was completed to determine whether there was a pattern of species richness with distance from the sea.

A. arenaria, *Poa billardierei* and two unidentified grasses were not included in the vegetation analysis. This is because these are all grasses and the herbicide that has been applied to the dunes at Mason Bay is grass-specific. Hence, the changes in abundance of these species may have been influenced by the application of herbicide and not necessarily burial. Therefore, any changes in abundance of these species would not reflect their natural response to increased burial.

Sedimentation analysis

The changes in plant community composition were related to changes in sedimentation to understand the influence of burial on the plant species present in the deflation surfaces. The digital elevation models presented in Chapter 3 were used to calculate sand accumulation for each quadrat. The same method used in Chapter 3 to calculate the change in elevation for the survey area was used to calculate these changes. The area of each quadrat was clipped from the 2015 and 2020 DEM. Using the Cut Fill tool in ArcGIS™, the 2020 DEM was taken away from the 2015 DEM to calculate the change in volume for each quadrat. The volumes were then converted into an average change in elevation. The change calculated was interpreted as erosion if the elevation had decreased and accretion if the elevation had increased. Sedimentation in each quadrat was compared with the analysis of changes in plant communities in the plots to determine if there was a relationship between burial and plant community composition.

The abundance of *F. spiralis* and *R. hookeri var. hookeri* in 2020 were compared with the sand accumulation in each individual quadrat between 2017 and 2020. These species were used as key indicator species because *F. spiralis* is the primary native sand binding species at Mason Bay and is expected to show a positive response to the increase in burial. *R. hookeri var. hookeri* was selected because it is the most dominant dune slack

species in the deflation surfaces at Mason Bay and understanding the response of this species to increased burial will provide an indication of the response of other dune slack species. The sand accumulation was calculated for every quadrat by using the change in elevation from the 2015 and 2020 DEM. The sand accumulation was converted into a yearly average change in elevation over a three-year period, between 2017 and 2020, by dividing the total sand accumulation by three. 2017 was used because, as established from the topographical profile change of P6 in Chapter 3 (Fig. 3.11), this is when sand started to enter the P6 deflation surface. The abundance was calculated by dividing the number of intercepts of the species by the total number of intercepts (81) for each quadrat. This was then converted into a percentage. The abundance of *F. spiralis* and *R. hookeri var. hookeri* in every quadrat was plotted against the sand accumulation for the corresponding quadrat in the landward and seaward plots. This showed the relationship between the sand accumulation that had occurred in each quadrat, with the abundance of *F. spiralis* and *R. hookeri var. hookeri*. *R. hookeri var. hookeri* was not present in the seaward plot in P6 in 2020, thus, no comparison with the abundance and sand accumulation was completed for this species in this plot.

5.3 Results

5.3.1 Plot-scale changes between 2015-2020

In the surveys completed in the plots in the deflation surfaces in 2015 and 2020, there were 21 plant species present (Table 5.1). In 2015, 18 species were recorded and in 2020, 16 species were recorded. Of these species, 13 were herbs and 4 were sedges. Seven of these species are classified as 'nationally vulnerable' or 'threatened' by the New Zealand Threat Classification System (Table 5.1) (de Lange *et al.*, 2017). The vegetation cover in all plots was relatively low (below 25%) (Fig. 5.4).

The greatest change in species richness was in the seaward plot in P6 (Fig. 5.3). Species richness in this plot declined from 17 species in 2015 to 5 species in 2020. In contrast, the seaward plots in P4 and P5 have maintained a higher species richness, with 13 and 15 species present in 2020. This shows there is a clear difference in the species richness in the seaward plots. There was also a difference in species richness between the landward and seaward plots. There were 5 and 6 more species present in the seaward plots in P4 and P5 in 2020 compared to the landward plots and this trend was consistent throughout the survey period. The opposite occurred in P6 where the landward plot had a higher species richness. These results indicate the sediment that has been deposited in the seaward half of the P6 deflation surface has influenced the species richness in the seaward plot.

The total vegetation cover was below 25% in most plots across the survey period (Fig. 5.4). The vegetation cover in the seaward plot in P6 was similar to the seaward plots in P4 and P5 in 2015, however, decreased steadily between 2015 and 2020. In 2020, the vegetation cover in the P6-S plot was less than 5%, indicating that it is now mostly covered in bare sand as sediment from the eroding upwind foredune has been deposited within this plot. Vegetation cover in the seaward plots in P4 and P5 was higher than the landward plots and in contrast to the reduction in cover in the P6-S plot, the vegetation cover in the other plots has only slightly fluctuated throughout the years.

The 'similarity index' expresses the similarity in the plant species recorded between each year surveyed. The majority of the plots in the deflation surfaces have become more

similar or showed little change in similarity between 2015 and 2020 (Fig. 5.5). The largest decrease in similarity was in the seaward plot in P6, which has slightly decreased in similarity over the six-year survey period (0.5 in 2015 to 0.4 in 2020), showing the plant species present in this plot have become increasingly different overtime. These results indicate that the sand accumulation that has occurred in the lee of the foredune has influenced the plant communities in this plot. The landward plots in P4 and P6 had the largest increase in similarity, particularly between 2018 and 2020.

The species diversity was consistent across the years surveyed in all plots, except for the seaward plot in P6 (Fig. 5.6). Species diversity in this plot steadily declined from 2.57 in 2015 to 1.42 in 2020. The diversity in the seaward plots in P4 and P5 was about 0.5 higher than the landward plots. This shows the deflation surface habitat closer to the foredune is suitable for a higher number of species compared to the landward half of the deflation surfaces.

The differences in the variables described above show the largest change in the deflation surfaces has occurred in the seaward plot in P6. The plots in the P4 and P5 deflation surfaces showed slight fluctuations, likely due to natural variability. In contrast, the differences in species richness, diversity and vegetation cover in the seaward plot in P6, which have not occurred in any other plot, have clearly been influenced by the sand accumulation that has occurred in the plot.

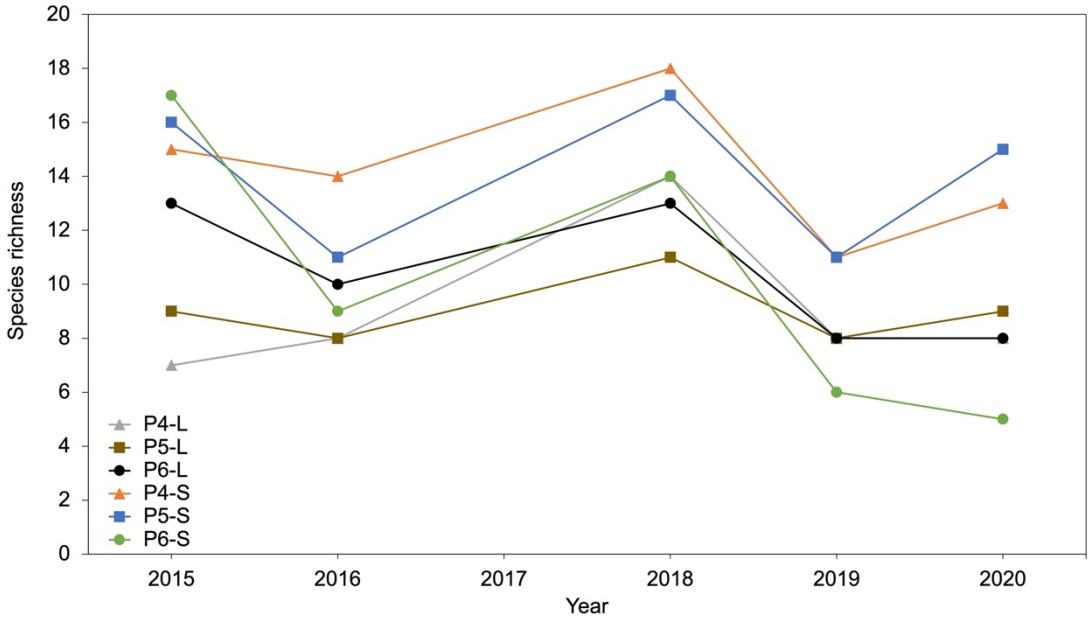

Figure 5.4: Species richness (total number of species present in the landward (L) and seaward (S) plots in P4, P5 and P6 between 2015 and 2020. Surveys were completed in 2015, 2016, 2018, 2019 and 2020.

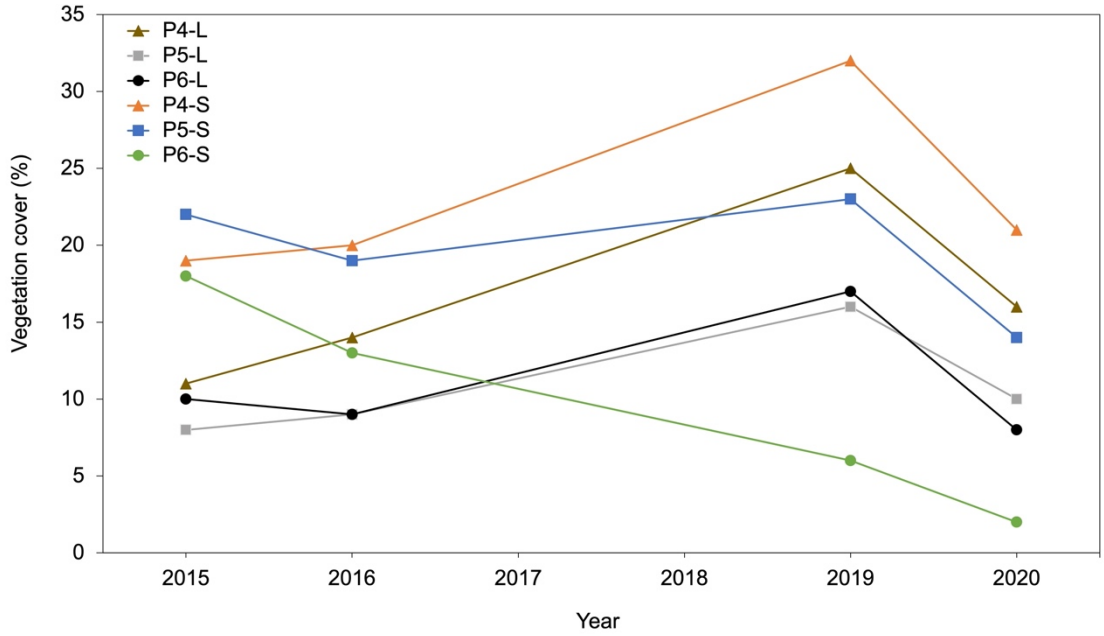

Figure 5.3: Vegetation cover (%) in the landward (L) and seaward (S) plots in P4, P5 and P6 between 2015 and 2020. Vegetation cover was calculated from the abundance of vegetation in the quadrats. Surveys were completed in 2015, 2016, 2019 and 2020.

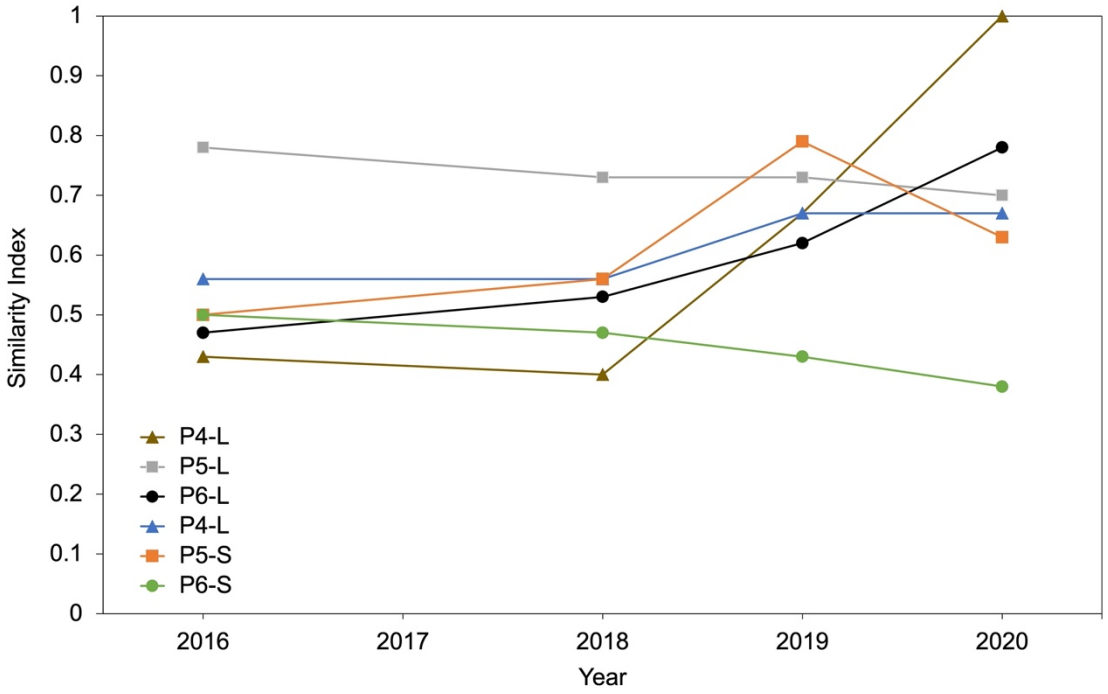

Figure 5.5: Jaccard similarity index calculated for the years surveys were completed in the landward (L) and seaward (S) plots in P4, P5 and P6. Each year represents the similarity with the previous year.

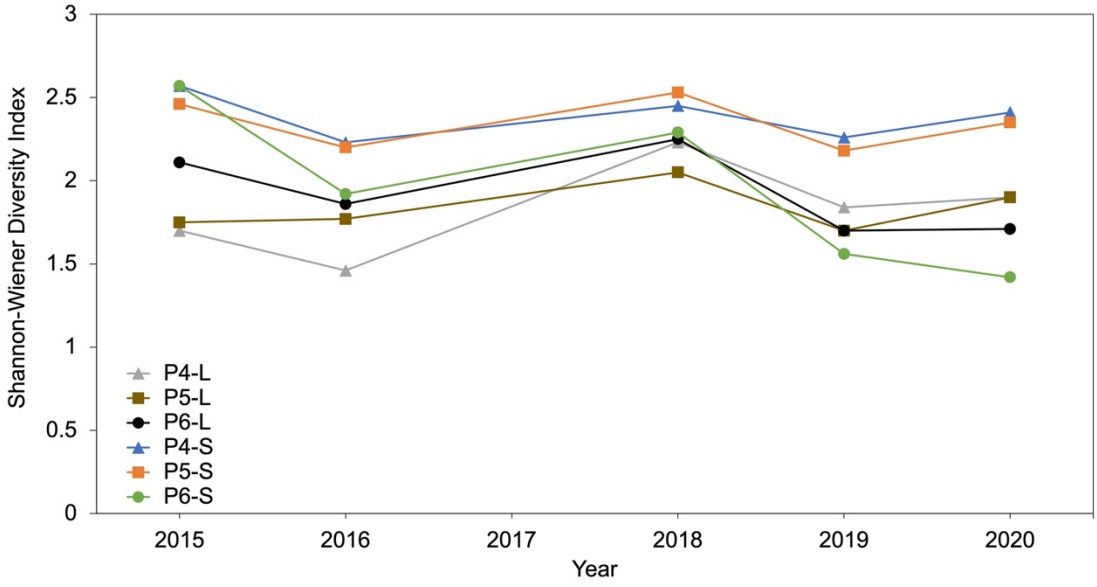

Figure 5.6: Shannon-Wiener diversity index for the landward (L) and seaward (S) plots in P4, P5 and P6 between 2015 and 2020. Surveys were completed in 2015, 2016, 2019 and 2020.

The photographs of the plots show that between 2015 and 2021 the plots have become increasingly sandier (Figs. 5.7-5.12). There has been an increase in the dominance of *F. spiralis*. In particular, *F. spiralis* nabkha have increased in size and number, as the presence of *F. spiralis* in the deflation surfaces has promoted the deposition of sand. The landward plots in P4 and P5 have had less sand accumulation compared to the seaward plots. This is in contrast to the landward plot in P6 where there has been a higher rate of deposition, leading to *F. spiralis* thriving and the development of a number of *F. spiralis* nabkha (Fig. 5.11).

The seaward plot in P6 experienced the greatest change between 2015 and 2021 (Fig. 5.12). This is expected since, as established in Chapter 3, there has been a high amount of sediment deposited in the lee of the foredune upwind of P6 and within the seaward plot in this parabolic. Between 2015 and 2021, the landscape has changed from a stony deflation surface to mainly bare sand, with occasional *F. spiralis* present. The plot represents a more hummocky, dunal landscape, predominantly associated with the presence of *F. spiralis*, as opposed to the deflation surface present in 2015.

Figure 5.7: Photograph of the landward plot in P4 (P4-L) in a) 2015 and b) 2021 (source: Teresa Konlechner).

Figure 5.8: Photograph of the seaward plot in P4 (P4-L) in a) 2015 and b) 2021 (source: Teresa Konlechner).

Figure 5.9: Photograph of the landward plot in P5 (P5-L) in a) 2015 and b) 2021 (source: Teresa Konlechner).

Figure 5.10: Photograph of the seaward plot in P5 (P5-S) in a) 2015 and b) 2021 (source: Teresa Konlechner).

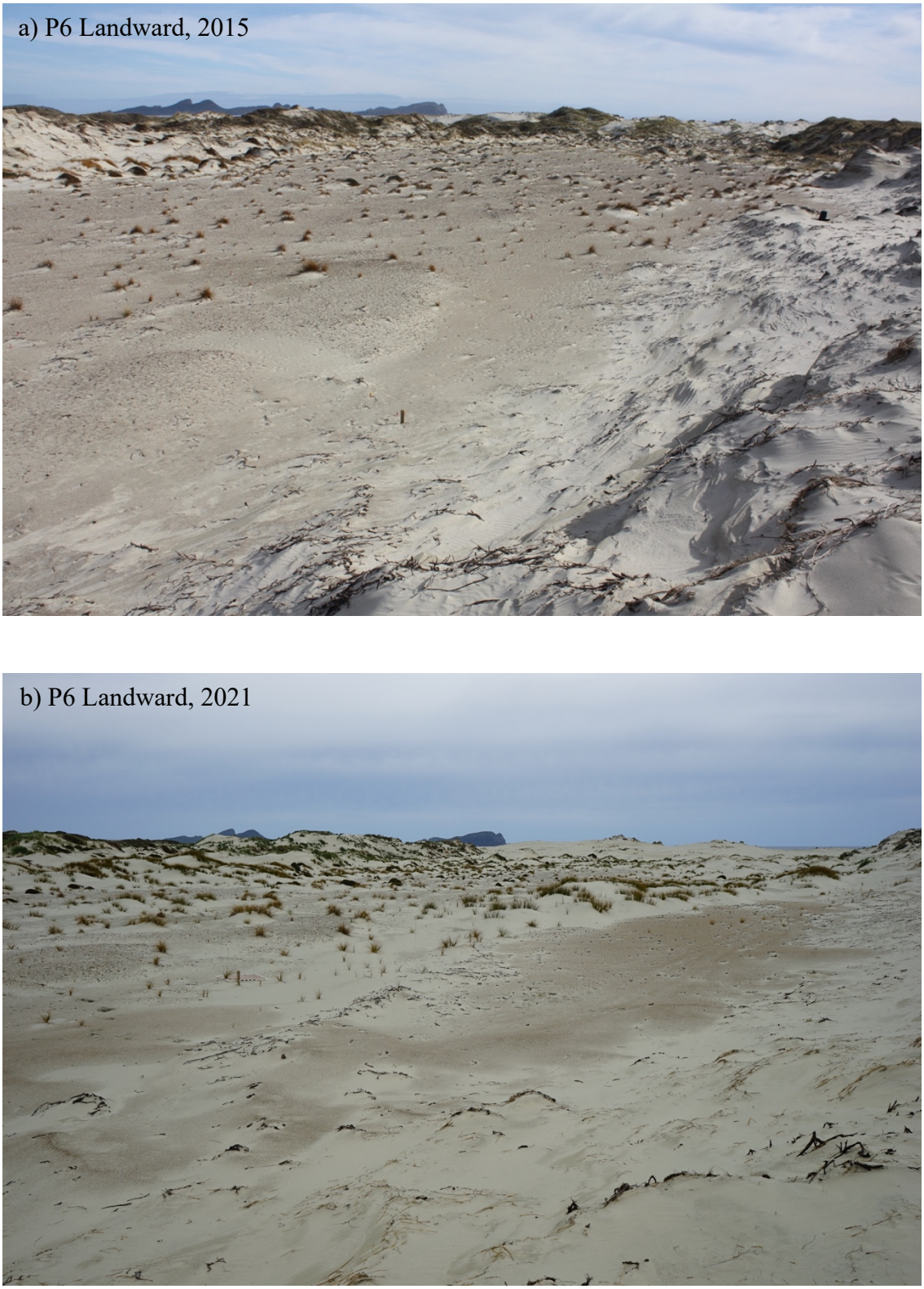

Figure 5.11: Photograph of the landward plot in P6 (P6-L) in a) 2015 and b) 2021 (source: Teresa Konlechner).

Figure 5.12: Photograph of the seaward plot in P6 (P6-S) in a) 2015 and b) 2021 (source: Teresa Konlechner).

5.3.2 Changes in plant communities between 2015 and 2020

Table 5.1: Species present in the surveys completed in 2015 and 2020, their structural class and functional type at Mason Bay and risk status according to the New Zealand Threat Classification system (de Lange *et al*., 2017). Three categories are recognised: primary dune builder, intermediate dune coloniser and dune slack species.

Species name	**Structural class**	**Functional type**	**Risk status**
Ficinia spiralis	Sedge	Primary dune builder	At risk
Carex flagellifera	Sedge	Intermediate dune coloniser	Not threatened
Coprosma acerosa	Shrub	Intermediate dune coloniser	At risk
Ficinia nodosa	Sedge	Intermediate dune coloniser	Not threatened
Isolepis cernua	Sedge	Intermediate dune coloniser	Not threatened
Pimelea lyallii	Shrub	Intermediate dune coloniser	At risk
Apium prostratum subsp. prostratum var. filiforme	Herb	Dune slack	Not threatened
Catsear	Herb	Dune slack	Not threatened
Colobanthus muelleri	Herb	Dune slack	Not threatened
Craspedia robusta var. pedicellata	Herb	Dune slack	Naturally uncommon
Epilobium komarovianum	Herb	Dune slack	Not threatened
Gentianella saxosa	Herb	Dune slack	Naturally uncommon
Hydrocotyle microphyilla	Herb	Dune slack	Not threatened
Lilaeopsis novae-zelandiae	Herb	Dune slack	Not threatened
Luzula banksiana var. banksiana	Rush	Dune slack	Not threatened
Moss	Moss	Dune slack	n/a
Myosotis pygmaea	Herb	Dune slack	At risk
Pratia angulata	Herb	Dune slack	Not threatened
Ranunculus acaulis	Herb	Dune slack	Not threatened
Ranunculus recens	Herb	Dune slack	Nationally vulnerable
Raoulia hookeri var. hookeri	Herb	Dune slack	At risk

Table 5.2: Species lost and gained from the landward and seaward plots in P4, P5 and P6 between 2015 and 2020. Species lost were present in 2015 but not present in 2020 and species gained were not present in 2015 but present in 2020.

Plot	Lost	Gained
Landward P4	*Carex flagellifera*	*Ranunculus recens*
	Catsear	*Luzula banksiana var. banksiana*
		Moss
Seaward P4	*Craspedia robusta var. pedicellata*	*Epilobium komarovianum*
	Carex flagellifera	*Isolepis cernua*
	Ranunculus acaulis	
Landward P5	*Carex flagellifera*	*Luzula banksiana var. banksiana*
		Moss
Seaward P5	*Carex flagellifera*	*Isolepis cernua*
	Craspedia robusta var. pedicellata	*Lilaeopsis novae-zelandiae*
	Apium prostratum subsp. prostratum var. filiforme	*Myosotis pygmaea*
Landward P6	*Gentianella saxosa*	
	Carex flagellifera	
	Myosotis pygmaea	
	Luzula banksiana var. banksiana	
Seaward P6	*Raoulia hookeri var. hookeri*	
	Gentianella saxosa	
	Moss	
	Carex flagellifera	
	Myosotis pygmaea	
	Luzula banksiana var. banksiana	
	Ficinia nodosa	
	Craspedia robusta var. pedicellate	
	Colobanthus muelleri	
	Hydrocotyle microphyilla	
	Pimelea lyallii	

The majority of the species present in the deflation surfaces are herbs and dune slack-specific species (Table 5.1). These species are tolerant to low levels of burial (mm/yr). The shrubs and sedges were classified as intermediate dune colonisers and are tolerant to cm of burial per year. *F. spiralis* is the only sand binder present in the Mason Bay dune system (excluding *A. arenaria*), and thus, was classified as a primary dune builder. *F. spiralis* is tolerant to the highest level of burial out of the species listed. Eight of the species present in the Mason Bay deflation surfaces are classified as 'nationally vulnerable', 'at risk' or 'naturally uncommon' (de Lange *et al*., 2017).

Between 2015 and 2020, the landward plots have lost fewer species compared to the seaward plots (Table 5.2). The majority of the plots have lost more species than they have gained, excluding the landward plots in P4, which gained 3 species, and P5, which gained 2 species. *C. flagellifera* was present in all plots in 2015, however, by 2020 was lost from all plots. The plots in P6 are the only plots that have not gained any species over the six-year survey period. The greatest loss of species has occurred in the seaward plot in P6, where 11 species have been lost. The majority of the species that have been lost in this plot are dune slack species.

Table 5.3: Results showing the number of plots (n = 6) species were present in 2015 and 2020, the mean vegetation cover (%) of each species, averaged over every quadrat surveyed (n = 150) and p-value (significance at p <0.05) calculated from the Wilcoxon signed-rank test. * Indicates a significant difference between the abundance in 2015 and 2020.

Species name	**2015 plots present**	**2015 mean cover (%)**	**2020 plots present**	**2020 mean cover (%)**	**P-value**
Apium prostratum subsp. prostratum var. filiforme	1	0.007	0	0	n/a
Carex flagellifera	6	0.618	0	0	<0.001*
Catsear	4	0.264	4	0.116	0.001*
Coprosma acerosa	6	4.983	6	2.471	<0.001*
Colobanthus muelleri	6	1.094	5	1.478	0.603
Craspedia robusta var. pedicellata	3	0.135	0	0	<0.001*
Epilobium komarovianum	0	0	1	0.117	0.016*
Ficinia nodosa	6	0.675	5	0.453	0.062
Ficinia spiralis	6	1.153	6	0.853	0.001*
Gentianella saxosa	5	0.321	3	0.107	0.001*
Hydrocotyle microphyilla	1	0.081	0	0	n/a
Isolepis cernua	0	0	2	0.162	0.002*
Lilaeopsis novae-zelandiae	0	0	1	0.007	n/a
Luzula banksiana var. banksiana	4	0.294	4	0.264	0.478
Moss	4	0.314	5	0.211	0.06
Myosotis pygmaea	4	0.033	2	0.035	0.949
Pimelea lyallii	3	0.047	1	0.015	0.107
Pratia angulate	1	0.007	0	0	n/a
Ranunculus acaulis	4	0.213	3	0.046	0.001*
Ranunculus recens	5	0.679	6	1.142	0.05
Raoulia hookeri var. hookeri	6	5.45	5	4.733	0.033*

Between 2015 and 2020, a number of species in the deflation surfaces experienced a change in abundance. In the surveys completed in 2015 and 2020, 21 species were recorded as present across all plots. Ten of these species showed a significant difference in the average abundance per quadrat in 2015 compared to 2020 (Table 5.3). The majority of the species recorded decreased in abundance over the study period. The species that

increased in abundance between 2015 and 2020 were *R. recens*, *C. muelleri* and the species that were not present in 2015, *E. komarovianum*, *I. cernua* and *L. novae-zelandiae*. In 2020, the abundance of each species was low (below 5%), showing the plots are dominated by bare sand. The most abundant species in both years were *R. hookeri var. hookeri* and *C. acerosa.*

The relative importance of each species present in the plots in 2015 and 2020 was calculated. The largest change of relative importance was in the seaward plot in P6. This is a result of the reduced species richness and change in plant community composition that has occurred in this plot. The seaward plot in P6 is the only seaward plot where *F. spiralis* has a high importance (Fig. 5.14). The change that has occurred in the seaward plot in P6 is different to what has occurred in all of the other plots in the deflation surfaces. This indicated the plant communities in this plot have changed in response to increased sand accumulation. In contrast, the five most dominant species present in the seaward plots in P4 and P5, were the intermediate dune colonisers, *C. acerosa* and *F. nodosa* and the dune slack species, *R. recens* and *C. muelleri* (Fig. 5.13). These were the most dominant species in the seaward plots in P4 and P5 in both 2015 and 2020. This shows there was little change in the relative importance of the species in these two plots over the study period.

There was a difference in the most important species in the seaward plots compared to the landward plots. *C. acerosa* was the dominant species in most of the seaward plots in both 2015 and 2020 (excluding P5-S, 2020) (Fig. 5.14). The cushion plant, *R. hookeri var. hookeri*, was the dominant species in all of the landward plots in 2015 and 2020 (Fig. 5.13). *C. muelleri* and *F. spiralis* were consistently the second and third most dominant species in the landward plots in both 2015 and 2020.

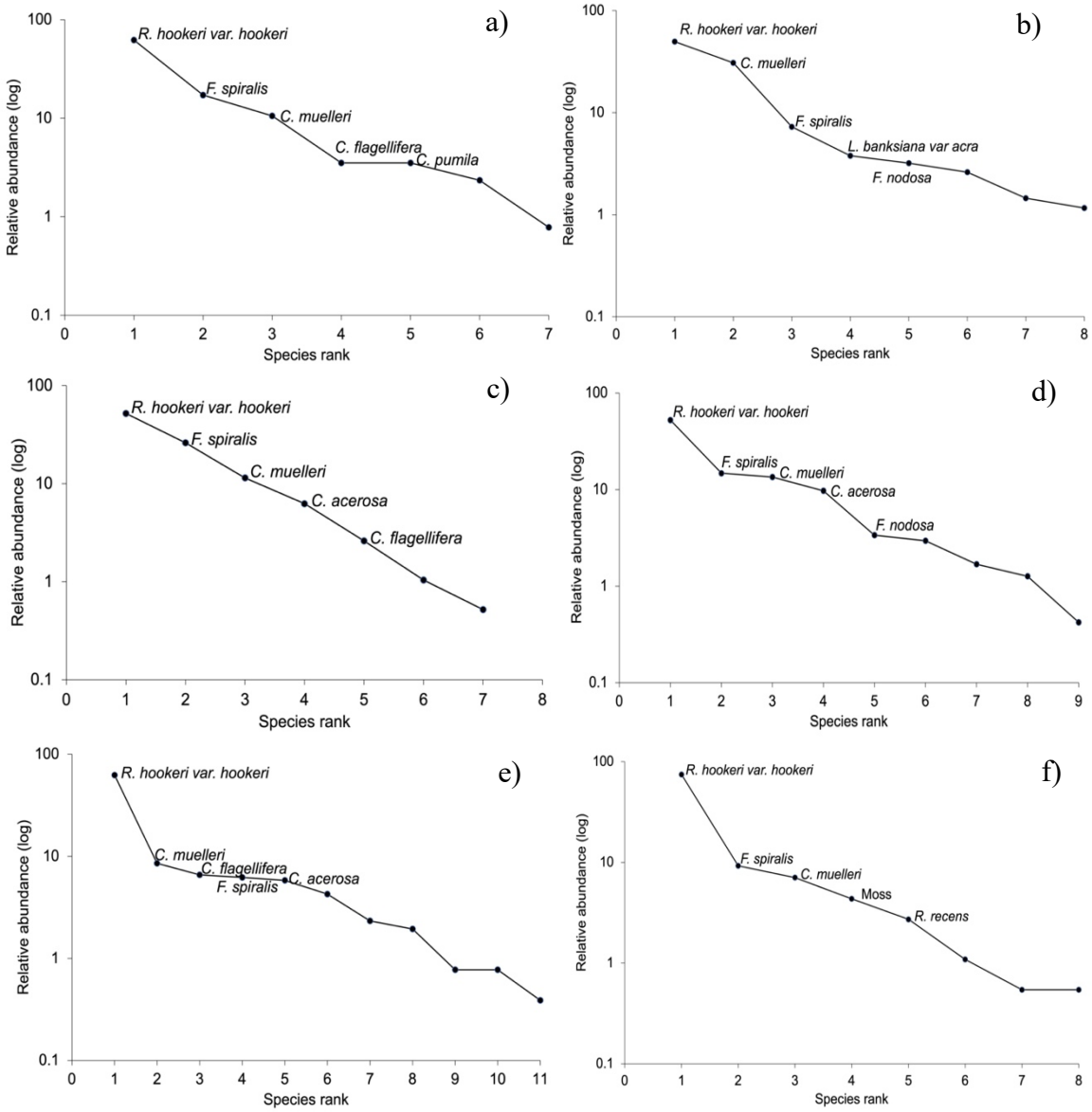

Figure 5.13: Relative importance of the species that occurred in the landward plots in 2015 (left) and 2020 (right); a) P4-L, 2015; b) P4-L, 2020; c) P5-L, 2015; d) P5-L, 2020; e) P6-L, 2015; f) P6-L, 2020. The relative abundance is presented on a log scale.

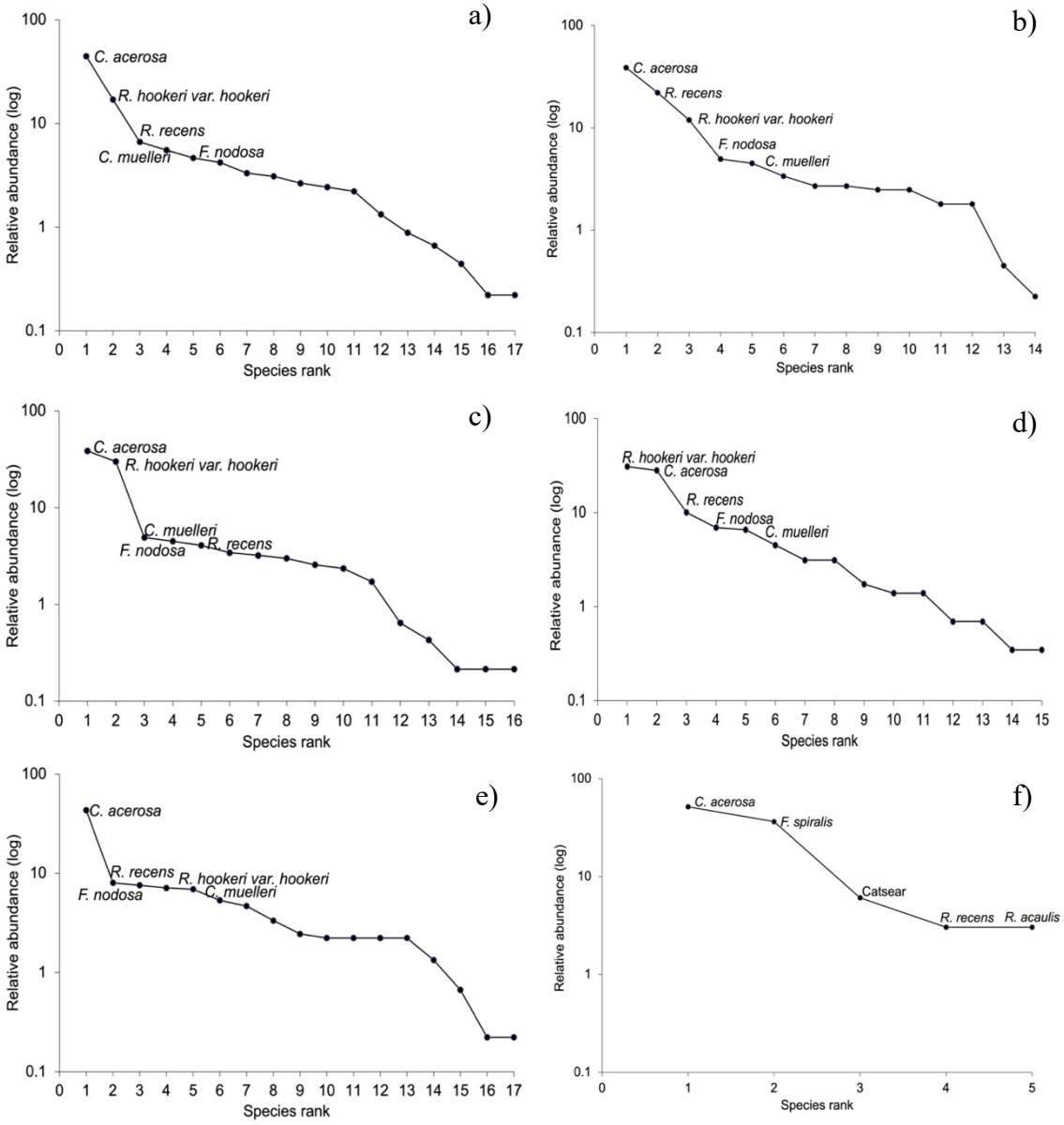

Figure 5.14: Relative importance of the species that occurred in the seaward plots in 2015 (left) and 2020 (right); a) P4-S, 2015; b) P4-S, 2020; c) P5-S, 2015; d) P5-S, 2020; e) P6-S, 2015; f) P6-S, 2020. The relative abundance is presented on a log scale.

The plant species present in the deflation surfaces were categorised based on their structural class: herb, shrub or sedge (Table 5.1). The sedges had the lowest vegetation cover of these three types of vegetation in both the seaward and landward plots, below 2.5% (Fig. 5.15 and 5.16). The vegetation cover of the sedges in the landward plots in P4 and P5 showed a similar trend, sightly decreasing in cover between 2015 and 2020 (Fig. 5.15c). The landward plot in P6 had a lower cover than the other plots throughout the monitoring period and showed little change between 2015 and 2020. The sedges in the seaward plots have fluctuated in vegetation cover (Fig. 5.16c). The largest change in sedge cover was in the seaward plot in P6, where it decreased from 2.5% in 2015 to 0.1%. in 2020. This is in contrast to the P4 and P5 seaward plots where there has been little change in sedge cover.

The shrubs had a higher vegetation cover in the seaward plots compared to the landward plots (Fig. 5.15 and 5.16). The shrubs had a low cover in the landward plots and showed a similar trend over the study period. In 2015, the shrub cover in the seaward plots was very similar, however, these plots have since diverged (Fig. 5.16b). The shrub cover in the seaward plot in P4 remained similar between 2015 and 2020. The seaward plot in P5 has steadily decreased in shrub cover. The largest decrease in shrub cover was in the seaward plot in P6. This occurred between 2016 and 2019, when shrub cover decreased from 7% in 2016 to 0.1% in 2019.

The herbs had the highest vegetation cover of the three structural groups. These are predominantly dune slack species and are the species most vulnerable to burial (Table 5.1). A similar trend was observed in the herb cover in the landward plots, increasing between 2015 and 2019, before decreasing slightly in 2020 (Fig. 5.15a). The cover of these species was highest in P4 in both the landward and seaward plots, where the least accretion has occurred. The herbs in the seaward plot in P4 showed a similar trend and have slightly increased in abundance over the study period (Fig. 5.16a). In contrast, the herb cover in the seaward plot in P6 decreased from 13% in 2016 to 0.01% in 2020. This shows the herbs have been unable to tolerate the sand accumulation that has occurred in this plot.

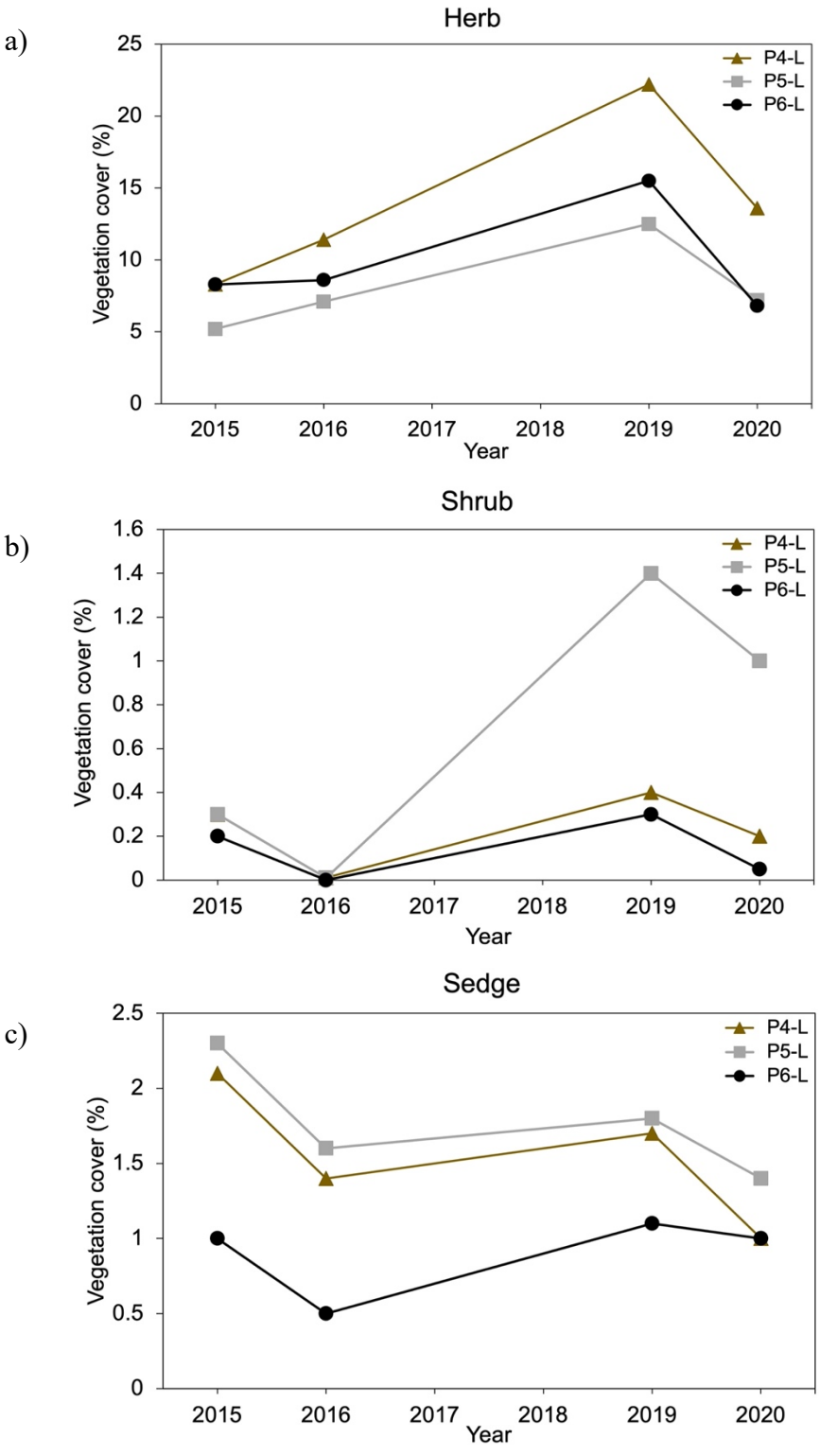

Figure 5.15: The vegetation cover (%) of three functional groups of plants that were present in the landward plots in the deflation surfaces of P4, P5 and P6 from surveys completed in 2015, 2016, 2019 and 2020; a) herb cover; b) shrub cover; c) sedge cover. Vegetation cover was calculated from the abundance of species present. Classifications of species are listed in Table 5.1.

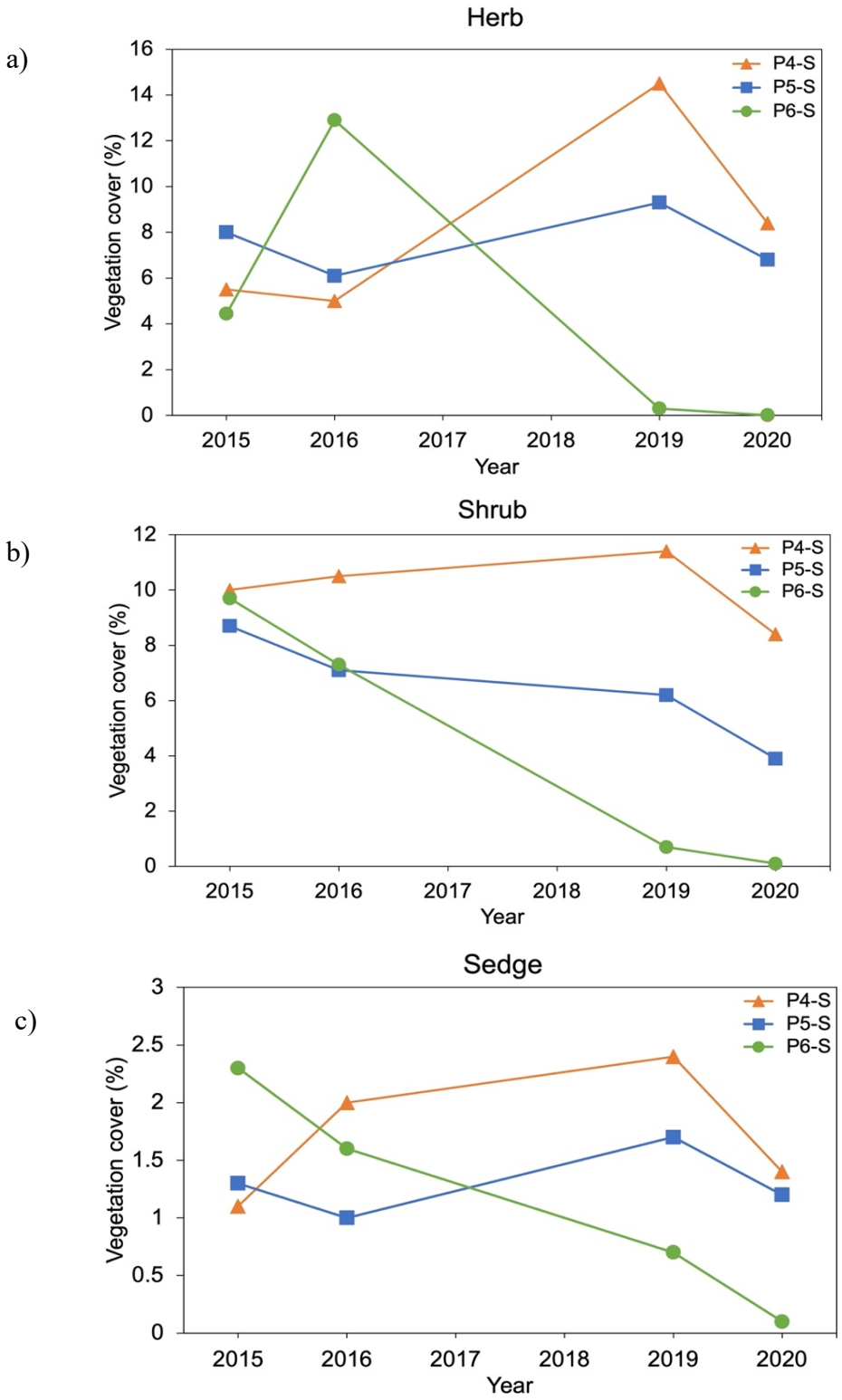

Figure 5.16: The vegetation cover (%) of three functional groups of plants that were present in the seaward plots in the deflation surfaces of P4, P5 and P6 from surveys completed in 2015, 2016, 2019 and 2020; a) herb cover; b) shrub cover; c) sedge cover. Vegetation cover was calculated from the abundance of species present. Classifications of species are listed in Table 5.1.

5.3.3 Relationship between changes in plant communities and burial

Accretion has occurred across the majority of the plots between 2015 and 2020 (Fig. 5.17). Some areas within the plots have eroded, which is more evident in the seaward plots. These areas of erosion are likely due to the breakdown of nabkha previously associated with the presence of *A. arenaria.* The greatest accretion has occurred in the seaward plot in P6 (Fig 5.17f), where there has been up to 1 m of accretion across most of the plot. High levels of accretion occurred in areas of the other plots, such as the NW corner of the landward plot in P6 (Fig. 5.17e), due to the presence and growth of *F. spiralis* nabkha, which have promoted higher rates of sediment deposition.

Accretion between 2015 and 2020 varied between the plots (Table 5.4). The lowest rate of accretion between 2015 and 2020 occurred in P4, where accretion was higher in the landward plot (7.47 cm) compared to the seaward plot (4.83 cm). This contrasts with the patterns of accretion in the P5 and P6 plots. Accretion in P5 was slightly higher than in P4, particularly in the seaward plot where the average accretion was 17.38 cm. This is likely due to sediment being transported around the P5/P6 trailing arm, from the foredune upwind of P6. The seaward plot in P6 has had the highest average accretion per quadrat, 58.71 cm, and ranged between 24-93 cm of accretion between 2015 and 2020.

The patterns of sand accumulation can be related to the changes in plant communities described above. The seaward plot in P6 experienced the greatest depth of accretion between 2015 and 2020. This is also the plot where the greatest loss in species richness, diversity and vegetation cover has occurred. This indicates that most of the species present in 2015 were unable to keep up with the rate of burial that occurred in this plot over the study period. This includes *F. spiralis*, which has a high tolerance to burial, however, has a low abundance in this plot, indicating the rate of accretion in this plot is too high for even the most burial tolerant species. The plant communities in the P4 and P5 plots were similar in the analysis completed and have not showed as much change as P6. Accretion in these plots is less than in the P6 plots and the plants have been exposed to similar burial conditions. Therefore, the majority of these plants have been able to keep up with the observed level of sand accumulation.

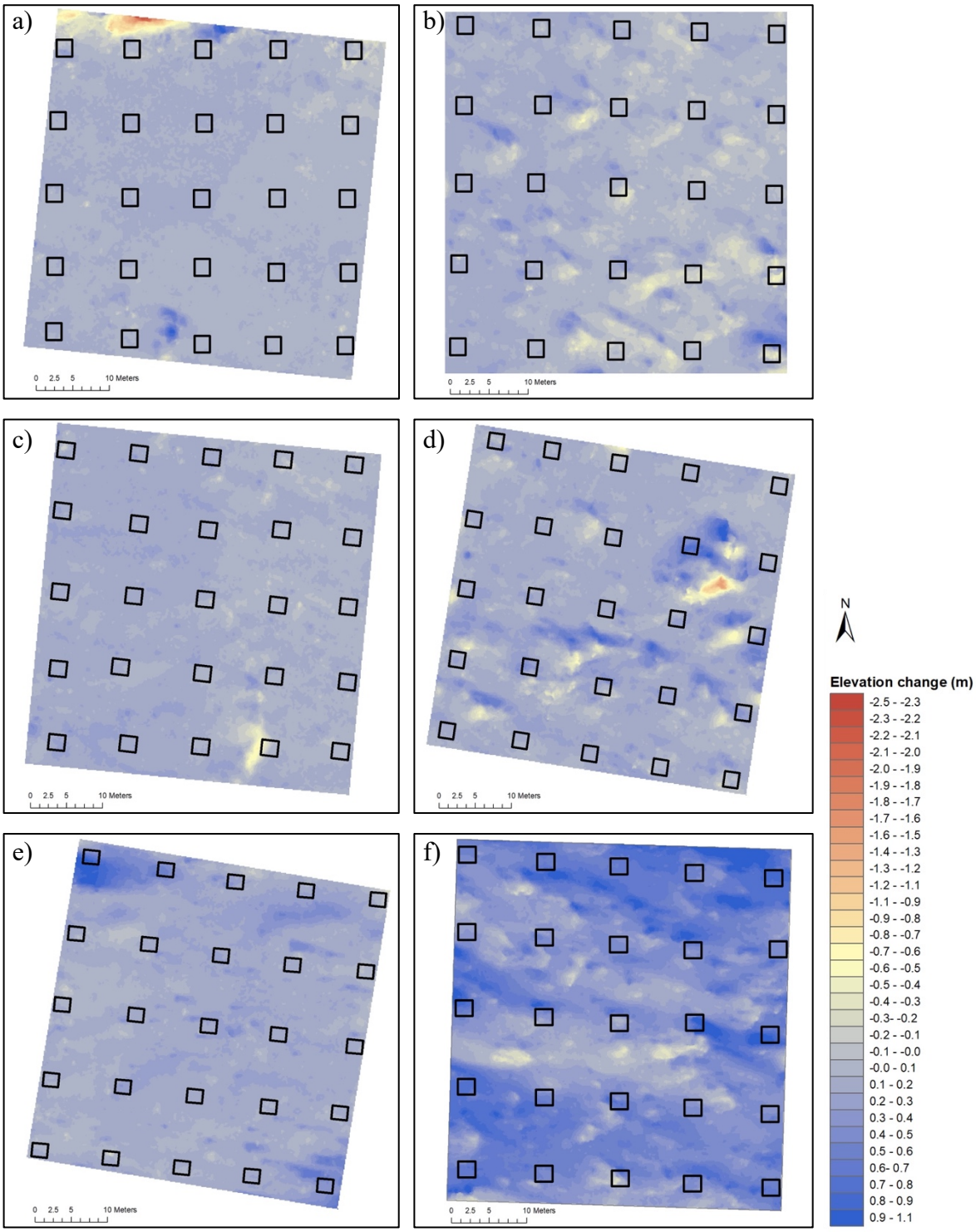

Figure 5.17: Digital elevation model showing the change in surface elevation (m) of the six plots located in the deflation surfaces of P4, P5 and P6 from November 2015 to June 2020: a) P4-L; b) P4-S; c) P5-L; d) P5-S; e) P6-L; f) P6-S. Blue represents an increase in elevation.

Table 5.4: The minimum, maximum and average accretion (cm) that has occurred in the 25 quadrats in each plot between 2015 and 2020. The accretion was calculated from the DEMs showing the elevation change between 2015 and 2020 (Fig. 5.17) and the average accretion of all quadrats in each plot was calculated.

Plot	Minimum accretion (cm)	Maximum accretion (cm)	Average accretion per quadrat (cm)
P4 Landward	-1.45	13.8	7.57
P4 Seaward	-22.91	17.34	4.83
P5 Landward	-9.6	20.89	11.93
P5 Seaward	0.44	71.44	17.38
P6 Landward	4.41	80.91	19.94
P6 Seaward	24.03	94.28	58.71

The average species richness per quadrat for each line of quadrats in the plots shows the relationship between species richness and distance from the sea (Fig 5.18). The western line of quadrats is represented by 1 on the x-axis and is the most seaward line of quadrats and the eastern line of quadrats is represented by 5 on the x-axis and is the most landward line of quadrats in the plot.

The seaward plots in P4 and P5 show there was no large difference in species richness over the lines of quadrats (Fig. 5.18). There was a slight decrease in species richness between 2015 and 2020. In contrast, there was a clear decrease in species richness in the seaward plot in P6 (Fig. 5.18f). There were no species present in the seaward-most line of quadrats and the middle line in the plot. This is due to the high rate of sand accumulation that has occurred in this plot, as very few species have been able to keep up with rate of sand accumulation.

The landward plots in both 2015 and 2020 decreased in species richness with distance inland and proximity to the apex of the parabolic. The plots in P4 and P5 increased in species richness across all lines of quadrats between 2015 and 2020. In contrast, the landward plot in P6 decreased in species richness between 2015 and 2020. In 2020, species richness in this plot slightly increased with distance inland. This is likely a result of the higher rate of sand accumulation in the lines of quadrats closer to the sea in P6.

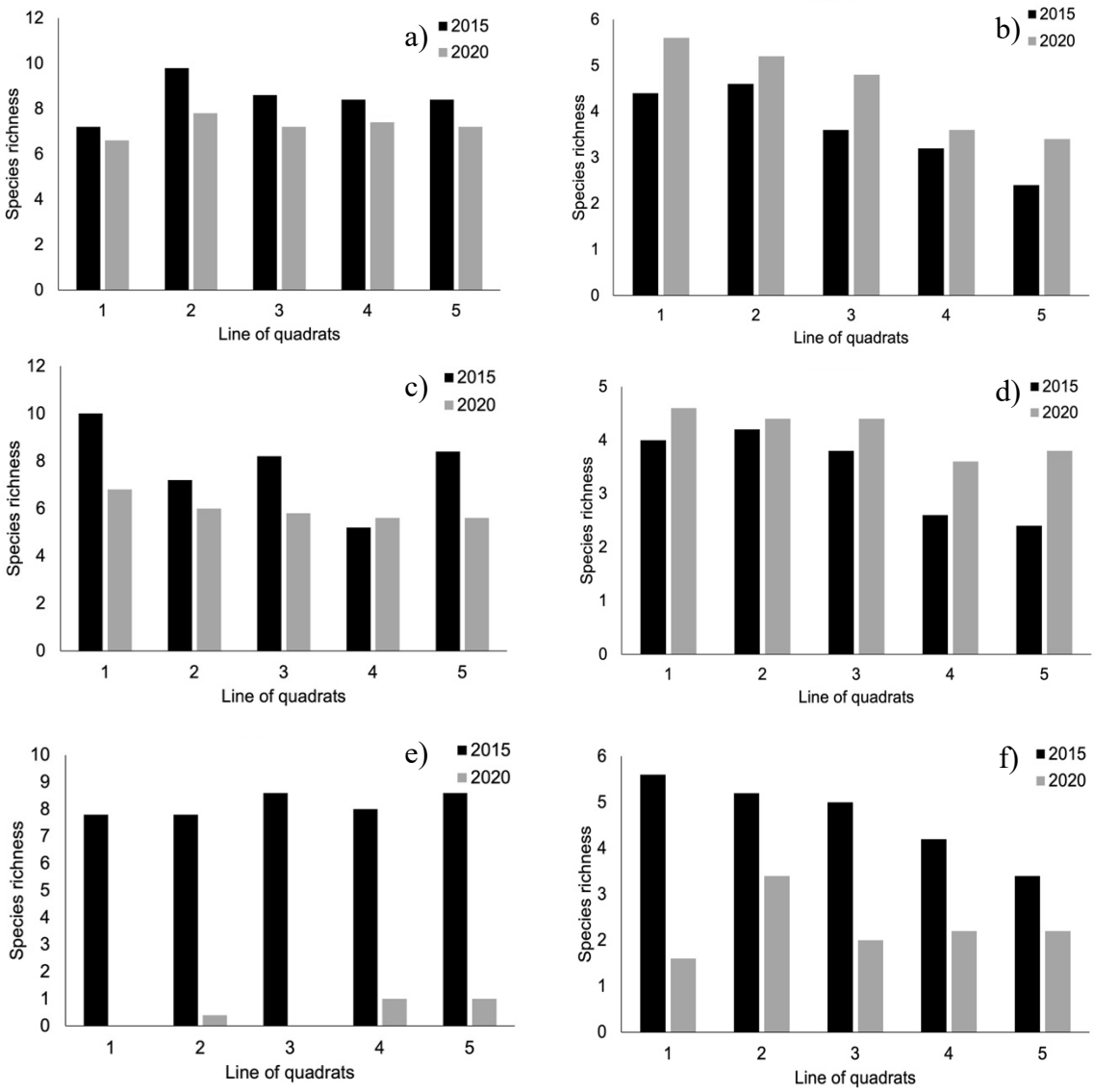

Figure 5.18: The average species richness in the quadrats in each line for a) P4-S; b) P4-L; c) P5-S; d) P5-L; e) P6-S; f) P6-L. Each line contains 5 quadrats separated by 10 m. Line 1 is the western-most line in the plot, closest to the sea and line 5 is the eastern-most line, furthest from the sea. The average species richness was calculated from the species richness of all quadrats (n=5) within each line.

The results indicate the critical threshold of burial *F. spiralis* is able to tolerate. There was variation in the relationship between abundance of *F. spiralis* and sand accumulation in the individual quadrats in the landward plots (Fig. 5.19a). In general, the abundance of *F. spiralis* was positively correlated with sand accumulation. Abundance was highest in areas of 4-7 cm of accretion per year. *F. spiralis* occurred less frequently in the seaward plots, where it had been largely displaced by *A. arenaria* prior to the commencement of the dune restoration programme. Therefore, there was not a strong relationship between *F. spiralis* abundance and sand accumulation (Fig. 5.19b). In the P4 and P5 plots, *F. spiralis* did not tolerate burial in excess of 10 cm per year. In the seaward P6 plot, *F. spiralis* was abundant in areas that experienced up to 28 cm of accretion per year, however, this appears to be the maximum rate of burial it could tolerate. Quadrats in this plot had accreted 58.71 cm on average between 2015 and 2020. The low abundance of *F. spiralis* in the seaward P6 plot shows that it was mostly unable to keep up with the rate of burial that has occurred.

R. hookeri var. hookeri is a non-sand binding, herb species that is highly abundant across the deflation surfaces in Mason Bay. It appears to be able to survive up to 8 cm of accretion per year in the landward plots (Fig. 5.20). It is most abundant in areas that recorded between 1-4 cm of accretion per year. It has been lost from the seaward plot in P6, showing that it is unable to withstand the level of accretion that has occurred here (20 cm/yr on average). A similar result was observed in the seaward P4 and P5 plots, where abundance peaked between 1-3 cm of accretion per year but was unable to tolerate accretion over 9 cm per year. Therefore, *R. hookeri var. hookeri* thrives in low rates of burial, between 1-4 cm of accretion per year and is unable to withstand higher rates.

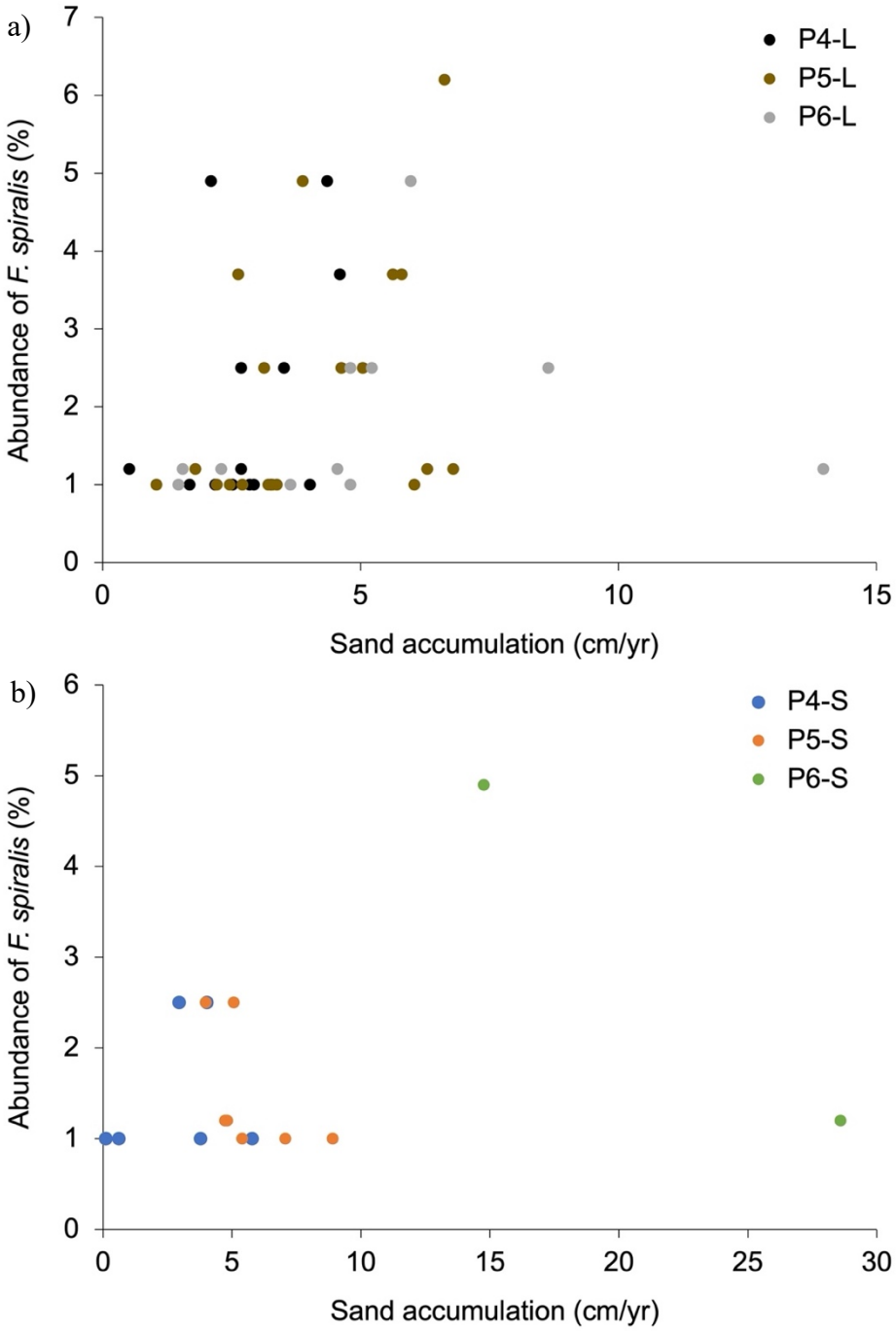

Figure 5.19: Relationship between the abundance of *F. spiralis* (%) and the level of sand accumulation (cm per year) for each individual quadrat in a) the landward plots in P4, P5 and P6 b) the seaward plots in P4, P5 and P6. The abundance was recorded in 2020 and sand accumulation was calculated as the average yearly change in elevation for each quadrat between 2017 and 2020. Note the different scales on the axes.

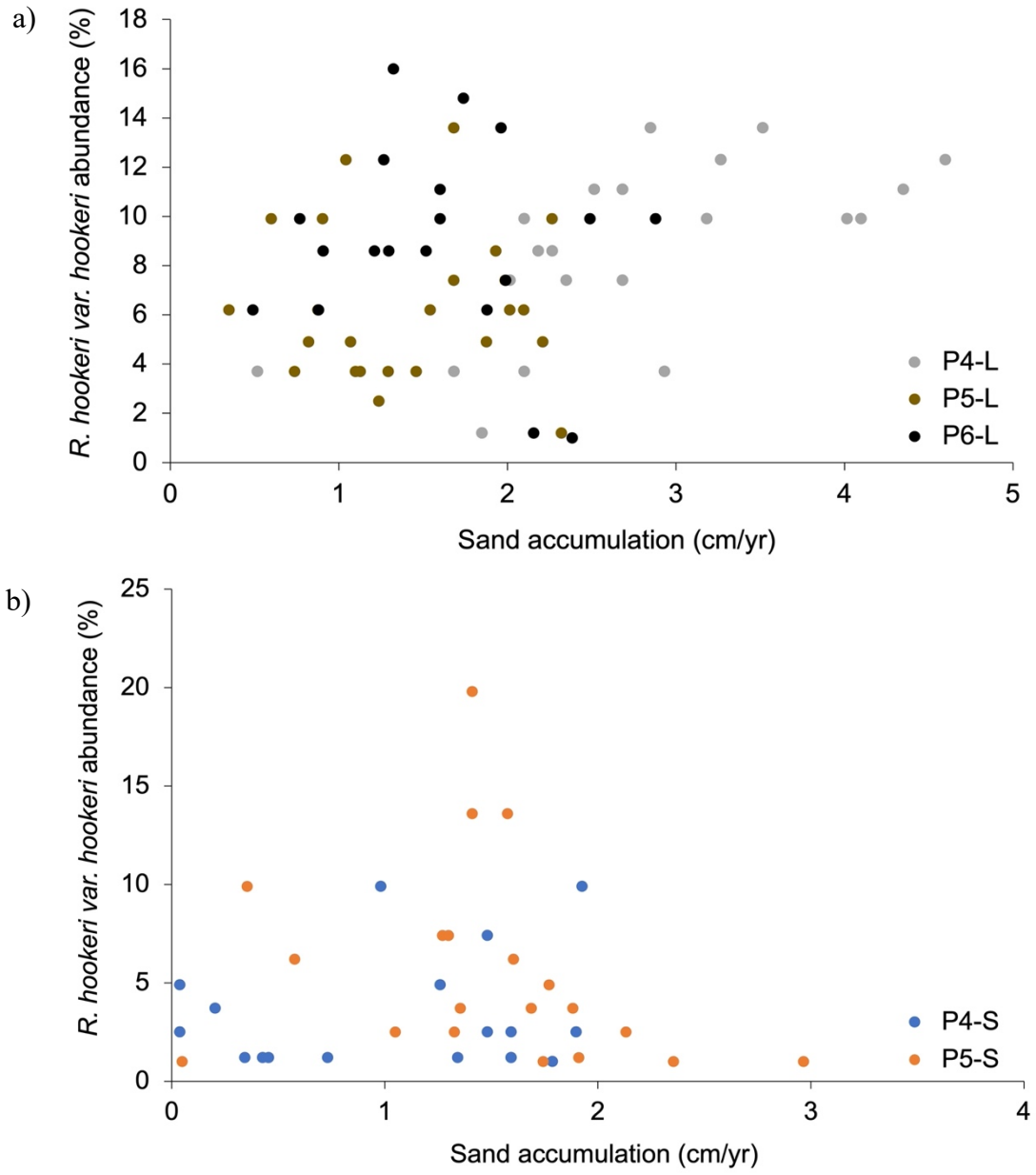

Figure 5.20: Relationship between the abundance of *R. hookeri var. hookeri* (%) and the level of sand accumulation (cm per year) for each individual quadrat in a) the landward plots in P4, P5 and P6; b) the seaward plots in P4 and P5. The abundance was recorded in 2020 and sand accumulation was calculated as the average yearly change in elevation for each quadrat between 2017 and 2020. Note the different scales on the axes.

5.4 Discussion

The plant communities affected in the deflation surfaces evolved during a period of zero sand input after the establishment of the *A. arenaria* foredune. Prior to this, low-lying, hummocky dunes, associated with *F. spiralis* occupied the landscape. Parabolic dunes developed alongside the introduction of *A. arenaria,* and the plant communities in the deflation surfaces comprised of primarily low-lying dune slack species. Foredune destabilization at Mason Bay has increased rates of sand transport into the deflation surfaces, and consequently, accretion from almost zero to dm/year between 2015 and 2020. This has impacted the plant communities in the deflation surfaces of the parabolic dunes, including plant community composition and vegetation cover. The most significant change has occurred in P6, where the adjacent foredune was sprayed with an effective herbicide (Hurricane^{TM}) during a trial that commenced in 2010. Significant sand transport into the deflation surfaces did not commence until after 2015 (Chapter 3), hence, this study has captured the response of the deflation surface plant communities to the progressive increase in sand accumulation in this area.

The greatest rate of sand accumulation occurred in the seaward plot in P6, where 24-93 cm of accretion has occurred across the quadrats between 2015 and 2020. This has clearly had a direct influence on the plant communities in this area. In 2015, this plot had a high species richness, with 17 species present and a similar vegetation cover to the seaward plots in P4 and P5. However, a large portion of the sand released from the foredune has been deposited in the seaward half of the P6 deflation surface, as the foredune has lowered and widened, extending further inland (Chapter 3). As a result, the habitat in the seaward P6 plot has transformed from a stable and stony deflation surface to a dunal landscape, that is predominantly bare sand. This has directly impacted the survival of plants here.

It was hypothesised that there would be a decrease in species richness and plant cover in the seaward plot in P6 as only plants tolerant to high levels of burial would be able to survive. This hypothesis was supported by the current study as vegetation cover decreased from 16% in 2015 to 2% in 2020, and only 5 species were recorded in the plot in 2020. It was also expected that there would be an increase in the abundance of *F.*

spiralis as this is one of the species most tolerant to burial in the Mason Bay dune system, however, the statistical analysis showed no change in the abundance of *F spiralis*. Despite this, the ground photos showed *F. spiralis* has increased in density and number, which indicates a change in vigour has occurred (Fig. 5.12).

As the landscape in the seaward P6 plot has transitioned from a deflation surface habitat to a dunal landscape, the plant communities have changed. Out of the 11 species that have been lost from this plot, 8 of these are dune slack species. This includes, *R. hookeri var. hookeri*, the most abundant species in the deflation surfaces across all parabolics in both 2015 and 2020 (Table 5.3). It appears that *R. hookeri var. hookeri* is able to survive low rates of burial (1-4 cm per year). However, the rate of sand accumulation in the seaward plot in P6 has proven to be too high for *R. hookeri var. hookeri* to tolerate, as this species has been lost from this plot. These findings are consistent with what occurred following restoration at Doughboy Bay where there was a decline in species richness and the species present were mostly dune-specific species, tolerant to higher rates of burial and aeolian activity, such as *F. spiralis* (Konlechner *et al.*, 2014).

It would be expected that once the release of sediment from the foredune slowed, the landscape will evolve into an undulating, dunal landscape and this will promote the establishment of dune-specific species. This includes the native sand-binding species, *F. spiralis*, which is anticipated to establish more widely. This is because the rate of change in the foredune environment is expected to eventually decline, resulting in more favourable conditions for *F. spiralis*. This has started to occur in the lee of the foredune, as sediment has been deposited in the seaward plot in P6 and *F. spiralis* has developed a sparse cover that was not present in 2015. This is likely to extend into the landward half of the P6 deflation surface, as more sediment is deposited here. Therefore, the area downwind of the foredune is expected to transition from a deflation to a dunal landscape, representative of the pre-*A. arenaria* landscape.

As expected, less change occurred in the P4 and P5 deflation surface plant communities compared to P6. The plant communities in both the seaward and landward plots in P4 and P5 followed similar trajectories throughout the monitoring period. This included the species richness, diversity and vegetation cover, as well as species gained or lost throughout the survey period. The deflation surfaces of these parabolics have received

less sand compared to P6, therefore, there has been a smaller change in the plant communities (7-17 cm of accretion on average per quadrat between 2015 and 2020). Sykes and Wilson (1990) found in a study of 30 sand dune species in New Zealand, many perennials survived partial burial, however, most did not survive complete burial. For example, creeping herbs were able to survive partial burial as they could regrow from small stolons that grew vertically. This explains why there has been little change in the P4 and P5 deflation surface communities, as the plants present have been able to keep up with the lower rate of sand accumulation that has occurred.

There were fluctuations in the plant communities throughout the survey period across all parabolics, showing these are dynamic plant communities that are variable in space and time. All plots have lost or gained a number of species and the species richness and abundance has fluctuated between 2015 and 2020. This indicates there are other factors that influence the plant communities and changes are not solely influenced by burial conditions. Plants present in dune slacks are exposed to factors such as low nutrient availability, a fluctuating water table and exposure to both wet and dry conditions (Grootjans *et al.*, 2008). *I. cernua* and *L. novae-zelandiae* were gained in the seaward plots in P4 and P5 in 2020, having not been identified as present in any of the previous surveys completed. The introduction of these species to the seaward plots in 2020 could be due to a change in conditions following the complete submersion of these plots in December 2019, when lakes formed in the deflation surfaces following a period of heavy rain, resulting in a damper environment (Fig. 5.21). The changes identified here show that regardless of the level of burial, these are very dynamic plant communities.

There were also a number of species identified in the plots that had a very low abundance. For example, *A. prostratum subsp. prostratum var. filiforme* was only found in one quadrat in 2015 and *P. lyallii* was only found in two quadrats in 2020. Therefore, deflation surface plant species exhibit spatial variability. This could be due to the limited dispersal abilities of these species resulting in them only being found in local patches of the deflation surfaces (Bossuyt *et al.*, 2005). These species could have also been widely displaced from the low-lying dunes associated with *F. spiralis* following *A. arenaria* invasion.

Figure 5.21: Lakes formed in the seaward half of the deflation surfaces following a period of heavy rain in December 2019. The P5 deflation surface is pictured, showing a lake that extended into the seaward plot in P5.

There was a difference in plant community composition between the landward and seaward plots. The seaward plots (excluding P6) consistently had a higher species richness and diversity compared to the landward plots throughout the survey period (5 more species in the seaward plot in P4 and 6 more species in P5 in the 2020 survey). This is because in parabolic dune deflation surfaces, pioneer species are found further from the coast and successional, intermediate species are found closer to the coast (Hesp, 1991). The landward plots were dominated by herbs including *R. hookeri var. hookeri* and *C. muelleri,* while the seaward plots had a larger dominance and abundance of *C. acerosa*, a woody shrub and other sedges (Fig. 5.15 and 5.16). This can be attributed to the differences in soil properties, as the sediment in the seaward plots is sandier compared to the stonier substrate in the landward plots. The deflation surfaces also slope towards the east, hence, are more exposed to stronger winds with distance inland. This reduces the deposition of sediment, and subsequently nutrients, making it a less suitable environment for plants to survive. This explains the observed patterns of plant community composition in the deflation surfaces as herbaceous species have a greater tolerance to disturbances compared to woody shrubs (Gallego-Fernández and Martínez, 2011).

There were also finer-scale, localised patterns of sedimentation that were influenced by the presence of *F. spiralis*. Sand binding plant species promote the deposition of sediment. *F. spiralis* is spread throughout the deflation surfaces at Mason Bay. The photographs of the plots show there has been an increase in sediment deposition in association with these plants. Sediment is predominantly deposited in the lee of *F. spiralis* during the prevailing westerly winds, however, during north-easterly wind events, the tails can be eroded, and sediment deposited on the opposite side, resulting in shadow dune reversal. In the landward P6 plot, the photos document the growth of a large nabkha where *F. spiralis* has established (Fig. 5.11). This is also evident in the DEM which shows there has been over 1 m of elevation gain between 2015 and 2020 in this quadrat (the NW quadrat, #20 in P6-L, Fig. 5.17e). Similarly, a number of nabkha have also established in the seaward plot in P6. The presence of nabkha has resulted in a variable pattern of sediment accumulation, superimposed on the landscape-scale changes described above, that is not consistent across the deflation surfaces. The increases in size and number of *F. spiralis* nabkha, and association of the presence of *F. spiralis* nabkha and increased sand accumulation, supports the hypothesis that *F. spiralis* would have a strong influence on the deposition of sediment in the deflation surfaces.

Hilton *et al.* (2019) described the extensive *A. arenaria* seedbank that has developed in the foredune at Mason Bay and it was expected this seed would be exposed and released downwind as the foredune progressively eroded. However, *A. arenaria* seedlings were not recorded in the plots in the deflation surfaces in surveys completed between 2015 and 2020. Therefore, seedlings blown downwind from the foredune were not being deposited within the deflation surfaces. This could be because *A. arenaria* seeds in the foredune are no longer viable, are being transported further inland, beyond the parabolic dunes or the deflation surface environment is not conducive to germination or recruitment. These results contrast with restoration at Doughboy Bay where emergence of *A. arenaria* seedlings persisted for years following the initial application of herbicide (Hilton and Konlechner, 2010). *A. arenaria* seedlings were found 16 years following the initial herbicide application at Doughboy Bay (Hilton *et al.*, 2019). This shows processes following restoration vary at different sites and are largely dependent on site-specific characteristics, which should be considered when forming conservation management strategies.

5.5 Conclusion

This chapter has described the changes in the deflation surface plant communities landward of the foredune at Mason Bay between 2015 and 2020. Permanent plots in the deflation surfaces have allowed for the monitoring of the plant communities present here since 2015. The results show these are dynamic plant communities, that are influenced by a number of factors, primarily burial.

It is clear that burial is a strong selective force in the study area. The destabilization of the foredune at Mason Bay has resulted in a significant increase in the transport and deposition of sediment downwind of the foredune. Half of this sediment has been deposited in the deflation surface of the parabolics. This has directly impacted the plant communities in P6 as most of the plants have been completely buried. Consequently, there has been a significant reduction in species presence and cover in the seaward half of the former P6 deflation surface.

The P6 deflation surface and plant communities are still transitioning, as sediment continues to be released from the foredune and deposited in the deflation surface. As the erosion of the foredune slows it is expected a scattered vegetation cover of plant communities with fewer species will develop in the former deflation surface. It is also expected the plant communities present will transform into a low diverse, dynamic dune-specific community, similar to the change in plant communities that occurred following restoration at Doughboy Bay (Konlechner *et al.*, 2014). As the foredune upwind of P4 and P5 continues to erode, it is expected the changes in plant communities observed in P6 will also occur in these deflation surfaces.

Chapter 6

Conclusion

6.1 Introduction

Dynamic dune restoration aims to restore active geomorphic processes to dune systems that have been stabilised (Arens *et al.*, 2013b; Darke *et al.*, 2016). Aeolian activity and the transfer of sand between the beach and within the hinterland promote geomorphic and ecological habitat diversity. However, there is very little understanding of the impacts of dynamic restoration, particularly for the downwind dune environment and associated plant communities. The current study examined the processes and impacts of restoration of a large *A. arenaria* foredune located at Mason Bay on the west coast of Rakiura/Stewart Island; an energetic temperate-latitude coast. The Department of Conservation have undertaken one of the largest dynamic dune restoration projects in the world at Mason Bay. The Mason Bay foredune is probably the largest ever to be deliberately destabilised. The removal of the invasive *A. arenaria* from the foredune commenced in 2010 and provided an exceptional opportunity to study the consequences of foredune devegetation on dune system development and associated plant communities.

This thesis examined the impacts of foredune devegetation on (i) dune system morphology; (ii) rates and processes of aeolian sediment transport and landscape evolution; and (iii) deflation surface plants and plant communities at Mason Bay. The study area comprised three parabolic dunes (P4-P6) located between Duck Creek and Martins Creek at Mason Bay. The foredune upwind of P6 was first sprayed with herbicide in 2010, while the foredune upwind of P4 and P5 was first sprayed five years later (2015). Consequently, these sections of associated foredune and parabolic dunes, which have different treatment and sedimentation histories, provide an exceptional opportunity to

understand the nature and rate of processes that occur following foredune devegetation. This chapter is a synthesis of the key findings from the research. Each of the research aims will be addressed and limitations to this study and the potential for future research in this area will be identified.

6.2 Research aims

6.2.1 Spatio-temporal patterns of sand erosion and deposition following foredune devegetation

Long-term monitoring of the dune system following foredune devegetation provided an opportunity to determine the changes in morphology of the foredune and parabolic dunes at Mason Bay, and the potential to quantify patterns of erosion and accretion. UAV and topographical surveys, as well as ground photos and soil pits were analysed to quantify the rate of change that has occurred within the foredune-parabolic dune complex at Mason Bay. Due to the slow release of sand following foredune devegetation, this chapter was predominantly focussed on the change that occurred between 2015 and 2020. It was expected the foredune would erode following devegetation and this sediment would be transported inland, however, it was not known how rapidly this would occur or where this sediment would be deposited.

Chapter 3 demonstrated that the morphology of the foredune upwind of P6 changed following devegetation at Mason Bay. The stoss face of the foredune progressively eroded, releasing sand, that was transported inland. About half of the eroded sediment has been deposited locally, in the immediate lee of the (moving) foredune crest. This area has experienced the highest net accretion within the parabolic (24,066 m^3 over a 12,594 m^2 area). During the period 2015 to 2020, the foredune became lower and wider and the crest shifted landward (Fig. 3.11). This pattern of deposition was attributed to the impact of topography on airflow over the foredune, which resulted in flow separation downwind of the foredune crest, reduced wind speeds and sand deposition. As air flows over the foredune, an eddy develops which reverses flow back towards the foredune, resulting in deposition of sediment (Walker and Hesp, 2013). Essentially, a large proportion of the sand eroded from the stoss face of the foredune was deposited in the lee of the foredune,

notwithstanding the increased potential for sand from the beach to enter the foredune system.

The rate of change in the foredune upwind of P6 was initially slow. This was attributed to a lag response caused by decaying plant matter, regrowth from rhizome buds in the foredune, inconsistencies in the application of herbicide and the response of *A. arenaria* to herbicide. In 2017, seven years following the first spray application, the rate of erosion rapidly increased and the rate of erosion on the stoss face of the foredune in the subsequent years has been consistently higher than the erosion between 2010-2017 (Fig. 3.11).

Foredune devegetation has influenced the morphology of P6 but barely affected P4 and P5. The highest rate of deposition within the deflation surfaces of the parabolic dunes occurred in P6. Deposition in the P6 deflation surface was primarily concentrated in the seaward half, where between 1-6 m of deposition has occurred. The depth of accretion has decreased with distance inland. Less than 10 cm of accretion was recorded near the apex of P6. Lower rates of deposition inland were attributed to the increasing exposure of the deflation surface to wind shear towards the depositional lobe. However, accretion in the deflation surface was not uniform, primarily due to the presence of *F. spiralis* nabkha, associated with higher rates of deposition. In contrast, most of the deflation surface in P4 and P5 experienced less than 20 cm of deposition (accretion ranged between 0-22 cm in the P4 deflation surface and primarily between 0-30 cm in the P5 deflation surface) (Fig. 3.21).

The depositional lobes of the parabolic dunes moved further inland following foredune devegetation (Fig. 3.15). The erosional face of the P6 depositional lobe lost up to 4 m in elevation and accreted up to 6 m in the lee of the lobe. Volume change calculations from the topographical profile showed that between 2004 and 2020, a section of the erosional face of the P6 depositional lobe has eroded 85.6 m^3 and accreted 236 m^3 in the lee (Fig. 3.15). The rate of accretion has been greater than the rate of erosion. This indicates that sediment transported downwind from the eroding foredune has been trapped within the depositional lobe in association with the native *F. spiralis*.

The erosion and accretion of the foredune and depositional lobes following foredune devegetation was quantified from the topographical profiles recorded between 2004 and 2020. Between this period, combined erosion on the stoss face of the foredune and erosional face of the depositional lobe was 576.2 m^3 and accretion in the lee of the foredune and depositional lobe was 566.3 m^3. The proportion of erosion was slightly higher than the rate of accretion. This indicates that less than 2% of the sediment eroded from the foredune and depositional lobe has been transported beyond the parabolic dunes, into the wider dune system. Therefore, a high proportion of the sediment eroded from the foredune has been retained within the foredune-parabolic dune complex.

These results provide the first substantive estimates of sand accretion downwind from a restored foredune. Previous research has established that the high and densely vegetated foredune that formed following the invasion of *A. arenaria* prevented the transfer of sediment inland (Petersen *et al.*, 2011). Following the devegetation of the foredune, blowouts formed across the stoss face, and the transfer of sediment between the beach and hinterland was re-established. The foredune has eroded and most of this sediment has been deposited in the immediate lee of the foredune, into the seaward half of P6 and within the P6 depositional lobe. These findings are consistent with other locations, such as the Netherlands and Canada, where mechanical removal of vegetation from sections of the foredune complex resulted in enhanced aeolian sediment transport and the foredune transformed into a lower and more hummocky morphology (Arens *et al.*, 2013b; Darke *et al.*, 2016; Ruessink *et al.*, 2018).

6.2.2 Rates, patterns and sources of aeolian sediment transport at Mason Bay

The devegetation of the foredune at Mason Bay provided an exceptional opportunity to understand rates and patterns of sand flux and resulting erosion/accretion across adjacent sections of the foredune-parabolic dune complex. Chapter 3 established the different foredune morphologies adjoining the parabolic dunes (P5 and P6) at Mason Bay due to the different treatment histories. The foredune upwind of P6 is lower, wider and unvegetated, whereas the foredune upwind of P5 is still similar to its pre-restoration morphology and retains some *A. arenaria* cover.

Two aeolian sediment transport experiments were completed during strong onshore wind events (15-20 ms^{-1}) to quantify the relative rates and patterns of sedimentation in the foredune-parabolic dune complex at Mason Bay (Chapter 4). The first experiment compared the rate of sediment transport downwind of a vegetated (P5) and devegetated (P6) foredune. The second experiment aimed to identify the source of sediment transported through a devegetated parabolic dune (P6), to establish whether the primary source of transported sediment was from the beach or the eroding foredune, at least in the particular wind conditions encountered during fieldwork. The frequency of strong wind events was also established to determine the relative importance of these particular conditions.

Foredune devegetation enhanced aeolian activity in P6. The rate of aeolian sediment transport recorded in the centre of the deflation surface in P6 was 575 times greater than downwind of the vegetated foredune (in P5). Increased aeolian activity has also been observed following vegetation removal from dunes in Canada and the Netherlands (Darke *et al.*, 2016; Arens *et al.*, 2013b). Topography had a strong influence on near-surface airflow. Between the foredune and the centre of the deflation surfaces, the incident winds were steered towards a westerly direction as wind flow crossed the foredune, in the direction of the orientation of the long axis of the parabolic dunes. These results were observed downwind of both the devegetated and vegetated foredune and are consistent with conceptual models of flow over similar foredunes (Bauer *et al.*, 2012).

Sand flux increased with distance inland across the deflation surface of P6. The rate of sediment transport was minimal at the rear of the beach, at the foredune toe, where sand flux was estimated to be less than 0.018 $kg/m^2/min$ (Table 4.6). The rate was an order of magnitude higher on the foredune crest, with sand flux between 0.48-0.51 $kg/m^2/min$. This suggests that the stoss face of the foredune was the primary source of sediment into the deflation surface of the parabolic dune, at least during the experimental conditions. The rate of sand flux recorded in the deflation surface and depositional lobe of P6 was the highest of the locations sampled, where between 0.90-1.65 $kg/m^2/min$ was in saltation. The rate of sand flux in the deflation surface and depositional lobe was similar. Therefore, sand is being transported across the length of the deflation surface during high wind events, into the depositional lobe of the parabolic dune. The primary source of sand transported across the deflation surface during strong wind events is unvegetated sand

deposited in the lee of the devegetated foredune and landward half of the deflation surface. This pattern is attributed to a cascading saltation effect. Sand eroded from the stoss face of the foredune initiates further sand transport across the lee slopes of the foredune, and the seaward half of the (former) deflation surface, which in turn entrains sand and increases saltation across the landward half of the deflation surface.

A high proportion of the sand eroded from the foredune has, to date, been deposited in the immediate lee of the migrating foredune crest and in the seaward half of the P6 deflation surface (Chapter 3). A two-stage model is proposed (Fig. 4.21). During lesser wind events (8-12 ms^{-1}), sand is eroded from the stoss face of the foredune and deposited in the lee of the foredune. In such conditions, the wind is not strong enough to cause the cascading saltation effect referred to above. During stronger winds (>15 ms^{-1}), that occurred during the experiments, the sand deposited in the lee of the foredune is an important source of sediment, which is entrained and transported into the depositional lobes of the parabolic dune. The findings from Chapter 4 show that sand is again entering the dune system landward of the foredune, in contrast to the findings of Petersen *et al.* (2011).

These results provide and insight into the future development of the foredune-parabolic dune complex. High rates of sand transport were recorded through the P6 deflation surface and into the depositional lobe under strong onshore winds (15-20 ms^{-1}). These findings were consistent with the results from Chapter 3 that showed there has been very little sand deposited in the landward half of the deflation surface of P6. Most of the sediment transported inland from the foredune has been trapped in the new depositional lobe, in association with *F. spiralis*. It was estimated that less than 2% of the sediment eroded from the foredune and depositional lobes has left the parabolic dune. These results are consistent with Buckley *et al*. (2016) who investigated sedimentation in the stonefield, located in the lee of the depositional lobe of the parabolic dunes. They recorded small rates of sand accumulation over a 9-month period. Net average accretion was 3.2 mm and a maximum accretion of 16 mm was recorded.

It is expected the rate of sand transported into the depositional lobe will reduce in response to the observed increase in the population of *F. spiralis* in the deflation surface and depositional lobe of P6. Increased accretion will occur in the deflation surface as the

number and size of *F. spiralis* nabkha increases and nabkha coalesce. It is expected the foredune will continue to erode, lower, and shift landward, potentially back to the pre-*A. arenaria* shoreline, and the foredune zone will eventually transform into a hummocky and dunal landscape, associated primarily with clumps of *F. spiralis* nabkha. This has started to occur in the lee of the foredune, representative of the pre-*A. arenaria* landscape. Consequently, most of the sediment transported onshore will be deposited within these hummocks.

6.2.3 The response of deflation surface plant communities to changes in sedimentation patterns

The deflation surfaces within the parabolic dunes provide a habitat for a range of plant species. The plant communities comprise primary sand binders, intermediate dune colonisers and dune slack species. Eight of the species in this habitat have been identified as 'nationally vulnerable', 'at risk' or 'nationally uncommon' (de Lange *et al.*, 2017). Therefore, it is important to understand the impact of foredune devegetation on these plant communities. Permanent plots located in the deflation surfaces of P4, P5 and P6 were surveyed over a six-year period, to understand the response of these plant communities to increased deposition. This long-term data allowed the response of the deflation surface plant communities to foredune devegetation to be quantified. Surveys commenced in 2015, prior to the deposition of large quantities of sand in the P6 deflation surface. It was expected there would be a change in species composition and abundance in response to changes in sand accumulation, because of the selective force of burial.

The greatest change in community composition occurred downwind of the devegetated foredune in P6 (Chapter 5), corresponding to the highest rates of sand accumulation. By 2020, this area contained large areas of bare sand. Very few plants survived the deposition that has occurred in this plot. They were not able to grow fast enough (vertically) to keep up with the high rate of burial; an average accretion of 58.71 cm per quadrat between 2015 and 2020 (accretion ranged between 24-93 cm). Consequently, this plot showed the largest decrease in species richness and abundance. Vegetation cover decreased from 16% in 2015 to less than 2% in 2020. Species richness also reduced from 17 species in 2015 to 5 species in 2020. A reduction in species richness also occurred following dynamic dune restoration at Doughboy Bay. Species composition shifted from

a non-native dominated community, to a community primarily composed of native species, reflective of plant communities associated with dynamic dunal environments (Konlechner *et al.*, 2014).

Plant communities in the P4 and P5 deflation surfaces experienced much less change over the same period. Lower rates of burial have occurred in the plots in these deflation surfaces (7-17 cm per quadrat on average between 2015 and 2020), and therefore, most species have been able to keep up with the rate of sand accretion that has occurred. However, these plots also experienced fluctuations in species richness and abundance between 2015 and 2020. Plant species were lost and gained from the plots in the P4 and P5 deflation surfaces (Table 5.2). *C. flagellifera* was present in every plot in 2015, however, was not present in any plot in 2020. *I. cernua* and *L. novae-zelandiae* were present in the seaward plots in P4 and P5 in 2020, however, were not identified in earlier surveys.

These results indicate other factors, in addition to burial, influence species composition. Important factors include the availability of nutrients and water. *I. cernua* and *L. novae-zelandiae* arrived in the deflation surfaces in the 2020 survey following flooding that occurred in December 2019 (Fig. 5.21). These species are associated with damp areas, therefore, the conditions in the deflation surfaces were suitable for these species to establish following this flooding event. Environmental conditions are important in determining species composition in deflation surfaces and species will colonise if the conditions are favourable (Hesp, 1991).

The seaward plots in P4 and P5 consistently had a higher species richness compared to the landward plots throughout the survey period. In 2020, there were 5 and 6 more species present in the seaward plots in P4 and P5 compared to the landward plots. This was attributed to the sediment and level of exposure in the deflation surfaces. The soil in the seaward plots is sandier compared to the stonier substrate in the landward plots. The landward plots are also more exposed to strong winds, therefore, there is less deposition of sediment, and thus, nutrients, required for plant growth. The herbaceous species, *R. hookeri var. hookeri* and *C. muelleri,* were the most abundant species in the landward plots, while the seaward plots had a higher abundance of *C. acerosa*, a woody shrub and other sedges (Fig. 5.13 and 5.14). The landward half of the deflation surface is more

exposed to stronger winds as the deflation surface slopes towards the east and, therefore, less sediment deposition occurs here (Chapter 3). This reduces the availability of nutrients required for plant growth. Herbaceous species have a greater tolerance to disturbances compared to woody shrubs (Gallego-Fernández and Martínez, 2011). Therefore, herbs are more likely to be able to survive in the landward half of the deflation surfaces.

It was expected *A. arenaria* seed would be released form the foredune and transported downwind as erosion of the foredune progressively exposed the seedbank. The existence of a large foredune seedbank at Mason Bay is well documented (Hilton *et al.*, 2019). However, *A. arenaria* seedlings were not recorded in the plots in the deflation surfaces between 2015-2020. This could be because *A. arenaria* seeds in the foredune are no longer viable, are being transported further inland, beyond the parabolic dunes, or the environment is not conducive to germination or recruitment. These results contrast with restoration at Doughboy Bay, where emergence of *A. arenaria* seedlings persisted for years following the initial application of herbicide (Hilton and Konlechner, 2010). This outlines the importance of understanding site-specific characteristics when forming conservation management strategies.

The changes in plant communities observed in P6 are indicative of what can be expected to occur within the foredune-parabolic complex as the dynamic restoration project continues. The sand deposited in the seaward half of the P6 deflation surface originates from the eroding foredune, as well as the eroding trailing arms of the parabolic dune. Sand deposition in the landward half of the P6 deflation surface has been minimal in comparison. Average accretion between 2015 and 2020 per quadrat in the seaward plot in P6 was 58.71 cm compared to 19.94 cm in the landward plot in P6. However, nabkha associated with *F. spiralis* have developed in the landward plot in P6 and the ground photos showed they have increased in size and number in the past five years. It is likely, therefore, that *F. spiralis* will increase in extent and density in the former deflation surface, as has occurred between 2015 and 2020 in the seaward plot in P6 (Fig. 5.12). This will promote the deposition of sand in the lee of the foredune and the area downwind of the foredune will transition from a deflation to a dunal landscape.

There will be winners and losers as a result of the change in the deflation surface landscape. *F. spiralis*, a nationally 'at risk' species and taonga to Māori, and other sedges are expected to thrive in the dunal landscape. *F. spiralis* is a key indicator species of active dune landscapes and the increase in habitat for this species will enhance diversity within the dune system. Prostrate, herbaceous species are predicted to be displaced from the deflation surfaces of the parabolic dunes. *M. pygmaea*, *R. recens* and *R. hookeri var. hookeri* are identified as 'at risk' or 'nationally vulnerable' (de Lange *et al.*, 2017). These low-lying species are unlikely to keep up with the rate of accretion that is anticipated to occur in the deflation surfaces, as has already occurred in the seaward plot in P6, where these species have been lost between 2015 and 2020. Therefore, the habitat for these species will be restricted to the section of the dunes inland of the parabolic dunes, in the stonefield and elsewhere in the dune system. It was found that less than 2% of the sediment eroded from the foredune and depositional lobes has been transported beyond the parabolic dunes, therefore, the stonefield habitat inland of these landforms will remain a habitat for low-lying, dune-slack species. As the foredune adjacent to P4 and P5 continues to erode following the removal of *A. arenaria*, it is also expected the same response observed in P6 will occur in the P4 and P5 deflation surfaces.

6.3 Concluding remarks

This study has shown that sand previously trapped in the *A. arenaria* foredune has slowly been released and redistributed within the adjoining parabolic dunes. The foredune has eroded, but the sand released has been primarily deposited in the lee of the foredune and within the seaward half of the P6 deflation surface. This has changed the downwind plant communities, resulting in a decrease in species richness and abundance in areas where there have been high rates of deposition, greater than 30 cm between 2015 and 2020. The removal of vegetation from the foredune has enhanced active processes of sedimentation, leading to high rates of stoss face erosion, albeit delayed, and deposition in two areas downwind of the foredune (i) directly in the lee of the foredune, within the P6 deflation surface; and (ii) within the P6 depositional lobe.

Findings from this research provide an insight to the impacts of foredune restoration via the removal of *A. arenaria*. The change from a deflation to dunal landscape in the

deflation surfaces shows this method of restoration is effective in restoring dynamic processes to the dunes, and to some degree, re-establishing the pre-*A. arenaria* landscape. Walker *et al*. (2013) identified six indicators of successful restoration following the mechanical removal of vegetation from a foredune in Canada; (i) increased aeolian activity; (ii) enlarged active sand surface area; (iii) positive sediment budgets; (iv) increased dune morphodynamics; (v) improved geomorphic diversity; and (vi) enhanced geomorphic resilience. The findings from this study show all six indicators have been achieved following restoration at Mason Bay. This has positive implications for restoring the dynamic plant communities found in active environments. This will be particularly important for the future preservation of these ecosystems, as habitats associated with active dune systems are being degraded throughout New Zealand (Holdaway *et al.*, 2012).

The foredune is expected to continue to lower and widen and shift landward. It is anticipated that the rate of change in the foredune environment will eventually decline as the height and slope of the stoss face declines. There was no foredune present prior to the invasion of *A. arenaria* to the Mason Bay dune system, therefore, it is likely the foredune will transition into a low-lying, Type 5 foredune (after Hesp, 1988), composed of *F. spiralis* nabkha. Eventually, bare surfaces created following devegetation will gradually decline as plants colonise (Arens *et al.*, 2013b). Thus, it can be expected the devegetated foredune environment will become more favourable for dune-specific plants, such as *F. spiralis*, and this will extend into the deflation surfaces of the parabolic dunes as more sediment is deposited here. This will result in a hummocky and dunal landscape. Therefore, restoration at Mason Bay will result in a greater diversity of habitats within the dune system that will enhance biodiversity.

6.4 Research limitations and future research

Estimates of aeolian sand flux during the reported experiments were limited by the environmental conditions that occurred during the experiments; albeit the relative results are more important than the absolute values. The two experiments were completed during a limited range of wind flow conditions. Wind speeds were strong during the experiments, 15-20 ms^{-1}, therefore, sediment transport data was not obtained under

lighter wind conditions (8-12 ms^{-1}). Consequently, the rate and patterns of sediment transport during lighter transport events could not be determined. As these events occur frequently at Mason Bay and were proposed to play an integral role in the deposition of sediment within the parabolic, this was a key limitation to this study. Sediment was also only observed during onshore winds, and therefore, the role of offshore winds transporting sediment towards the sea could not be investigated.

Future research at Mason Bay will aid in understanding the dune system response to foredune devegetation. Continued monitoring of the sand dunes at Mason Bay will be integral to understanding the implications of remobilisation. This includes monitoring both the morphology and ecology of the dune system. Repeated surveys provide valuable data that aid in understanding changes in the landscape (Darke *et al.*, 2016).

Further sediment transport experiments under different wind conditions will also improve understanding of sedimentation at Mason Bay. This includes sediment transport under offshore, NE winds, that did not occur during the fieldtrips completed. This will gain an insight into the importance of offshore winds in redistributing sediment throughout the dune system. Furthermore, relating the sediment transport experiments to rates of erosion and deposition within the parabolic dune will enhance understanding of the significance of strong wind events. Delgado-Fernandez *et al.* (2018) related sediment flux measurements to topographical change within an active parabolic dune and found strong wind events played a significant role in the geomorphic development of these landforms. Comparing sediment flux rates to patterns of erosion and accretion within the foredune-parabolic dune complex at Mason Bay will aid in understanding the significance of strong wind events on landform development.

Research on the landscape beyond the parabolic dunes will aid in understanding the response of the wider dune system to devegetation. Sediment transport experiments completed showed sediment was being transported into the P6 depositional lobe and a small proportion, further inland. However, the amount of sand that is transported beyond the depositional lobe has not been quantified. It appears to be a small fraction of the total eroded from the foredune and the *A. arenaria*-dominated depositional lobe but may still be important in the long-term sand budget of the stonefield, in the lee of the parabolic dunes.

References

Alcántara-Carrió, J. & Alonso, I. (2002) Measurement and prediction of aeolian sediment transport at Jandía Isthmus (Fuerteventura, Canary Islands). *Journal of Coastal Research,* 18(2), 300-315.

Anderson, J.L. & Walker, I.J. (2006) Airflow and sand transport variations within a backshore-parabolic dune plain complex: NE Graham Island, British Columbia, Canada. *Geomorphology,* 77, 17-34.

Andreotti, B., Claudin, P. & Pouliquen, O. (2010) Measurements of the aeolian sand transport saturation length. *Geomorphology,* 123, 343-348.

Arens, S.M. (1996) Patterns of sand transport on vegetated foredunes. *Geomorphology,* 17, 339-350.

Arens, S.M. & Geelen, L.H.W.T. (2006) Dune landscape rejuvenation by intended destabilisation in the Amsterdam water supply dunes. *Journal of Coastal Research,* 22(5), 1094-1107.

Arens, S.M., Mulder, J.P.M., Slings, Q.L., Geelen, L.H.W.T. & Damsma, P. (2013b) Dynamic dune management, integrating objectives of nature development and coastal safety: Examples from the Netherlands. *Geomorphology,* 19, 205-213.

Arens, S.M., Slings, Q.L. & Geelen, L.H.W.T. (2013a) Restoration of dune mobility in The Netherlands. In: Martínez, M.L., Gallego-Fernández, J.B. & Hesp, P.A (eds.) *Restoration of Coastal Dunes*. Berlin, Springer, pp. 107-124.

Arens, S.M., Slings, Q.L. & De Vries, C.N. (2004) Mobility of a remobilised parabolic dune in Kennemerland, The Netherlands. *Geomorphology,* 59, 175-188.

Arens, S.M., Slings, Q.L., Geelen, L.H.W.T. & Van der Hagen, H.G.J.M. (2007) Implications of environmental change for dune mobility in the Netherlands. In: *International Conference on Management and Restoration of Coastal Dunes, Minist. de Medio Ambiente, Santander, Spain*, pp. 3-5.

Bagnold, R.A. (1941) *The physics of blown sand and desert dunes*. London, Chapman & Hall.

Bakker, E.S. & Olff, H. (2003) Impact of different-sized herbivores on recruitment opportunities for subordinate herbs in grasslands. *Journal of Vegetation Science,* 14, 465-474.

Bar, P. (2013) Restoration of coastal sand dunes for conservation of biodiversity: The Israeli experience. In: Martínez, M., Gallego-Fernández, J.B. & Hesp, P.A. (eds.) *Restoration of Coastal Dunes*. Berlin, Springer, pp. 173-186.

Barchyn, T.E. & Hugenholtz, C.H. (2013) Reactivation of supply-limited dune fields from blowouts: A conceptual framework for state characterization. *Geomorphology,* 201, 172-182.

Barchyn, T.E., Martin, R.L., Kok, J.F. & Hugenholtz, C.H. (2014) Fundamental mismatches between measurements and models in aeolian sediment transport prediction: The role of small-scale variability. *Aeolian Research*, 15, 245-251.

Bauer, B.O. & Davidson-Arnott, R. (2002) A general framework for modeling sediment supply to coastal dunes including wind angle, beach geometry, and fetch effects. *Geomorphology,* 49, 89-108.

Bauer, B.O. & Davidson-Arnott, R.G.D. (2014) Aeolian particle flux profiles and transport unsteadiness. *Journal of Geophysical Research: Earth Surface,* 119(7), 1542-1563.

Bauer, B.O., Davidson-Arnott, R.G.D., Hesp, P.A., Namikas, S.L., Ollerhead, J. & Walker, I.J. (2009) Aeolian sediment transport on a beach: Surface moisture, wind fetch, and mean transport. *Geomorphology,* 105, 106-116.

Bauer, B.O., Davidson-Arnott, R.G.D., Walker, I.J., Hesp, P.A. & Ollerhead, J. (2012) Wind direction and complex sediment transport response across a beach-dune system. *Earth Surface Processes and Landforms,* 37, 1661-1677.

Biel, R.G., Hacker, S.D., Ruggiero, P., Cohn, N. & Seabloom, E. (2017) Coastal protection and conservation on sandy beaches and dunes: context-dependent tradeoffs in ecosystem service supply. *Ecosphere,* 8(4), e01791.

Bird, T.L.F., Bouskila, A., Groner, E. & Kutiel, P.B. (2020) Can vegetation temoval successfully restore coastal dune biodiversity? *Applied Sciences,* 10, 2310.

Bossuyt, B., Honnay, O. & Hermy, M. (2005) Evidence for community assembly constraints during succession in dune slack plant communities. *Plant Ecology,* 178(2), 201-209.

Brunbjerg, A.K., Svenning, J. & Ejrnaes, R. (2014) Experimental evidence for disturbance as key to the conservation of dune grassland. *Biological Conservation,* 174, 101-110.

Buckley, E.C.B., Hilton, M.J., Konlechner, T.M. & Lord, J.M. (2016) Downwind sedimentation and habitat development following *Ammophila arenaria* removal and dune erosion, Mason Bay, New Zealand. *Journal of Coastal Research,* 75, 268-272.

Buffa, G., Fantinato, E. & Pizzo, L. (2012) Effects of disturbance on sandy coastal ecosystems of N-Adriatic coasts (Italy). In: Lameed, G.A. (ed.) *Biodiversity enrichment in a diverse world*. Rijeka, InTech, pp. 339-372.

Bullard, J.E. (1997) A note on the use of the" Fryberger method" for evaluating potential sand transport by wind. *Journal of Sedimentary Research*, 67(3), 499-501.

Butterfield, G.R. (1999) Near-bed mass flux profiles in aeolian sand transport: High-resolution measurements in a wind tunnel. *Earth Surface Processes and Landforms,* 24, 393-412.

Casella, E., Drechsel, J., Winter, C., Benninghoff, M. & Rovere, A. (2020) Accuracy of sand beach topography surveying by drones and photogrammetry. *Geo-Marine Letters,* 40(2), 255-268.

Cockayne, L. (1909) *Report on the sand dunes of New Zealand: The geology and Botany, with their economic bearing.* Wellington, Government Printers.

Creer, J., Litt, E., Ratcliffe, J., Rees, S., Thomas, N. & Smith, P. (2020) A comment on some of the conclusions made by Delgado-Fernandez et al. (2019). "Is 're-mobilisation' nature conservation or nature destruction? A commentary". *Journal of Coastal Conservation,* 24(29).

Darke, I.B., Eamer, J.B.R., Beaugrand, H.E.R. & Walker, I.J. (2013) Monitoring considerations for a dynamic dune restoration project: Pacific Rim National Park Reserve, British Columbia, Canada. *Earth Surface Processes and Landforms,* 38, 983-993.

Darke, I.B., Walker, I.J. & Hesp, P.A. (2016) Beach-dune sediment budgets and dune morphodynamics following coastal dune restoration, Wickaninnish Dunes, Canada. *Earth Surface Processes and Landforms,* 41, 1370-1385.

Davidson-Arnott, R.G.D. & Bauer, B.O. (2009) Aeolian sediment tranposrt on a beach: Thresholds, intermittency, and high frequency variability. *Geomorphology*, 105(1-2), 117-126.

Davidson-Arnott, R., Hesp, P., Ollerhead, J., Walker, I., Bauer, B., Delgado-Fernandez, I. & Smyth, T. (2018) Sediment budget controls on foredune height: Comparing simulation model results with field data. *Earth Surface Processes and Landforms,* 43(9), 1798-1810.

De Lange, P.J., Rolfe, J.R., Barkla, J.W., Courtney, S.P., Champion, P.D., Perrie, L.R., Beadel., Ford, K.A., Breitwieser, I., Schönberger, I., Hindmarsh-Walls, R., Heenan, P.B. & Ladley, K. (2017) *Conservation Statuts of New Zealand Vascular Plants*. New Zealand Threat Classification Series 22, New Zealand Department of Conservation.

De Winter, R.C. and Ruessink, B.G. (2017) Sensitivity analysis of climate change impacts on dune erosion: case study for the Dutch Holland coast. *Climatic Change*, 141, 685-701.

Delgado-Fernandez, I. & Davidson-Arnott, R. (2011) Meso-scale aeolian sediment input to coastal dunes: The nature of aeolian transport events. *Geomorphology,* 126, 217-232.

Delgado-Fernandez, I., Smyth, T.A.G., Jackson, D.W.T., Smith, A.B. & Davidson-Arnott, R.G.D. (2018) Event-scale dynamics of a parabolic dune and its relevance for mesoscale evolution. *Journal of Geophysical Research: Earth Surface,* 123, 3084-3100.

Doody, J.P. (2001) *Coastal conservation and management: An ecological perspective*. Kluwer, Dordrecht, Springer Science+Business Media.

Durán, O. & Moore, L.J. (2013) Vegetation controls on the maximum size of coastal dunes. *PNAS,* 110(43), 17217-17222.

Durán, O., Silva, M.V.N., Bezerra, L.J.C., Herrmann, H.J. & Maia, L.P. (2008) Measurements and numerical simulations of the degree of activity and vegetation cover on parabolic dunes in north-eastern Brazil. *Geomorphology*, 102(3-4), 460-471.

Eamer, J.B.R., Darke, I.B. & Walker, I.J. (2013) Geomorphic and sediment volume responses of a coastal dune complex following invasive vegetation removal. *Earth Surface Processes and Landforms,* 38(10), 1148-1159.

Ejrnaes, R., Bruun, H.H. & Graae, B.J. (2006) Gradient analysis of dry grassland vegetation in Denmark. *Journal of Vegetation Science,* 11, 573–584.

Elko, N., Brodie, K., Stockdon, H., Nordstrom, K., Houser, C., McKenna, K., Moore, L., Rosati, J., Ruggiero, P., Thuman, R. & Walker, I. (2016) Dune management challenges on developed coasts. *Shore & Beach,* 84(1), 15-28.

Ellis, J.T., Li, B., Farrell, E.J. & Sherman, D.J. (2009) Protocols for characterizing aeolian mass-flux profiles. *Aeolian Research,* 1, 19-26.

Everard, M., Jones, L. & Watts, B. (2010) Have we neglected the societal importance of sand dunes? An ecosystem services perspective. *Aquatic Conservation: Marine and Freshwater Ecosystems,* 20, 476-487.

French, K., Mason, T.J. & Sullivan, N. (2011) Recruitment limitation of native species in invaded coastal dune communities. *Plant Ecological,* 212, 601-609.

Gallay, M., Lloyd, C.D., McKinley, J. & Barry, L. (2013) Assessing modern ground survey methods and airborne laser scanning for digital terrain modelling: A case study from the Lake District, England. *Computers & Geosciences,* 51, 216-227.

Gallego-Fernández, J.B. & Martínez, M.L. (2011) Environmental filtering and plant functional types on Mexican foredunes along the Gulf of Mexico. *Écoscience,* 18(1), 52-62.

Gao, J., Kennedy, D.M. & Konlecher, T. (2020) Coastal dune mobility over the past century: A global review. *Progress in Physical Geography,* 44(6), 814-836.

Garciá-Mora, M.R., Gallego-Fernández, J.B. & Garciá-Novo, F. (1999) Plant functional types in coastal foredunes in relation to environmental stress and disturbance. *Journal of Vegetation Science,* 10, 27-34.

Goble, R.J., Mason, J.A., Loope, D.B. & Swinehart, J.B. (2004) Optical and radiocarbon ages of stacked paleosols and dune sands in the Nebraska Sand Hills, USA. *Quaternary Science Reviews,* 23, 1173-1182.

Godínez-Alvarez, H., Herrick, J.E., Mattocks, M., Toledo, D. & Van Zee, J. (2009) Comparison of three vegetation monitoring methods: Their relative utility for ecological assessment and monitoring. *Ecological Indicators,* 9, 1001-1008.

Goldsmith, V. (1989) Coastal sand dunes as geomorphological systems. *Proceedings of the Royal Society of Edinburgh,* 96B, 3-15.

Goldsmith, V. & Golik, A. (1980) Sediment transport model of the southeastern Mediterranean Coast. *Marine Geology,* 37, 147-175.

Gonçalves, J.A. & Henriques, R. (2015) UAV photogrammetry for topographic monitoring of coastal areas. *ISPRS Journal of Photogrammetry and Remote Sensing,* 104, 101-111.

Grootjans, A.P., Adema, E.B., Bekker, R.M. & Lammerts, E.J. (2008) Why coastal dune slacks sustain a high biodiversity. In: Martínez, M.L. & Psuty, N.P.(eds.) *Coastal Dunes*, Berlin, Heidelberg, Springer, pp. 85-101.

Hansen, E., DeVries-Zimmerman, S., van Dijk, D. & Yurk, B. (2009) Patterns of wind flow and aeolian deposition on a parabolic dune on the southeastern shore of Lake Michigan. *Geomorphology*, 105(1-2), 147-157.

Hart, A.T., Hilton, M.J., Wakes, S.J. & Dickinson, K.J.M. (2012) The impact of *Ammophila arenaria* foredune development on downwind aerodynamics and parabolic dune development. *Journal of Coastal Research,* 28(1), 112-122.

Heathfield, D.K. & Walker, I.J. (2011) Analysis of coastal dune dynamics, shoreline position, and large woody debris at Wickaninnish Bay, Pacific Rim National Park, British Columbia. *Canadian Journal of Earth Sciences,* 48, 1185-1198.

Hesp, P. (1988) Morphology, dynamics and internal stratification of some established foredunes in southeast Australia. *Sedimentary Geology,* 55, 17-41.

Hesp, P. (1984) The formation of sand “beach ridges” and foredunes. *Search*, 15(9-10), 289-291.

Hesp, P. (2002) Foredunes and blowouts: Initiation, geomorphology and dynamics. *Geomorphology,* 48, 245-268.

Hesp, P.A. (1989) A review of biological and geomorphological processes involved in the initiation and development of incipient foredunes. *Proceedings of the Royal Society of Edinburgh,* 96B, 181-201.

Hesp, P.A. (1991) Ecological processes and plant adaptations on coastal dunes. *Journal of Arid Environments,* 21, 165-191.

Hesp, P.A. (1999) The beach backshore and beyond. In: Short, A.D. (ed.) *Handbook of beach and shoreface morphodynamics*. London, Wiley, pp. 145-170.

Hesp, P.A. (2013) Conceptual models of the evolution of transgressive dune field systems. *Geomorphology,* 199, 138-149.

Hesp, P.A. & Hilton, M. (2013) Restoration of foredunes and transgressive dunefields: Case studies from New Zealand In: Martínez, M., Gallego-Fernández, J.B. & Hesp, P.A. (eds.) *Restoration of Coastal Dunes*, Berlin, Springer, pp. 67-92.

Hesp, P.A. & Martínez, M.L. (2007) Disturbance processes and dynamics in coastal dunes. In: Johnson, E.A. & Miyanishi, K. (eds.) *Plant disturbance ecology: the process and the response*. United States of America, Academic Press, 215-247.

Hesp, P., Martínez, M., Miot da Silva, G., Rodríguez-Revelo, N., Gutierrez, E., Humanes, A., Laínez, D., Montaño, I., Palacios, V., Quesada, A., Storero, L., Trilla, G.G. and Trochine, C. (2011) Transgressive dunefield landforms and

vegetation associations, Doña Juana, Veracruz, Mexico. *Earth Surface Processes and Landforms,* 36, 285-295.

Hesp, P.A. & Thom, B.G. (1990) Geomorphology and Evolution of Active Transgressive dunefields. In: Nordstrom, K. F., Psuty, N. P. & Carter, B. (eds.) *Coastal Dunes, Form and Process*. Chichester, Wiley, pp. 253-288.

Hesp, P.A. & Walker, I.J. (2013) Coastal dunes. In: Shroder, J., Lancaster, N., Sherman, D.J. & Baas, A.C.W. (eds.) *Treatise on Geomorphology*. San Diego, Academic Press, pp. 328–355.

Hilton, M., Duncan, M. & Jul, A. (2005) Processes of *Ammophila arenaria* (marram grass) invasion and indigenous species displacement, Stewart Island, New Zealand. *Journal of Coastal Research,* 21(1), 175-185.

Hilton, M., Konlechner, T., McLachlan, K., Lim, D. & Lord, J. (2019) Long-lived seed banks of *Ammophila arenaria* prolong dune restoration programs. *Journal of Coastal Conservation,* 23, 461-471.

Hilton, M., Nickling, B., Wakes, S., Sherman, D., Konlechner, T., Jermy, M. & Geoghegan, P. (2017) An efficient, self-orienting, vertical-array, sand trap. *Aeolian Research,* 25, 11-21.

Hilton, M.J. (2006) The loss of New Zealand's active dunes and the spread of marram grass (*Ammophila arenaria*). *New Zealand Geographer,* 62, 105-120.

Hilton, M.J. & Konlechner, T.M. (2010) A review of the marram grass eradication program (1999–2009), Stewart Island, New Zealand. *Proceeding of the 17th Australasian Weeds Conference, Christchurch, New Zealand, 26-30 September 2010*. pp 386-389.

Holdaway, R.J., Wiser, S.K. & Williams, P.A. (2012) A threat status assessment of New Zealand’s naturally uncommon ecosystems. *Conservation Biology*, 4, 619-629.

Hoonhout, B. & de Vries, S. (2017) Field measurements on spatial variations in aeolian sediment availability at the Sand Motor mega nourishment. *Aeolian Research,* 24, 93-104.

Howe, M., Litt, E. & Pye, K. (2012) Rejuvenating Welsh dunes. *British Wildlife,* 24, 85-94.

Hubbard, D.M. & Dugan, J.E. (2003) Shorebird use of an exposed sandy beach in southern California. *Estuarine, Coastal and Shelf Science,* 58S, 41-54.

Hugenholtz, C.H. (2010) Topographic changes of a supply-limited inland parabolic sand dune during the incipient phase of stabilization. *Earth Surface Processes and Landforms*, 35(14), 1674-1681.

Hugenholtz, C.H. & Wolfe, S.A. (2005) Recent stabilization of active sand dunes on the Canadian prairies and relation to recent climate variations. *Geomorphology*, 68(1-2), 131-147.

Ierodiaconou, D., Schimel, A.C. & Kennedy, D.M. (2016) A new perspective of storm bite on sandy beaches using unmanned aerial vehicles. *Zeitschrift fu ̈r Geomorphologie, Supplementary Issues*, 60(3), 123–137.

Ievinsh, G. (2006) Biological basis of biological diversity: physiological adaptation of plants to heterogeneous habitats along a sea coast. *Acta Universitatis Latviensis,* 710, 53-79.

Jackson, D.W.T., Costas, S., González-Villanueva, R. & Cooper, A. (2019) A global 'greening' of coastal dunes: An integrated consequence of climate change? *Global and Planetary Change,* 182, 103026.

Jackson, N.L. & Nordstrom, K.F. (2013) Aeolian sediment transport and morphologic change on a managed and an unmanaged foredune. *Earth Surface Processes and Landforms,* 38, 413-420.

Jackson, N.L., Nordstrom, K.F., Feagin, R.A. & Smith, W.K. (2006) Coastal geomorphology and restoration. *Geomorphology,* 710, 53-79.

Johnson, P. (1992) *The Sand Dune and Beach Vegetation Inventory of New Zealand. II. South Island and Stewart Island.* Christchurch: Land Resources Scientific Report No.16, Department of Scientific and Industrial research, 278p.

Jungerius, P.D. & Van der Meulen, F. (1989) The development of dune blowouts, as measured with erosion pins and sequential air photos. *Catena*, 16(4-5), 369-376.

Keijsers, J.G.S., De Groot, A.V. & Riksen, M.J.P.M. (2015) Vegetation and sedimentation on coastal foredunes. *Geomorphology,* 228, 723-734.

Konlecher, T. & Hilton, M. (2009) The potential for marine dispersal of *Ammophila arenaria* (marram grass) rhizome in New Zealand. *Journal of Coastal Research,* 1, 434-437.

Konlechner, T.M., Buckley, E.E.C.B., Hilton, M.J. & Wakes, S.J. (2016) Downwind dune dynamics following *Ammophila arenaria* invasion. *Journal of Coastal Research,* 75(1), 298-302.

Konlechner, T.M., Hilton, M. & Arens, S.M. (2014) Transgressive dune development following deliberate de-vegetation for dune restoration in The Netherlands and New Zealand. *International Journal of Geoscience and the Environment,* 33, 141-152.

Kraus, M.J. (1999) Paleosols in clastic sedimentary rocks: Their geologic applications. *Earth-Science Reviews,* 47, 41-70.

Lancaster, N. (1988) Controls of eolian dune size and spacing. *Geology*, 16(11), 972-975.

Lancaster, N. (2009) Aeolian features and processes. In: Young, R. & Norby, L. (eds.) *Geological Monitoring*. Boulder, The Geological Society of America Inc, pp.1-25.

Lee, J.-M., Park, J.-Y. & Choi, J.-Y. (2013) Evaluation of sub-aerial topographic surveying techniques using total station and RTK-GPS for applications in macrotidal sand beach environment. *Journal of Coastal Research,* 65, 535-540.

Levin, N., Kidron, G.J. & Ben-dor, E. (2008) A field quantification of coastal dune perennial plants as indicators of surface stability, erosion or deposition. *Sedimentology,* 55(4), 751-772.

Li, Z.S. & Ni, J.R. (2003) Sampling efficiency of vertical array aeolian sand traps. *Geomorphology,* 52(3-4), 243-252.

Lithgow, D., Martínez, M.L., Gallego-Fernández, J.B., Hesp, P.A., Flores, P., Gachuz, S., Rodríguez-Revelo, N., Jiménez-Orocio, O., Mendoza-González, G. & Álvarez-Molina, L.L. (2013) Linking restoration ecology with coastal dune restoration. *Geomorphology,* 199, 214-224.

Lomba, A., Alves, P. & Honrado, J. (2008) Endemic sand dune vegetation of the Northwest Iberian Peninsula: Diversity, dynamics, and significance for bioindication and monitoring of coastal landscapes. *Journal of Coastal Research,* 24(2B), 113-121.

Luna, M.C.M., Parteli, E.J.R., Durán, O. & Herrmann, H.J. (2011) Model for the genesis of coastal dune fields with vegetation. *Geomorphology,* 129, 215-224.

Luzuriaga, A.L., Escudero, A., Olano, J.M. & Loidi, J. (2005) Regenerative role of seed banks following an intense soil disturbance. *Acta Oecologica,* 27, 57-66.

Lynch, K., Jackson, D.W.T. & Cooper, A. (2009) Foredune accretion under offshore winds. *Geomorphology,* 105, 139-146.

Magurran, A.E. (1988) *Ecology, diversity and its measurement*. New Jersey, Princeton University Press.

Marshall, J.K. (1965) Corynephorus canescens (L.) P. Beauv. as a model for the *Ammophila* problem. *The Journal of Ecology*, 53(2), 447-463.

Martínez, M., Gallego-Fernández, J.B. & Hesp, P.A. (2013) *Coastal Dunes: Ecology and Conservation.* Berlin, Springer.

Martínez, M. & Psuty, N. (2004) *Coastal Dunes: Ecology and Conservation*. *Ecological Studies*. Berlin, Springer.

Martínez, M., Psuty, N. & Lubke, R.A. (2004) A perspective on coastal dunes. In: Martínez, M. & Psuty, N. (eds.) *Coastal Dunes: Ecology and Conservation*. Berlin, Springer, pp. 3-10.

Martínez-Carricondo, P., Agüera-Vega, F., Carvajal-Ramírez, F., Mesas-Carrascosa, F.-J., García-Ferrer, A. & Pérez-Porras, F.-J. (2018) Assessment of UAV-photogrammetric mapping accuracy based on variation of ground control points. *International Journal of Applied Earth Observation and Geoinformation,* 72, 1-10.

Martinho, C.T., Hesp, P.A. & Dillenburg, S.R. (2010) Morphological and temporal variations of transgressive dunefields of the northern and mid-littoral Rio Grande do Sul coast, Southern Brazil. *Geomorphology,* 117, 14-32.

Maun, M.A. (1994) Adaptations enhancing survival and establishment of seedlings on coastal dune systems. *Vegetatio,* 111, 59-70.

Maun, M.A. (1998) Adaptations of plants to burial in coastal sand dunes. *Canadian Journal of Botany,* 76, 713-738.

Maun, M.A. (2009) *The biology of coastal sand dunes*. New York, Oxford University Press.

McIntosh, R.P. (1980) The background and some current problems of theoretical ecology. *Synthese*, 43(2), 195-255.

Miller, E.M., Gornish, E.S. & Buckley, H.L. (2010) Climate and coastal dune vegetation: disturbance, recovery, and succession. *Plant Ecological,* 206, 97-104.

Miot Da Silva, G. & Hesp, P. (2010) Coastline orientation, aeolian sediment transport and foredune and dunefield dynamics of Moçambique Beach, Southern Brazil. *Geomorphology,* 120, 258-278.

Moloney, J.G., Hilton, M.J., Sirguey, P. & Simons-Smith, T. (2018) Coastal dune surveying using a low-cost remotely piloted aerial system (RPAS). *Journal of Coastal Research,* 34(5), 1244-1255.

Morton, R.A., Leach, M.P., Paine, J.G. & Cardoza, M.A. (1993) Monitoring beach changes using GPS surveying techniques. *Journal of Coastal Research*, 702-720.

Musila, W.M., Kinyamario, J.I. & Jungerius, P.D. (2001) Vegetation dynamics of coastal sand dunes near Malindi, Kenya. *African Journal of Ecology,* 39, 170-177.

Namikas, S.L. (2003) Field measurement and numerical modling of aeolian mass flux distributions on a sandy beach. *Sedimentology,* 50, 303-326.

Ni, J.R., Li, Z.S. & Mendoza, C. (2002) Vertical profiles of aeolian sand mass flux. *Geomorphology,* 49, 205-218.

Nickling, W. & Davidson-Arnott, R. (1990) Aeolian sediment transport on beaches and coastal sand dunes. *Proceedings Canadian Symposium on Coastal Sand Dunes*, 1-35.

Nordstrom, K.F. (2008) *Beach and Dune Restoration*. New York, Cambridge University Press.

Nordstrom, K.F., Jackson, N.L., Hartman, J.M. & Wong, M. (2007) Aeolian sediment transport on a human-altered foredune. *Earth Surface Processes and Landforms,* 32, 102-115.

Nordstrom, K.F., Lampe, R. & Vandemark, L.M. (2000) Reestablishing naturally functioning dunes on developed coasts. *Environmental Management,* 25(1), 37-51.

Pardo-Pascual, J.E., Garcia-Asenjo, L., Palomar-Vazquez, J. & Garrigues-Talens, P. (2005) New methods and tools to analyze beach-dune system evolution using a Real-Time Kinematic Global Positioning System and Geographic Information System. *Journal of Coastal Research,* 49, 34-39.

Parttridge, T.R. (1992) Vegetation recovery following sand mining on coastal dunes at Kaitorete Spit, Canterbury, New Zealand. *Biological Conservation*, 61, 59-71.

Petersen, P.S., Hilton, M.J. & Wakes, S.J. (2011) Evidence of aeolian sediment transport across an *Ammophila arenaria*-dominated foredune, Mason Bay, Stewart Island. 67, 174-189.

Pikcart, A.J. (2013) Dune restoration over two decades at the Lanphere and Ma-le'l dunes in Northern Califronia. In: Martínez, M., Gallego-Fernández, J.B. & Hesp, P.A. (eds.) *Restoration of Coastal Dunes*, Berlin, Springer, pp. 159-171.

Pickart, A.J., Miller, L.M. & Duebendorfer, T.E. (1998) Yellow bush lupine invasion in northern California coastal dunes I. Ecological impacts and manual restoration techniques. *Restoration Ecology,* 6(1), 59-68.

Poortinga, A., Keijsers, J.G.S., Visser, S.M., Riksen, M.J.P.M. & Baas, A.C.W. (2015) Temporal and spatial variability in event scale aeolian transport on Ameland, The Netherlands. *GeoResJ*, 5, 23-35.

Provoost, S., Jones, L.M. & Edmondson, S.E. (2011) Changes in landscape and vegetation of coastal dunes in northwest Europe: a review. *Journal of Coastal Conservation,* 15, 207-226.

Pye, K. (1983) Coastal dunes. *Progress in Physical Geography,* 7, 531-557.

Pye, K. & Blott, S.J. (2017) Evolution of a sediment-starved, over-stabilised dunefield: Kenfig Burrows, South Wales, UK. *Journal of Coastal Conservation,* 21, 685-717.

Pye, K. & Tsoar, H. (1990) *Aeolian sand and sand dunes*. London, Unwin Hyman.

Ranwell, D. (1958) Movement of vegetated sand dunes at Newborough Warren, Anglesey. *Source: Journal of Ecology,* 46, 83-100.

Real, R. & Vargas, J.M. (1996) The probabilistic basis of Jaccard's Index of Similarity *Systematic Biology,* 45(3), 380-385.

Rotnicka, J. (2013) Aeolian vertical mass flux profiles above dry and moist sandy beach surfaces. *Geomorphology,* 187, 27-37.

Ruessink, B.G., Arens, S.M., Kuipers, M. & Donker, J.J.A. (2018) Coastal dune dynamics in response to excavated foredune notches. *Aeolian Research,* 31, 3-17.

Sanz-Ablanedo, E., Chandler, J., Rodríguez-Pérez, J. & Ordóñez, C. (2018) Accuracy of Unmanned Aerial Vehicle (UAV) and SfM photogrammetry survey as a function of the number and location of ground control points used. *Remote Sensing,* 10, 1606.

Seabloom, E.W., Ruggiero, P., Hacker, S.D., Mull, J & Zarnetske (2013) Invasive grasses, climate change, and exposure to storm-wave overtopping in coastal dune ecosystems. *Global Change Biology*, 19, 824-832.

Shannon, C.E. (1948) A mathematical theory of communication. *Bell System Technical Journal*, 27, 379-423.

Sherman, D.J & Li, B. (2009). Predicting aeolian sand transport rates: A reevaluation of models. *Aeolian Research*, 3(4), 371-378.

Shieh, G., Jan, S.-L. & Randles, R.H. (2007) Power and sample size determinations for the Wilcoxon signed-rank test. *Journal of Statistical Computation and Simulation,* 77(8), 717-724.

Sigren, J.M., Figlus, J. & Armitage, A.R. (2014) Coastal sand dunes and dune vegetation: Restoration, erosion, and storm protection. *Shore & Beach,* 82(4), 5-12.

Smyth, T.A.G., Delgado-Fernandez, I., Jackson, D.W.T., Yurk, B. & Rooney, P. (2020) Greedy parabolics: Wind flow direction within the deflation basin of parabolic dunes is governed by deflation basin width and depth. *Progress in Physical Geography: Earth and Environment,* 44(5), 643-660.

Smyth, T.A.G., Jackson, D. & Cooper, A. (2014) Airflow and aeolian sediment transport patterns within a coastal trough blowout during lateral wind conditions. *Earth Surface Processes and Landforms,* 39(14), 1847-1854.

Stallins, J.A. (2005) Stability domains in barrier island dune systems. *Ecological Complexity*, 2(4), 410-430.

Sun, Y., Hasi, E., Liu, M., Du, H., Guan, C. & Tao, B. (2016) Airflow and sediment movement within an inland blowout in Hulun Buir sandy grassland, Inner Mongolia, China. *Aeolian Research,* 22, 13-22.

Sykes, M.T. & Wilson, J.B. (1990) An experimental investigation into the response of New Zealand sand dune species to different depths of burial by sand. *Acta Botanica Neerlandica*, 39, 171-181.

Tsoar, H. (2005) Sand dunes mobility and stability in relation to climate. *Physica A: Statistical Mechanics and its Applications,* 357(1), 50-56.

Tsoar, H. & Blumberg, D.G. (2002) Formation of parabolic dunes from barchan and transverse dunes along Israel's Mediterranean coast. *Earth Surface Processes and Landforms,* 27, 1147-1161.

van Boxel, J.H., Jungerius, P.D., Kieffer, N. & Hampele, N. (1997) Ecological effects of reactivation of artificially stabilized blowouts in coastal dunes. *Journal of Coastal Conservation,* 3, 57-62.

Van der Meulen, F., Bakker, T.W.M. & Houston, J.A. (2004) The costs of our coast: Examples of dynamic dune management from Western Europe. In: Martinéz, M.L. & Psuty, N.P. (eds.) *Coastal Dunes, Ecology and Conservation*, Berlin, Springer, pp. 259-276.

Van Dijk, P.M., Arens, S.M. & Van Boxel, J.H. (1999) Aeolian processes across transverse dunes. II: Modelling the sediment transport and profile development. *Earth Surface Processes and Landforms,* 24, 319-333.

Walker, I.J. & Barrie, J.V. (2006) Geomorphology and sea-level rise on one of Canada's most sensitive coasts: Northeast Graham Island, British Columbia. *Journal of Coastal Research*, SI39, 220-226.

Walker, I.J., Eamer, J.B.R. & Darke, I.B. (2013) Assessing significant geomorphic changes and effectiveness of dynamic restoration in a coastal dune ecosystem. *Geomorphology,* 199, 192-204.

Walker, I.J. & Hesp, P.A. (2013) Fundamentals of aeolian sediment transport: Airflow over dunes. In: Shroder, J., Lancaster, N., Sherman, D.J. & Baas, A.C.W. (eds.) *Treatise on Geomorphology*. San Diego, Academic Press, pp. 109–133.

Wiedemann, A.M. & Pickart, A. (1996) The *Ammophila* problem on the Northwest Coast of North America. *Landscape and Urban Planning,* 34, 287-299.

Wiedemann, A.M. & Pickart, A.J. (2004) Temperate zone coastal dunes. In: Martínez, M.L. & Psuty, N.P. (eds.) *Costal dunes, ecology and conservation*. Berlin, Springer, pp. 53–65.

Willis, A.J. (1989) Coastal sand dunes as biological systems. *Proceedings of the Royal Society of Edinburgh,* 96B, 17-36.

Willis, A.J., Folkes, B.F., Hope-Simpson, J.F. & Yemm, E.W. (1959) Braunton Burrows: The dune system and its vegetation. *Journal of Ecology,* 47(2), 249-288.

Yizhaq, H., Ashkenazy, Y., Levin, N. & Tsoar, H. (2013) Spatiotemporal model for the progression of transgressive dunes. *Physica A,* 392, 4502-4515.

Zarnetske, P.L., Ruggiero, P., Seabloom, E.W. & Hacker, S.D. (2015) Coastal foredune evolution: The relative influence of vegetation and sand supply in the US Pacific Northwest. *Journal of the Royal Society Interface,* 12, 20150017.